Functional Characterization of Target of Rapamycin (TOR) Signalling in Physcomitrella

Elie Saliba[1], Sebastian N. W. Hoernstein[2], Nico van Gessel[1], Alexander Sentimenti[2], Karoline M. V. Höß[1], Juliana Parsons[1], Eva L. Decker[1], Pitter F. Huesgen[2,3], Henrik Toft Simonsen[4], Ralf Reski[1,3]

[1]Plant Biotechnology, Faculty of Biology, University of Freiburg, Schaenzlestr. 1, 79104 Freiburg, Germany

[2]Biochemistry and Functional Proteomics, Faculty of Biology, University of Freiburg, Schaenzlestr. 1, 79104 Freiburg, Germany

[3]CIBSS – Centre for Integrative Biological Signalling Studies, University of Freiburg, Schaenzlestr. 18, 79104 Freiburg, Germany

[4]Laboratoire Biotechnologies Végétales Plantes aromatiques et médicinales, Université Jean Monnet, St. Étienne 42023, France

Corresponding author: ralf.reski@biologie.uni-freiburg.de

ORCID IDs

Elie Saliba: 0000-0003-4617-9782

Sebastian N.W. Hoernstein: 0000-0002-2095-689X

Nico van Gessel: 0000-0002-0606-246X

Alexander Sentimenti: 0009-0006-7679-5315

Karoline M.V. Höß: 0009-0001-7928-6253

Juliana Parsons: 0000-0001-6261-2342

Eva L. Decker: 0000-0002-9151-1361

Pitter F. Huesgen: 0000-0002-0335-2242

Henrik Toft Simonsen: 0000-003-3070-807X

Ralf Reski: 0000-0002-5496-6711

Acknowledgements

We are grateful to Michael N. Hall, Barbara Di Ventura, Bruno André, Claudio De Virgilio, Riko Hatakeyama, Elena Kozgunova, Sjon Hartman, and Ekkehard Schulze for strains and plasmids. We thank Sarah Courbier for including our samples in some of her TOR activity assays. We also thank Agnes Novakovic and Richard Haas for technical assistance, and Anne Katrin Prowse for language editing.

Abstract

Target of rapamycin (TOR) is a conserved protein kinase and an important signalling hub in eukaryotes. The moss Physcomitrella (*Physcomitrium patens*) is a model organism for plant physiology, development, and evolution. However, little is known about TOR signalling in non-vascular plants, including Physcomitrella. Here, we report the effects of inhibiting TOR signalling in Physcomitrella. We identified and characterized Physcomitrella 12-kD FK506-binding protein (FKBP12), which binds TOR in the presence of rapamycin. Whereas the growth of wild-type protonema is unaffected by rapamycin, overexpressing endogenous *FKBP12* rendered the plant susceptible to the inhibitor in a dose-dependent manner. Likewise, protonema growth was inhibited when the TOR-specific ATP-competitive inhibitor AZD8055 was present in the culture. We show that rapamycin and AZD8055 have pleiotropic effects, as they delay cell cycle progression and development, induce chlorosis, inhibit photosynthesis, and alter total protein content. Additionally, we identified and characterized PpTOR, PpLST8, and PpRAPTOR, key components of TOR complex 1 (TORC1), whereas RICTOR and mSIN1 of TORC2 are not encoded by the moss genome. We found that PpLst8 substitutes its homolog in yeast to allow cell growth. Physcomitrella mutants were generated with a conditional downregulation of *PpTOR*, *PpLST8*, and *PpRAPTOR*, respectively. They were impaired in growth. Finally, we show TOR-dependent phosphorylation of a well-known TOR phospho-target, the ribosomal protein RPS6, via LC-MS/MS. Collectively, our results show that Physcomitrella growth and development is positively controlled by a conserved TOR kinase. We suggest to further dissect TOR signalling in Physcomitrella in order to elucidate signalling integration via TORC1 in plants.

Keywords

AZD8055, bryophyte, cell cycle, plant TOR, photosynthesis, TORC1

Key message

The evolutionary conserved TOR kinase positively controls growth and development of the moss Physcomitrella, development and function of its chloroplasts, its protein synthesis and cell cycle progression.

Introduction

All living organisms rely on sensing and responding to their surroundings. The information that is taken up by a significant number of external and internal sensors has to be processed and integrated. Depending on the nature of the information, this is done by complex macroscopic structures (e.g., the trigger hairs on bladderworts or the eyes of animals) or molecular sensors acting through signalling pathways within the cell. One of the most crucial and conserved signalling hubs in eukaryotes is Target of Rapamycin (TOR), best known for its role in controlling metabolism, cell growth, proliferation and survival, mainly in response to nutrients, energy, and environmental stresses (Loewith and Hall 2011; Liu and Xiong 2022; Wang et al. 2025).

TOR is an atypical serine/threonine kinase and a member of the phosphatidylinositol (PI) 3-kinase-related protein kinases (PIKKs) family (Keith and Schreiber 1995). It was originally identified in a genetic screen for yeast (*Saccharomyces cerevisiae*) mutants that could grow in the presence of rapamycin (Heitman et al. 1991a), a macrolide antibiotic from the bacterium *Streptomyces hygroscopicus* (Sehgal et al. 1975; Vezina et al. 1975). TOR proteins are found in most eukaryotes and exhibit high amino acid (aa) sequence similarity (Maegawa et al. 2015; Tatebe and Shiozaki 2017; Liu et al. 2025). They contain five functional domains: HEAT (Huntington, Elongation factor 3, regulatory subunit A of PP2A, TOR1) repeats at the N-terminus, FAT (FRAP-ATM-TRRAP) and FRB (FKBP-Rapamycin-Binding) in the middle of the protein, and the kinase and FATC (Carboxy-terminal FAT) domains at the C-terminus (Tatebe and Shiozaki 2017). Rapamycin inhibits TOR by forming a ternary complex with the highly conserved 12-kDa FK506-binding protein (FKBP12) and the FRB domain, thus restricting its kinase domain (Heitman et al. 1991b; Choi et al. 1996; Yang et al. 2013).

In yeast and mammals, TOR is the catalytic subunit of two high-molecular-mass complexes, TORC1 and TORC2, with distinct architecture and function (Loewith et al. 2002). Yeast TORC1 is formed by either TOR1 or TOR2, LST8 (Lethal with Sec Thirteen 8), KOG1 (Kontroller of Growth 1), and TCO89, while TORC2 exclusively contains TOR2, LST8, AVO1/2/3 (Adheres Voraciously (to TOR2) 1/2/3), and BIT2/61 (Binding Partner of TOR2 protein) (Loewith et al. 2002; Reinke et al. 2004). Mammalian mTORC1 includes mTOR, mLST8, RAPTOR (Regulatory-Associated Protein of TOR), the homolog of yeast KOG1, and two additional proteins, DEPTOR

(DEP domain-containing TOR-interacting protein) and PRAS40 (Proline Rich AKT Substrate 40 kDa). Similar to mTORC1, mTORC2 shares core components (mTOR, mLST8, and DEPTOR) and includes the yeast AVO1 and AVO3 homologs mSIN1 and RICTOR, along with PROTOR1/2, equivalents of BIT2/61 (Loewith and Hall 2011; Liu and Xiong 2022). TORC1, but not TORC2, is sensitive to rapamycin (Loewith et al. 2002). This feature was instrumental in elucidating the function of these complexes, with TORC1 regulating transcription, translation, metabolism, and autophagy to ensure cell growth and survival, while TORC2 has specific roles in actin cytoskeleton organization and cell wall integrity (Loewith et al. 2002; Loewith and Hall 2011).

In algae and flowering plants, the composition of TOR complexes is less well understood, with no evidence for the existence of TORC2 (Liu et al. 2025). The plant TOR complex consists of TOR, LST8, and RAPTOR. In Arabidopsis (*Arabidopsis thaliana*), which has one *TOR*, two *RAPTOR*, and two *LST8*, with only *RAPTOR1* and *LST8-1* being predominantly expressed, homozygous null mutants of *Attor* are embryo lethal (Menand et al. 2002), whereas *Atraptor1* or *Atlst8-1* knock-out plants show embryo developmental arrest and severe growth defects, respectively (Deprost et al. 2005; Moreau et al. 2012). At the cellular level, studies mainly conducted in Arabidopsis revealed that TOR responds to nutrients, energy, light, hormones, biotic and abiotic stresses to regulate transcription, translation, metabolism, autophagy, and hormone signalling (Liu et al. 2025; Wang et al. 2025). At the organismal level, it affects all Arabidopsis developmental stages (Liu et al. 2025). These studies, along with others carried out in algae, have been crucial in understanding the functional evolution of TOR. They also uncovered plant-specific regulations and functions, such as TOR activation by light and auxin through the plant-specific ROP2 GTPase (Moreau et al. 2012; Li et al 2017), and its critical role in promoting photosynthetic activity (Couso et al. 2021; D'Alessandro et al. 2024).

In all examined species, TOR mediates its function by fine tuning the activity via phosphorylation of a large array of downstream effector proteins (Battaglioni et al. 2022; Liu et al. 2025). One key effector that is primarily activated by TORC1 is p70 ribosomal S6 kinase 1 (S6K1), which further phosphorylates its primary substrate ribosomal protein S6 (RPS6) (Jacinto and Lorberg 2008; Battaglioni et al. 2022; Liu et al. 2025). This TORC1-S6K1-RPS6 signalling branch mainly regulates ribosome biogenesis and protein translation (Jacinto and Lorberg 2008; Battaglioni et al. 2022;

Liu et al. 2025). In humans, S6K1 is predominantly phosphorylated by mTORC1 on threonine 389 (Kim et al. 2002), while RPS6 mostly undergoes phosphorylation on serines 240 and 244 in an mTORC1-S6K1-dependent manner (Roux et al. 2007). In Arabidopsis, S6K1 and RPS6, along with their TOR-dependent phosphorylation sites, are conserved. AtS6K1 and AtS6K2 are phosphorylated on threonines 449 and 455, respectively (Schepetilnikov et al. 2011). AtRPS6A and AtRPS6B are phosphorylated on Ser240, equivalent to the Ser240 in HsRPS6, and have also been found phosphorylated on Ser237 (Dobrenel et al. 2016). Although these findings underscore the deep evolutionary conservation of TOR signalling mechanisms, our understanding of this pathway in non-vascular land plants, such as the moss Physcomitrella (new species name *Physcomitrium patens*), remains less well explored.

Physcomitrella is a rather small moss in the family Funariaceae (Ostendorf et al. 2021), and a premier model system for studying the biology of non-vascular plants, evolutionary developmental (evo-devo) biology, and cell biology (Reski 2018; Rensing et al. 2020). This prominence is due to its simple body plan (Reski 1998), ease of genetic manipulation due to a yeast-like high rate of homologous recombination in mitotic cells (Strepp et al. 1998; Hohe et al. 2004; Ermert et al. 2019), and its evolutionary position (Beike et al. 2015). One remarkable feature of Physcomitrella is its ability to grow in the form of a filamentous tissue, the protonema, in suspension cultures (Hohe and Reski 2005). This system offers a homogenous and rapidly proliferating biological platform that is also amenable to large-scale propagation under controlled conditions, providing a uniform population of cells (Hohe et al. 2002) for experimental manipulation, genetic engineering, and physiological studies (Decker and Reski 2007). Moreover, the addition of chemicals, such as hormones or inhibitors, leads to a uniform exposure of every single cell without concentration gradients or effects of a gellant (Reski and Abel 1985; Hadeler et al. 1995). Consequently, Physcomitrella protonema in suspension is ideal for molecular genetics, cell biology, and high-throughput functional analyses (Egener et al. 2002; Schween et al. 2005). By capitalizing on these features, Physcomitrella provided important new insights into the evolution of developmental processes (Khraiwesh et al. 2010; Horst et al. 2016; Resemann et al. 2021; Kozgunova et al. 2022; Hoernstein et al. 2023). Therefore, dissecting TOR in Physcomitrella will contribute to clarifying how this signalling hub

operates across the green lineage, informing comparative studies between algae and land plants.

This study reports TOR signalling inhibition in the moss Physcomitrella, thus addressing a major gap in our understanding of TOR signalling evolution and function in non-vascular plants. We identified and characterized core components of this pathway, including FKBP12, TOR, LST8, RAPTOR, and RPS6, and demonstrated their evolutionary conservation. Specifically, we established a Physcomitrella genetic system sensitive to rapamycin, determined optimal conditions for inhibitor sensitivity experiments using rapamycin and AZD8055, an ATP-competitive inhibitor of mTOR (Chresta et al. 2010), constructed conditional RNAi Pptorc1 mutants, and found PpTOR-dependent phosphorylation of PpRPS6 at Ser241 as an essential step toward developing a TOR kinase activity assay.

Results

Moss growth is resistant to rapamycin

As TOR is a master regulator of eukaryotic cell and organismal growth (Liu et al. 2025), we investigated whether its role in growth promotion is conserved in moss. To start with, we added rapamycin to protonema on solid medium or in a suspension culture, and evaluated plant growth. We found that Physcomitrella growth is resistant to rapamycin. Neither the addition of 10 µM of the inhibitor, which is 100-fold higher than the one used to inhibit yeast growth (Heitman et al. 1991a), nor the treatment for a long period of up to 18 days impacted biomass accumulation (**Figure 1A**). Likewise, Physcomitrella growth was not affected by rapamycin in suspension cultures (**Figure 1B**). The fact that Physcomitrella is resistant to rapamycin has been stated before (Menand et al. 2002), however, without disclosing culture conditions or reporting data.

Resistance to rapamycin appears to be widespread in algae and vascular plants. For instance, growth of Arabidopsis seedlings on solid medium is resistant to 10 µM rapamycin (Sormani et al. 2007; Ren et al. 2012). Similarly, growth of broad bean (*Vicia faba*) and rice (*Oryza sativa*) is not inhibited, and only high concentrations of the inhibitor could moderately retard growth of tomato (*Solanum lycopersicum*) seedlings (Xu et al. 1998; Xiong et al. 2016; Bakshi et al. 2017). Two algae, the red alga *Cyanidioschyzon merolae* and the green alga *Auxenochlorella pyrenoidosa*, are also

resistant to rapamycin (Imamura et al. 2013; Zhu et al. 2022). Several reasons were suggested: 1) inability of rapamycin to enter plant cells, 2) inability of the FKBP12-rapamycin complex to bind the FRB domain in plant TOR, and/or 3) inability of plant FKBP12 to bind rapamycin or TOR due to a reduced affinity to the drug or a low *FKBP12* expression level. Despite the fact that Arabidopsis seedlings are slightly sensitive to rapamycin when submerged in a liquid medium (Xiong and Sheen 2012), it is unlikely that the resistance of algae and plants to the inhibitor is due to poor uptake, or a default in FKBP12-rapamycin-FRB complex formation. In line with this, growth of the green alga Chlamydomonas is sensitive to rapamycin (Crespo et al. 2005). Furthermore, the FRB domain of AtTOR was able to complex with rapamycin and ScFKBP12 (Sormani et al. 2007). Moreover, Arabidopsis seedlings became moderately sensitive to rapamycin when *AtFKBP12* expression was increased, a phenotype that is enhanced when human, yeast, or tomato *FKBP12* were ectopically overexpressed (Ren et al. 2012; Xiong and Sheen 2012). In line with this, Chlamydomonas was more sensitive when aa residues in the rapamycin-binding pocket of CrFKBP12, namely glycine 53 or glutamate 54, where substituted with their human or yeast equivalents (Crespo et al. 2005). This suggests that a reduced affinity of plant FKBP12 to rapamycin and/or a low expression level of endogenous FKBP12 are behind plant resistance to rapamycin.

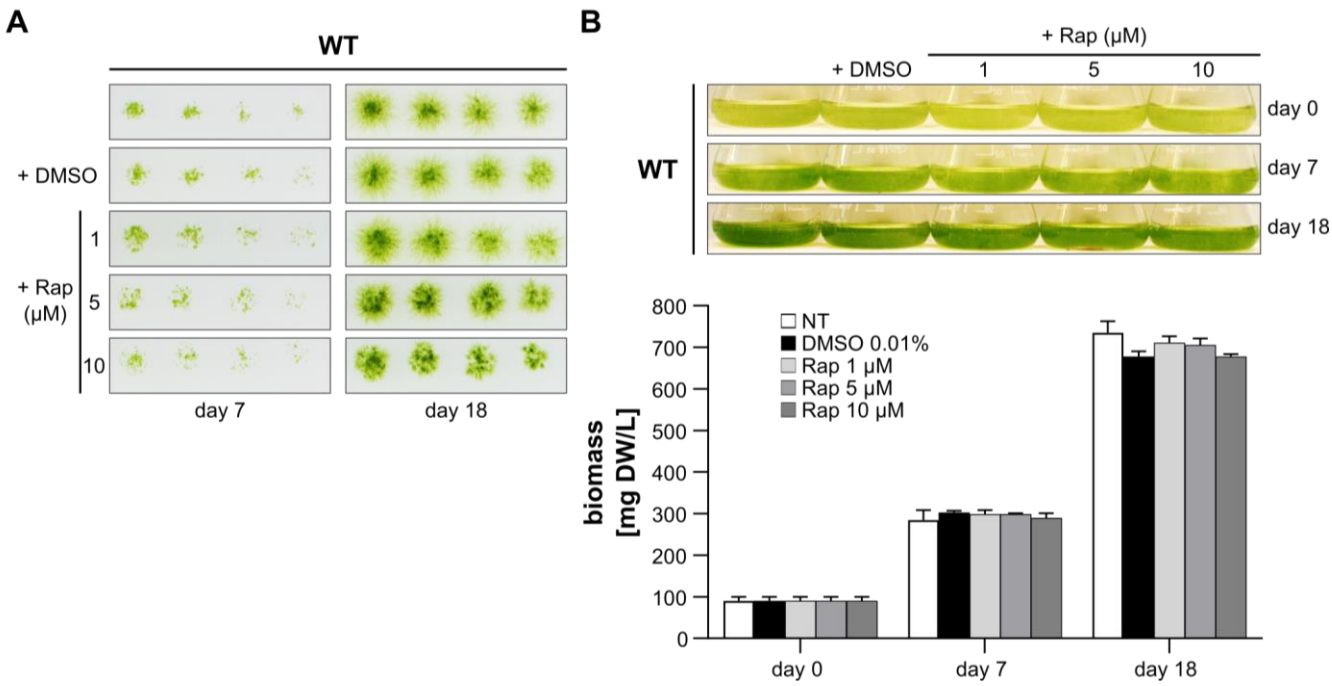

Fig. 1 Physcomitrella growth is insensitive to rapamycin.
A Wild-type protonema from a weekly sub-cultured suspension were prepared at a density of 400 mg DW/L in Knop ME pH 5.8. One-fold serial dilutions were conducted and 15 µL were spotted on solid Knop ME pH 5.8 plates supplemented with medium (NT=not treated), DMSO 0.01%, or rapamycin (Rap) 1, 5, or 10 µM. Plates were photographed at day 7 and 18 of incubation under 70 µmol photons m^{-2} s^{-1} at 22 °C in a 16 h/8 h light/dark cycle. **B** Same protonema as in panel **A**, except that they were prepared at a density of 100 mg DW/L. Aliquots of 25 mL were established in 100 mL Erlenmeyer flaks and subjected to the same treatments as in panel A. Flasks were incubated under 70 µmol photons m^{-2} s^{-1} at 22 °C in a 16 h/8 h light/dark cycle with shaking at 125 rpm. Top: Flasks were photographed at day 0 and days 7 and 18 following incubation. Bottom: Plant material from flasks in panel above were collected and biomass was determined. Bars represent averages of three biological replicates (n=3); error bars represent standard deviations (SD).

FKBP12 is conserved in Physcomitrella and functional in yeast

A BLASTP search with AtFKBP12 as a query identified Physcomitrella FKBP12 with 76% sequence identity (**Figure 2A**). It is encoded by a single gene, *Pp3c1_27870*, on chromosome 1. A query of the *PEATmoss* gene expression database (www.peatmoss.plantcode.cup.unifreiburg.de; Fernandez-Pozo 2023) revealed that it is lowly expressed in all tissues (**Supplementary Figure S1**). To evaluate if Physcomitrella's resistance to rapamycin is due to a reduced affinity of PpFKBP12 toward the inhibitor, and/or low expression, we first analysed whether aa residues involved in the interaction between HsFKBP12 and rapamycin are conserved in PpFKBP12. Four of these amino acids (Tyr27, Asp38, Gln53, Glu54) are not present in PpFKBP12 (**Figure 2A**, black arrows). Instead, a cysteine, a tryptophan, a glycine, and an arginine occupy these positions, respectively. Hence, it is possible that the presence of these aa impairs the interaction between PpFKBP12 and rapamycin in Physcomitrella. To test this hypothesis, we generated five PpFKBP12 mutants with single or multiple substitutions of these aa with their human counterparts (**Figure 2B**; mutants PpFKBP12^{C26Y}, PpFKBP12D^{W40D}, PpFKBP12$^{C26Y-W40D}$, PpFKBP12 $^{M56K-G57Q-R58E}$, and PpFKBP12$^{C26Y-W40D-M56K-G57Q-R58E}$). As for Gly57 in PpFKBP12, the two aa on both sides were additionally replaced by their human homologs (PpFKBP12$^{M56K-G57Q-R58E}$ and PpFKBP12$^{C26Y-W40D-M56K-G57Q-R58E}$ variants). This decision was adopted since a CrFKBP12 mutant bearing a lysine, a glutamine, and a glutamate at the respective positions conferred more sensitivity of Chlamydomonas cells to rapamycin than the WT protein (Crespo et al. 2005). Two additional mutants were generated, in

which Arg58 was not substituted with its human homolog, but rather with its yeast one (**Figure 2B**; PpFKBP12$^{M56V-R58Q}$ and PpFKBP12$^{M56V-R58Q}$). We did so because Chlamydomonas showed its highest sensitivity to rapamycin when expressing the yeast-like CrFKBP12$^{M52V-E54Q}$ mutant (Crespo et al. 2005).

To investigate if these mutated PpFKBP12 isoforms exhibit higher affinity to rapamycin than the WT protein, we evaluated their ability to replace ScFKBP12 in a yeast complementation assay. Yeast *fkbp12Δ* cells grow normally in the presence of rapamycin on minimal solid medium containing galactose as a carbon source, unless *ScFKBP12* is ectopically expressed from a plasmid under the galactose-inducible GAL1 promoter (Heitman et al. 1991b; Crespo et al. 2005). We expressed WT *PpFKBP12* or mutant variants driven by the GAL1 promoter in the yeast *fkbp12Δ* strain and spotted them onto galactose plates supplemented with rapamycin. Surprisingly, we found that PpFKBP12 is moderately capable of restoring the sensitivity to rapamycin of yeast *fkbp12Δ* cells (**Figure 2B**). When the double amount of rapamycin was used (200 nM), which is still a relatively low concentration, those cells did not grow at all, which indicated that PpFKBP12 can substantially complex with rapamycin and mediate its inhibitory action on TOR, at least in yeast. As for the mutant variants, all but PpFKBP12^{W40D} complemented the rapamycin-resistant phenotype of *fkbp12Δ* cells, and, when growth was evaluated from plates with 100 nM rapamycin, we found that these mutants were more efficient than WT PpFKBP12 in mediating rapamycin action. Intriguingly, yeast expressing PpFKBP12^{C26Y} behaved like those expressing ScFKBP12 (**Figure 2B**). This indicates that having a tyrosine at position 26 instead of a cysteine is required for PpFKBP12 to strongly bind rapamycin. The importance of this tyrosine is highlighted by its ability to reverse the effect of the W40D mutation, and to further enhance the affinity to rapamycin of PpFKBP12$^{M56K-G57Q-R58E}$ and PpFKBP12$^{M56V-R58Q}$, even in the presence of the W40D mutation (**Figure 2B**). Asp38 in HsFKBP12 is involved in a hydrogen bond with rapamycin (Choi et al. 1996), and therefore, it was unexpected that the W40D substitution in PpFKBP12 results in a loss-of-function mutant. The effect of the other substitutions correlates with their role in establishing the bond with rapamycin in human FKBP12.

Taken together, FKBP12 is conserved in Physcomitrella and is able to mediate rapamycin action in yeast *fkbp12Δ* cells. However, and despite the fact that certain aa substitutions in PpFKBP12 enhanced its affinity to the drug, these results could not

fully explain why Physcomitrella is strongly resistant to rapamycin. Because PpFKBP12 could significantly inhibit yeast growth in the presence of rapamycin, it is very likely that a low expression level of endogenous *FKBP12* is a reason of rapamycin resistance in Physcomitrella.

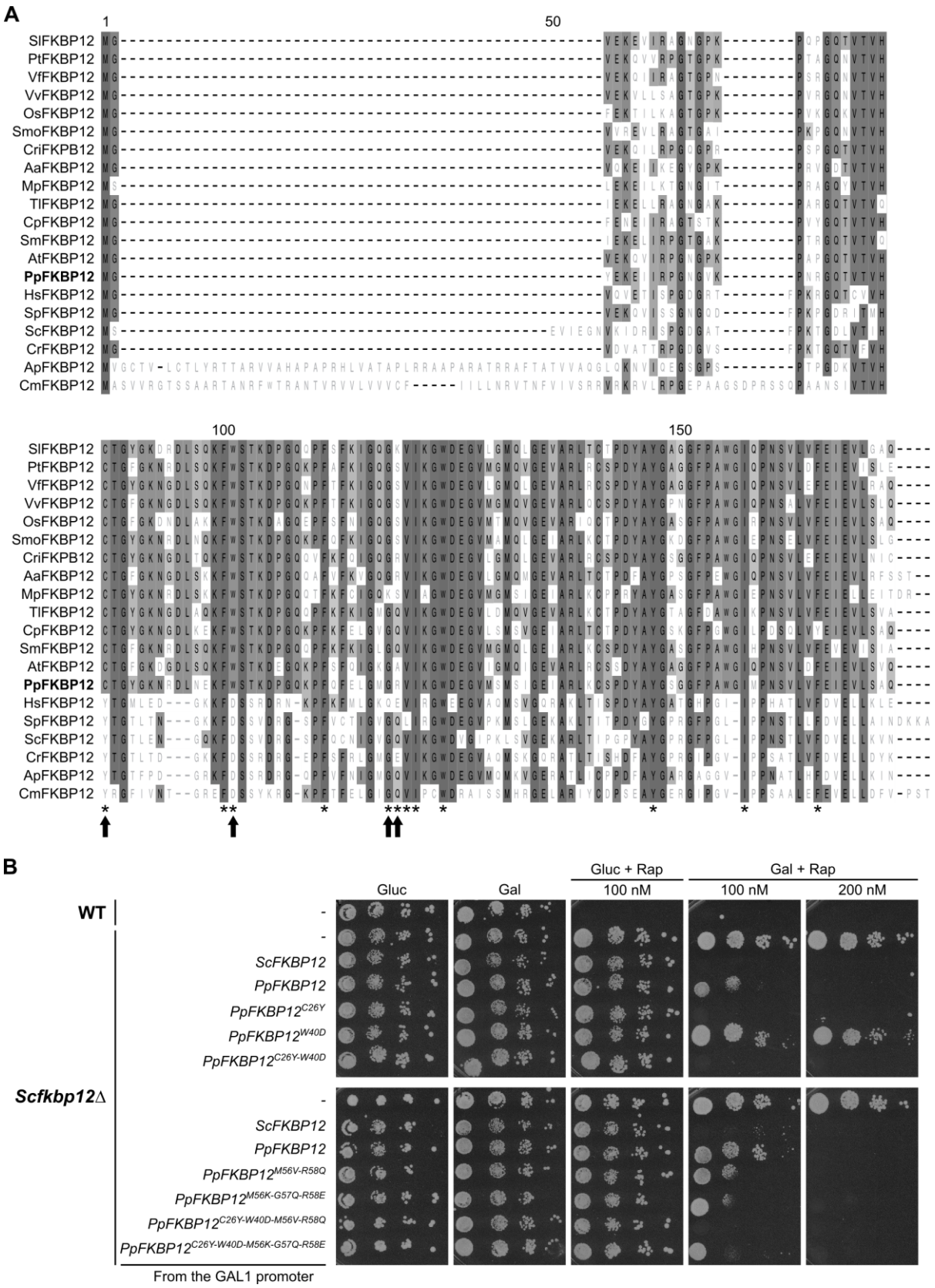

Fig. 2 FKBP12 is conserved in Physcomitrella and is able to mediate rapamycin action in yeast.

A Multiple sequence alignment of FKBP12 proteins from Physcomitrella (bold) and representative organisms: *Anthoceros angustus* (Aa), *Arabidopsis thaliana* (At), *Auxenochlorella pyrenoidosa* (Ap), *Calohypnum plumiforme* (Cp), *Ceratopteris richardii* (Cri), *Chlamydomonas reinhardtii* (Cr), *Cyanidioschyzon merolae* (Cm), *Homo sapiens* (Hs), *Marchantia polymorpha* (Mp), *Oryza sativa* (Os), *Physcomitrium patens* (Pp), *Populus trichocarpa* (Pt), *Saccharomyces cerevisiae* (Sc), *Schizosaccharomyces pombe* (Sp), *Selaginella moellendorffii* (Smo), *Solanum lycopersicum* (Sl), *Sphagnum magellanicum* (Sm), *Takakia lepidozioides* (Tl), *Vicia faba* (Vf), *Vitis vinifera* (Vv). Majority consensus amino acids are shaded in grey. Asterisks indicate residues from human FKBP12 that interact with rapamycin. Arrows indicate amino acids within the rapamycin-binding pocket of HsFKBP12 that are not conserved in PpFKBP12. **B** Yeast complementation assay of the *fkbp12Δ* mutant. Wild-type MH272-3c yeast strain transformed with an empty vector (p415 GAL1), and mutant MH274-1a (*fkbp12Δ*) strain transformed with either p415 GAL1 or p415 GAL1-derived vectors expressing different *FKBP12* variants, were grown in SD-Leu or SGal-Leu suspension cultures. Cultures were normalized to an optical density (OD) at 660 nm of 0.1, subjected to 10-fold serial dilutions, and 15 µL of each dilution were spotted onto SD-Leu or SGal-Leu plates supplemented with DMSO (0.02%) or with rapamycin at 100 or 200 nM. Plates were incubated at 30°C for 5 days.

A rapamycin-sensitive moss mutant

A Physcomitrella mutant with acquired sensitivity to rapamycin will enable the functional characterization of PpTOR. Therefore, we engineered transgenic lines that ectopically express *PpFKBP12-cMyc* or *PpFKBP12*^{C26Y}*-cMyc* under the control of the CaMV 35S promoter and terminator from a construct that contains DNA sequences homologous to the PIG1 locus, which enables targeted and stable integration into the moss genome (Okano et al. 2009). Since Arabidopsis plants overexpressing *HsFKBP12* or *ScFKBP12* showed more sensitivity to rapamycin than those overexpressing the endogenous gene (Ren et al. 2012; Xiong and Sheen et al. 2012), we decided to additionally generate Physcomitrella mutants overexpressing the yeast *ScFKBP12-cMyc* or the human *HsFKBP12-cMyc*.

After transformation of protoplasts, regeneration, and selection on hygromycin, between 102 and 115 different plants per DNA construct were obtained. From these, between 32 and 62 different plants per DNA construct were analysed by PCR for correct integration of the expression cassettes at the PIG1 locus. Between 22% and 31% of these plants showed targeted integration in the moss genome. In addition to targeted integration, multiple and random integrations can occur (Kamisugi et al. 2006; Hoernstein et al. 2023). Therefore, we employed qPCRs on genomic DNA to determine the copy numbers of the integrated expression cassettes. We aimed to

select lines with only a single copy of the integrated construct, or with similar copy numbers. Our screen for lines with one copy of the expression cassettes led to the identification of one transgenic plant (ESPB001) containing *PpFKBP12-cMyc* (**Figure 3A**). Interestingly, the addition of 10 µM rapamycin for 7 days to protonema from this plant in a suspension culture slightly impacted their growth (**Figure 3A**). This indicates that one extra copy of *PpFKBP12* is capable of enhancing the sensitivity of Physcomitrella to rapamycin, and that endogenous levels of PpFKBP12 are not high enough to mediate this response. We expected, however, a higher sensitivity to the drug since *PpFKBP12-cMyc* was expressed from the 35S promoter, which usually provides moderate to strong expression levels in Physcomitrella (Horstmann et al. 2004; Niederau et al. 2024). However, it appears that the 35S driven expression of *PpFKBP12-cMyc* in Physcomitrella is not strong enough to enable high sensitivity to rapamycin, while the 35S driven expression of *ScFKBP12* in Arabidopsis conferred resistance to the inhibitor (Ren et al. 2012). This hypothesis was validated when we tested the sensitivity to 10 µM rapamycin of transgenic plants with increasing copy numbers of the *PpFKBP12-cMyc* cassette, which correlated with an increasing amount of the synthetized protein (**Figure 3**), consistent with previous observations in transgenic Physcomitrella lines (Ruiz-Molina et al. 2022). We observed that the more copies were introduced, the more Physcomitrella became sensitive to rapamycin, with one line showing a drastic decrease in biomass accumulation when compared to the control (**Figure 3**). Starting with a protonema suspension at around 100 mg DW/L, ESPB003 reached, after 7 days, 302 ± 2 mg DW/L in the presence of DMSO versus 148 ± 4 mg DW/L in the presence of rapamycin. On the other hand, plants expressing *PpFKBP12^{C26Y}-cMyc* did not gain more sensitivity to rapamycin than those with *PpFKBP12-cMyc* (**Figure 3**; line ESPB002 vs line ESPB006 with equivalent copies of the integration cassettes, 109 ± 19 and 111 ± 8, respectively). This result is in line with our finding that both variants can replace ScFKBP12 in the yeast complementation assay (**Figure 2C**; panel 200 mM rapamycin). As for the lines expressing *ScFKBP12-cMyc* or *HsFKBP12-cMyc*, we saw that rapamycin could only slightly affect their growth (**Figure 3A**). This may be due to inefficient synthesis of the respective proteins regardless of how many expression cassettes are present in these lines (**Figure 3B**).

In conclusion, we generated a Physcomitrella mutant with high levels of PpFKBP12 that was highly sensitive to rapamycin. This suggests that Physcomitrella's resistance

to this inhibitor is mainly due to a low expression level of endogenous *PpFKBP12* (**Supplementary Figure S1**). FKBP12 is highest expressed in spores with FPKM (fragments per kilobase of transcript per million mapped reads) values of less than 80 and less than 40 in protonema. These are rather low expression values compared to photosynthesis-related genes, which can have FPKM levels of more than 700 or even beyond 5000 (Niederau et al. 2024). However, rapamycin did not fully arrest the growth of the mutant. This might be due to PpFKBP12 protein levels being still not high enough to mediate a full action of rapamycin. Another plausible explanation is that TORC1 function(s) essential for cell growth and proliferation cannot be fully inhibited by the FKB12-rapamycin-TOR complex, as suggested for the effect of rapamycin on fission yeast (*Schizosaccharomyces pombe*), Arabidopsis, and Chlamydomonas (Weisman et al. 1997; Menand et al. 2002; Crespo et al. 2005). Here, rapamycin drastically inhibited protonema biomass accumulation (**Figure 3A**), an effect also seen in transgenic Arabidopsis seedlings expressing *ScFKBP12* from the 35S promoter with one or several copies of the recombinant expression cassette (Ren et al. 2012). Thus, the observed inhibition may represent the maximal achievable effect of rapamycin on Physcomitrella under these conditions. In conclusion, we found that rapamycin can inhibit Physcomitrella growth, indicating the presence of a functional TOR signalling pathway in this plant.

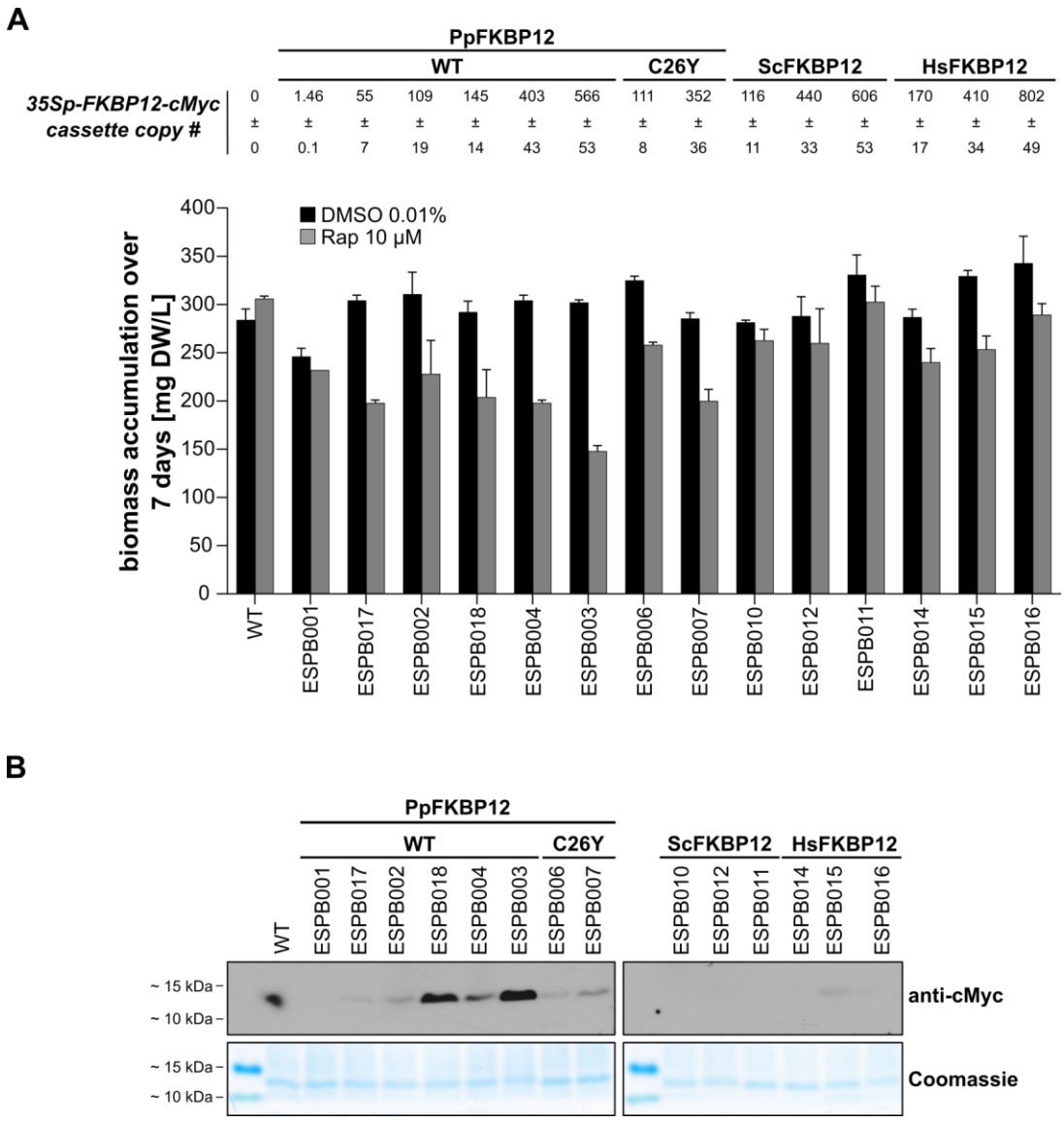

Fig. 3 Establishment of a rapamycin-sensitive Physcomitrella line overexpressing endogenous FKBP12.

A Top. Copy number count of the different *35Sp-FKBP12-cMyc* expression cassettes determined via qPCR in the selected transgenic lines. Bottom. Determination of protonema biomass accumulation over 7 days in the presence of 10 µM rapamycin. Protonema from weekly sub-cultured suspensions of the indicated lines were prepared at a density of 100 mg DW/L in Knop ME pH 5.8. Aliquots of 25 ml were established in 100 mL Erlenmeyer flaks and subjected to treatment with 0.01% DMSO or 10 µM rapamycin. Suspensions were incubated for 7 days under 70 µmol photons m^{-2} s^{-1} at 22 °C in a 16 h/8 h light/dark cycle. Plant material was collected and biomass was determined. Bars represent means of two to three biological replicates; error bars represent standard deviations (SD). **B** Protonema of the indicated lines were grown as suspensions in Knop ME pH 5.8. Tissues were harvested, crude protein extracts were prepared, and FKBP12-cMyc was immunoblotted with anti-cMyc antibody. Protein loading control by Coomassie staining is depicted below.

Multiple effects of TOR inhibition

To determine whether the observed effect of rapamycin is specific and mediated through PpTOR, rather than resulting from nonspecific toxicity, we evaluated the growth of the Physcomitrella line overexpressing *PpFKBP12* in the presence of decreasing concentrations of rapamycin (10 µM, 5 µM, 1 µM). We found that the lower the concentration of rapamycin, the smaller its effect on protonema biomass accumulation is (**Figure 4A**). This supports the conclusion that the effect of rapamycin is specific and likely mediated through PpTOR. Notably, the strongest effect was observed at a concentration of 10 µM. Therefore, this concentration was subsequently used.

Apart from rapamycin, mTOR and AtTOR can be inhibited by a set of chemicals that act as ATP-competitive inhibitors, such as AZD8055 (Chresta et al. 2010; Montané and Menand 2013). In Arabidopsis, AZD8055 is highly specific to the TOR kinase (Perdoux et al. 2024). Unlike rapamycin, AZD8055 achieves more complete inhibition of TOR (Van Leene et al. 2019; Liu et al. 2024), which could be useful to elucidate TOR functions that are resistant to rapamycin. Therefore, we additionally evaluated the effects of AZD8055 on Physcomitrella protonema biomass accumulation. Similar to rapamycin, we recorded a dose-dependent response, with 10 µM of AZD8055 completely blocking protonema growth (**Figure 4B**). These results suggest that AZD8055 can also be applied to study TOR action in Physcomitrella, and may be best suited if a complete inhibition of the signalling pathway is required.

Whether with rapamycin or AZD8055, protonemata turned yellow under TOR inhibition (**Figure 4**), an effect seen in other photosynthetic organisms as well (Caldana et al. 2013; Upadhyaya and Rao 2019). We measured total chlorophyll contents in the Physcomitrella line overexpressing *PpFKBP12* before and after the addition of 10 µM rapamycin, and found a significant decline when compared to the control (**Figure 4C**). The same was observed when 5 µM AZD8055 was applied to WT protonema (**Figure 4C**). TOR is crucial for regulating chlorophyll synthesis, and chloroplast development and function (Couso et al. 2021; Liu and Xiong 2022; D'Alessandro et al. 2024). Light microscopy revealed that chloroplasts had shrunk to such extend that they were difficult to spot in some cells (**Figure 4D**), indicating that TOR inhibition affects shape and abundance of chloroplasts in Physcomitrella, which can explain the observed decrease in chlorophyll levels. This decline likely includes autophagy, as TOR is a

central regulator of autophagy in plant energy stress responses (Neufeld 2010; Feng et al. 2025).

Unexpectedly, we observed a progressive decline in chlorophyll content between day 0 and days 7/18 also in the controls, which were treated with DMSO (**Figure 4C**). This decline cannot be attributed to changes in chloroplast morphology or quantity in chloronema cells, the juvenile protonemal cells predominant at day 0. Instead, the differentiation of chloronema into caulonema, which are elongated cells with fewer chloroplasts (Reski and Cove 2004), likely explains the reduced chlorophyll levels. Consistent with this, caulonema formation increased remarkably by days 7 and 18 as compared to day 0 (**Supplementary Figure S2**).

In Chlamydomonas and Arabidopsis, TOR inhibition impacts chloroplast functions (Couso et al. 2021; D'Alessandro et al. 2024). This can be assessed by measuring the maximal efficiency of photosystem II (PSII), which reflects the photosynthetic activity of a plant and is not affected by variations in chlorophyll levels. To test whether chloroplast functions in Physcomitrella are affected by TOR inhibition, we measured chlorophyll fluorescence in protonema treated with rapamycin or AZD8055 and calculated the PSII maximum quantum yield (Fv/Fm). Treatment of protonema with rapamycin or AZD8055 resulted in a drop of the photosynthetic efficiency. In protonema of *OE PpFKBP12*, we measured an Fv/Fm of 0.763 ± 0.002 with 0.01% DMSO vs 0.667 ± 0.017 with 10 µM rapamycin after 3 days of treatment. With 5 µM AZD8055, WT protonema showed an Fv/Fm value of 0.591 ± 0.008 vs 0.766 ± 0.002 for those treated with 0.01% DMSO (**Figure 4E**).

Next, we investigated if Physcomitrella TOR also governs other cellular mechanisms such as protein homeostasis and cell division, as reported for other organisms (Liu and Xiong et al. 2022; Liu et al. 2025). We found that TOR inhibition led to a drop in cellular total soluble protein content (**Figure 4F**) and to delays in cell cycle progression (**Figure 4G**). The addition of rapamycin resulted in chloronema cells accumulating in the G1 phase of the cell cycle, similar to observations in yeast (Barbet et al. 1996), whereas under normal conditions, Physcomitrella chloronema is congregated at the G2/M transition (Schween et al. 2003). AZD8055 treatment of protonema did not result in the formation of a pronounced peak of cells arrested at G1. However, it substantially reduced the number of cells accumulating with duplicated DNA content and increased

the counted events with a fluorescence intensity below 200, thus suggesting cell cycle arrest (**Figure 4G**).

Collectively, we found that TOR signalling is crucial for regulating chlorophyll synthesis and chloroplast development and function, protein synthesis, and cell cycle progression in Physcomitrella, underscoring its evolutionary conserved function in plants.

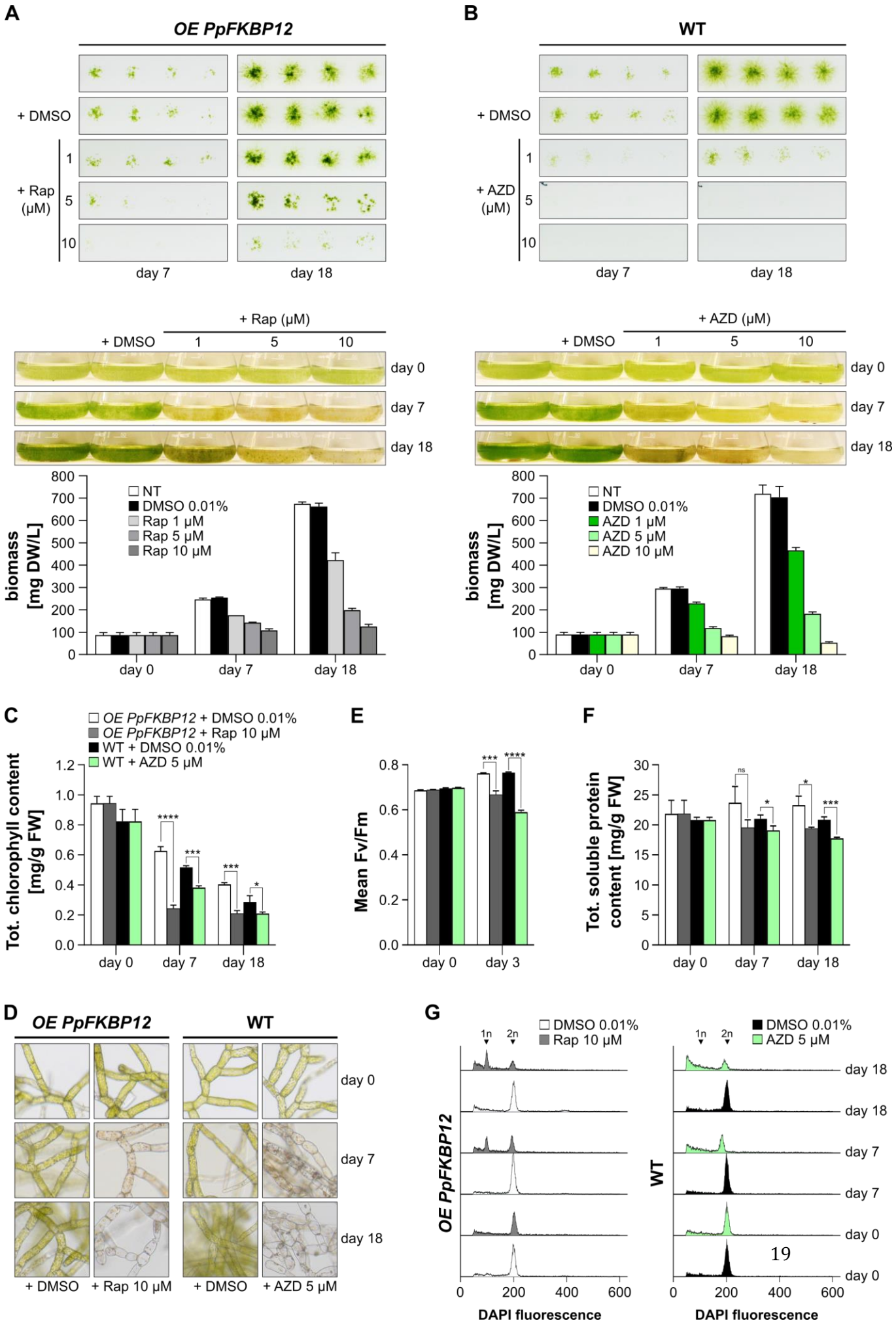
A
OE PpFKBP12
+ DMSO
+ Rap (µM)
1
5
10
day 7
day 18
B
WT
+ DMSO
+ AZD (µM)
1
5
10
day 7
day 18
+ Rap (µM)
+ DMSO
1
5
10
day 0
day 7
day 18
+ AZD (µM)
+ DMSO
1
5
10
day 0
day 7
day 18
biomass [mg DW/L]
NT
DMSO 0.01%
Rap 1 µM
Rap 5 µM
Rap 10 µM
AZD 1 µM
AZD 5 µM
AZD 10 µM
C
OE PpFKBP12 + DMSO 0.01%
OE PpFKBP12 + Rap 10 µM
WT + DMSO 0.01%
WT + AZD 5 µM
Tot. chlorophyll content [mg/g FW]
E
Mean Fv/Fm
day 3
F
Tot. soluble protein content [mg/g FW]
D
OE PpFKBP12
WT
+ DMSO
+ Rap 10 µM
+ AZD 5 µM
G
DMSO 0.01%
Rap 10 µM
AZD 5 µM
1n
2n
DAPI fluorescence

473

Fig. 4 TOR inhibition impacts Physcomitrella growth, induces chlorosis, inhibits photosynthesis, alters total protein content, and delays cell cycle progression.
A Same experiment as in Fig. 1, except that the ESPB003 line overexpressing *PpFKBP12* was analysed. **B** Same experiment as in Fig1, except that AZD8055 (AZD) instead of rapamycin was used. **C** Chlorophyll content determination in protonema under same growth conditions as in panels A and B at the indicated treatment concentrations. **D** Light microscopy images of protonema under same growth conditions as in panels A and B at the indicated treatment concentrations. **E** Photosynthetic activity measured in protonema under same growth conditions as in panels A and B at the indicated treatment concentrations. Same legend as in panel C. **F** Total protein content in protonema under same growth conditions as in panels A and B at the indicated treatment concentrations. Same legend as in panel C. **G** Histograms of flow cytometric analyses of DAPI stained isolated nuclei of protonema under same growth conditions as in panels A and B at the indicated treatment concentrations. The abscissa represents the channel numbers corresponding to the relative fluorescence intensities of analysed particles (liner mode), while the ordinate indicates the number of counted events (~5000 counts). 1n and 2n refer to DNA content. Significance levels (*$p < 0.05$, **$p < 0.01$, and ***$p < 0.001$, and ****$p < 0.0001$) are based on multiple unpaired t-tests, each performed on data from three independent biological replicates.

Physcomitrella encodes TOR, LST8 and RAPTOR

In yeast and mammals, the TOR kinase operates in distinct cellular complexes with different functions, namely TORC1 and TORC2. Therefore, our next step was to determine whether the main protein components of these complexes exist in Physcomitrella and whether they have maintained conserved functions. Using the Arabidopsis peptide sequences of TOR, LST8-1, and RAPTOR1 as queries, a BLASTP analysis revealed the presence of single genes in the Physcomitrella genome that code for putative homologs of AtTOR and AtLST8-1, whereas four different putative PpRAPTOR proteins are encoded. These genes are *Pp3c6_4910* and *Pp3c11_25160* for PpTOR and PpLST8*,* respectively. Those encoding the PpRAPTOR proteins are *Pp3c9_4770*, *Pp3c25_7220*, *Pp3c17_3950* and *Pp3c15_3360* (hereafter referred to *PpRAPTOR1*, *PpRAPTOR2, PpRAPTOR3, and PpRAPTOR4*, respectively). A structural domain analysis reveals the presence of all known functional domains within these proteins (**Figure 5A**). Publicly available transcription data indicates that they are expressed at low to moderate levels similar to FKBP12 across all tissue types (**Supplementary Figure S1**). Whereas Arabidopsis

and Physcomitrella encode one *TOR* gene each, Physcomitrella encodes one *LST8* gene and Arabidopsis two. The difference is more pronounced with the *RAPTOR* genes, of which Arabidopsis encodes two and Physcomitrella four. This expansion indicates neofunctionalisation of the *RAPTOR* genes in Physcomitrella.

For a functional analysis, we tested whether the moss genes could substitute their yeast homologs in promoting yeast cell growth. In yeast, *TOR*, *LST8* and *RAPTOR* are essential genes (Loewith et al. 2002). Therefore, we used three well-described yeast strains in which the expression of the respective genes could be shut down by shifting the cells from galactose to glucose. Those strains are SW137-4b, RL57-2d, and RL93a (Loewith et al. 2002; Wullschleger et al. 2005; Díaz-Troya et al. 2008). *S. cerevisiae* has two *TOR* genes, *TOR1* and *TOR2*. TORC1 contains either of them, but *TOR2* is exclusive for TORC2. However, the formation of both complexes is essential for the viability of yeast cells. Therefore, SW137-4b lacks *TOR1* and expresses *TOR2* from the galactose-inducible GAL1 promoter. As for RL57-2d and RL93a, *LST8* and *RAPTOR* were placed under the GAL1 promoter, respectively. We introduced plasmids expressing the respective Physcomitrella full-length cDNA under the strong and constitutive GPD (Glyceraldehyde-3-Phosphate Dehydrogenase) promoter into these yeast strains and analysed their growth on synthetic minimal plates, containing either galactose or glucose as the carbon source. A WT TB50a yeast strain and mutants containing empty vectors served as positive and negative controls, respectively, for growth on plates with glucose.

Surprisingly, only PpLST8 could complement its respective yeast mutant (**Figure 5B**, **Supplementary Figure S3**), revealing that PpLST8 is a functional homolog of ScLST8. This also indicates that PpLST8 can bind ScTOR and ScRAPTOR to form a complex in yeast. In contrast, none of the four Physcomitrella RAPTORs could substitute for its yeast homolog. This is not due to the use of an incorrect strain, since the introduction of a plasmid expressing ScRAPTOR restored yeast growth in the presence of glucose (**Supplementary Figure S3**). Likewise, PpTOR could not complement its yeast homolog. Here, the low degree of conservation of the HEAT and FAT domains with 23% and 28% sequence identity, respectively (**Figure 5A**), could result in improper assembly, function, and localization of ScTORC. This hypothesis is supported by the findings that rice TOR (OsTOR) could not rescue yeast *tor* mutants either, but a chimeric TOR protein with the yeast HEAT and FAT domains and the rest

from OsTOR could (Maegawa et al. 2025). In yeast, RAPTOR interacts with its C-terminal WD40 domains with the HEAT repeats of TOR, whereas its N-terminus is positioned next to the TOR kinase domain, likely bringing substrates into the vicinity of the catalytic region (Adami et al. 2007). Because the WD40 domains of ScRAPTOR and PpRAPTOR1 share 46% of sequence identity, and the HEAT repeats share only 16% of sequence identity (**Figure 5A**), it is likely that the domains of PpRAPTOR1 are not conserved enough to allow biogenesis of ScTORC1. So far, only OsRAPTOR2 has been able to support growth of a thermosensitive yeast *raptor* mutant (Maegawa et al. 2025). This assay was conducted at 37°C, a temperature that could strengthen the interaction between OsRAPTOR2 and ScTOR, which under normal growth conditions is very weak, if not absent. We did not find homologs of key TORC2 proteins, such as RICTOR and mSIN1, in Physcomitrella, which is in line with the findings in other photosynthetic organisms.

In summary, Physcomitrella LST8 is functionally conserved and complements its yeast homolog, whereas neither Physcomitrella TOR nor its four RAPTOR proteins rescued the respective yeast mutants. Despite conserved domain architectures, critical sequences or structural divergences, particularly in regions mediating protein-protein interactions, may prevent proper assembly and function of TORC1 in yeast. Further experiments like the one conducted with yeast/rice chimeric TOR could confirm this.

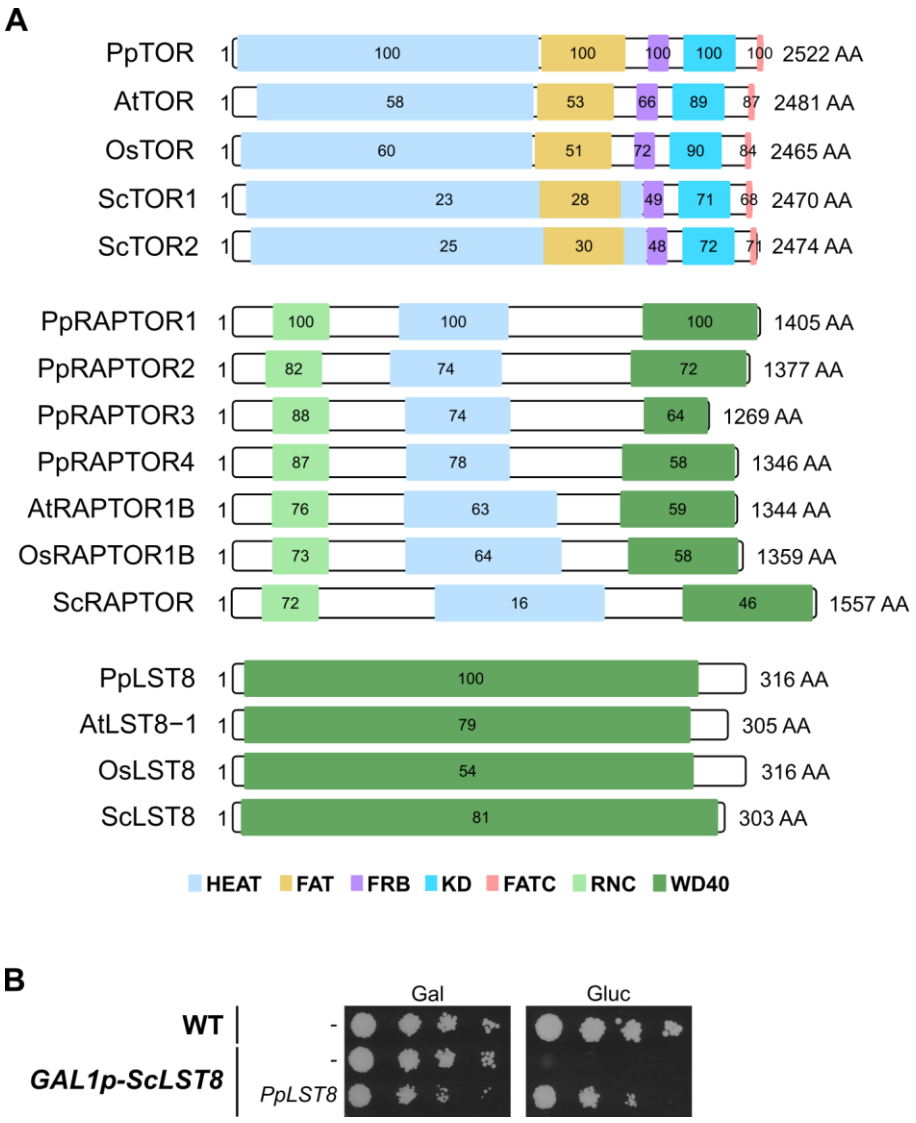

Fig. 5 TOR, LST8 and RAPTOR are conserved in Physcomitrella.
A Conserved protein domains of PpTOR, PpLST8, or the four PpRAPTOR paralogs with homologs from *A. thaliana* (At), *O. sativa* (Os), *S. cerevisiae* (Sc). Values in domain boxes indicate percentage of shared identity with the respective homologous Physcomitrella domain. **B** Complementation of a yeast *lst8* mutant with the Physcomitrella *LST8* cDNA. Wild-type TB50a yeast strain and mutant RL57-2d expressing *ScLST8* from the galactose-inducible GAL1 promoter were initially grown as suspensions in rich medium containing galactose as a carbon source (YPGal). Strains were transformed with pESPB019 (empty vector) or pESPB020 (pESPB019-derived vector expressing *PpLST8*) and selected on SGal-Leu plates. Selected transformants were grown for 6 h at 30°C in SD-Leu suspension cultures. Cultures were normalized to an OD (660 nm) of 0.2, subjected to 10-fold serial dilutions, and 15 µL of each dilution were spotted onto SGal-Leu or SD-Leu plates, which were incubated at 30°C for 5 days. Plates were scanned upside down with the lid open on a Canon CanoScan 9000F scanner.

Downregulation of TOR, LST8 or RAPTOR delays development

Next, we investigated whether a reduced expression of PpTORC1 subunit genes impacts not only Physcomitrella growth, but also its development. Specifically, we evaluated whether TOR activity influences the developmental transition from two-dimensional (2D) to three-dimensional (3D) growth in Physcomitrella, also known as budding (Reski and Abel 1985). The 2D to 3D transition is a key developmental innovation of land plants (Weeks et al. 2025). To investigate this, WT protonemal tissue derived from suspension culture was transferred onto solid Knop ME media supplemented with either 0.02% glucose or 1 µM AZD8055 as described in Hoernstein et al. (2023). Plates without any supplementation served as controls. The formation of leafy gametophores was subsequently monitored over time. In the presence of 1 µM AZD8055, gametophore development was markedly suppressed throughout the observation period. In contrast, the number of gametophores began to increase noticeably from day 12 onwards in the control condition, with an even more pronounced promotion observed on plates containing 0.02% glucose (**Figure 6A**). The same effect was observed when employing 1% sucrose instead of 0.02% glucose (**Supplementary Figure S4**). This demonstrates that inhibition of TOR activity in Physcomitrella not only impairs growth (**Figure 4**) but also development (**Figure 6A**). Conversely, supplementation with glucose or sucrose, which are known to promote TOR activity in plants and mammals, promotes developmental progression in Physcomitrella. Likewise, sugar availability affects developmental progression in Physcomitrella via cyclin D (Lorenz et al. 2003), suggesting a feedback loop between nutrients, TOR activity, cyclin D expression, and the cell cycle in moss.

Next, we generated Physcomitrella mutants with estradiol-inducible RNA interference (RNAi), targeting transcripts of individual genes encoding PpTORC1 subunits. This inducible approach was chosen to avoid experimental difficulties associated with the essential nature of these genes, as reported for other organisms (Loewith et al. 2002; Menand et al. 2002; Deprost et al. 2005; Moreau et al. 2012). Additionally, by designing the RNAi construct to target conserved regions, it is possible to attenuate the four PpRAPTOR paralogs simultaneously.

The screen of 60 hygromycin-resistant clones on solid Knop ME plates containing estradiol led to the identification of at least one transgenic line for each of the RNAi construct, that showed an altered developmental phenotype, reflected by the reduced

number and size of the gametophores (**Figure 6B**). One particular line, *Pptor-RNAi-65'-27*, which expresses an RNAi construct targeting the 500-bp coding region (561-1060) of *PpTOR*, equivalent to the one used to generate the Arabidopsis estradiol-inducible *tor* RNAi lines (Xiong and Sheen 2012), did not develop any gametophores on the estradiol-containing plate, whereas only few were spotted on the control plate containing DMSO (**Figure 6B**). This altered differentiation of the *Pptor-RNAi-65'-27* line observed in the absence of estradiol could be due to leakage in the estradiol-inducible RNAi system, as such issues have been reported previously (Nakaoka et al. 2012). Off-target effects could also account for this phenotype. However, we sought to reduce this likelihood by isolating distinct RNAi mutant lines for each gene, where in each line a different region within the transcript sequence is being targeted. We observed consistent phenotypes between these lines (**Figure 6B**), indicating that the developmental phenotypes observed here result from the knock-down of these genes.

It is well documented that organisms with low TOR signalling, including plants, are generally more susceptible to TOR inhibitors, such as rapamycin and AZD8055, at low concentrations (Montané et al. 2013; Jordan et al. 2014; Saliba et al. 2018). This increased sensitivity facilitates screens for mutants with reduced TOR activity. Since the Physcomitrella lines exhibited slightly altered differentiation under control conditions, we grew them on plates containing 1 µM AZD8055, which still allows growth (**Figure 4B**). If the RNAi systems in these lines are leaky, one would expect them to develop fewer gametophores than WT, which was the case (**Figure 6B**). Remarkably, the *Pptor-RNAi-65'-27* line barely grew. The altered differentiation of the other lines was more evident when quantified by counting gametophores. With line *Ppraptors-RNAi-69'-14* being the only exception, the presence of AZD8055 reduced the number of gametophores per colony (WT 8.45 ± 2.83, *Pplst8-RNAi-61'-40* 1.25 ± 1.09, *Pplst8-RNAi-63'-38* 2.00 ± 1.22, *Pptor-RNAi-65'-27* 0.00 ± 0.00, *Pptor-RNAi-67'-17* 2.25 ± 0.83, *Ppraptors-RNAi-69'-14* 4.25 ± 1.92, and *Ppraptors-RNAi-71'-25* 3.50 ± 1.12, **Figure 6C**), suggesting a reduced TOR signalling in these transgenics, most likely because of RNAi leakage. Addition of estradiol to the AZD8055-containing plates further reduced the number of gametophores in the majority of the analysed colonies, indicating that the estradiol-inducible RNAi systems in these lines were triggered further (**Figure 6C**). Together, the knockdown of *PpTORC1* subunit genes reduces the number of gametophores per colony, highlighting the importance of TOR signalling

for developmental progression in Physcomitrella, which is in line with our observations under TOR activity inhibiting conditions.

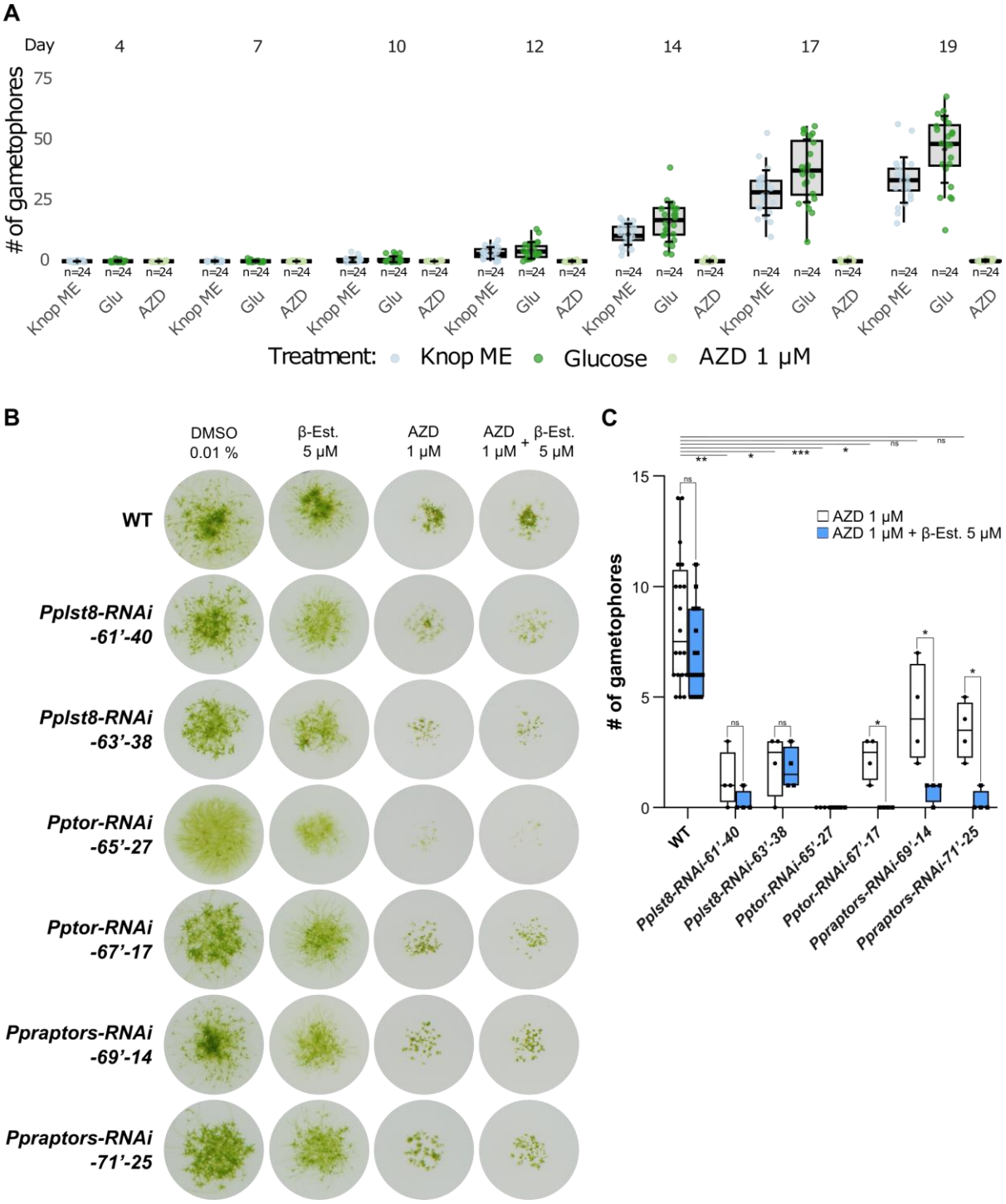

Fig. 6 Downregulation of TOR, LST8 or RAPTOR alters Physcomitrella growth.
A Box plot showing the number of gametophores per colony, counted after transferring 25-day-old WT protonema on Knop ME agar plates, or plates supplemented with 0.02% glucose or 1 µM AZD8055 (n = 24). Data are represented as mean +-SD. 15 µL droplets at a density

of 440 mg DW/L were spotted. **B** Weekly sub-cultured protonema in suspension of Wild-type, ESPB020 (*Pplst8-RNAi-61'-40*), ESPB024 (*Pplst8-RNAi-63'-38*), ESPB027 (*Pptor-RNAi-65'-27*), ESPB032 (*Pptor-RNAi-67'-17*), ESPB035 (*Ppraptors-RNAi-69'-14*), and ESPB040 (*Ppraptors-RNAi-71'-25*) lines were prepared at a density of 100 mg DW/L in Knop ME pH 5.8. One-fold serial dilutions were conducted and 50 µL were spotted on solid Knop ME pH 5.8 plates supplemented with 0.01% DMSO, 5 µM β-Estradiol (β-Est.), 1 µM AZD8055, or with 5 µM β-Estradiol and 1 µM AZD8055. Plates were photographed at week 4 of incubation under 70 µmol photons m^{-2} s^{-1} at 22 °C in a 16 h/8 h light/dark cycle. **C** Box plot showing the number of gametophores per colony of the indicated lines, 4 weeks after incubation on solid Knop ME pH 5.8 plates supplemented with 1 µM AZD8055, or, with 5 µM β-Estradiol and 1 µM AZD8055. Counting was performed on 19 wild-type colonies, and on 4 colonies of each of the transgenic lines. The box plots depict the mean (horizontal line within the box) of the data, the interquartile range (box), and the 1.5x interquartile range (whiskers). The significance level (*$p < 0.05$, **$p < 0.01$, and ***$p < 0.001$, and ****$p < 0.0001$) between the AZD8055-treated WT line and each of the AZD8055-treated RNAi lines is based on a one-way ANOVA followed by a post hoc multiple comparison test against the WT group. A multiple unpaired t-tests, with correction for multiple comparisons using the False Discovery Rate (FDR) method set at 0.05, was used to determine statistical significance (*$p < 0.05$, **$p < 0.01$, and ***$p < 0.001$, and ****$p < 0.0001$) between AZD8055 and AZD8055 + β-Estradiol-treated samples.

TOR-dependent phosphorylation of RPS6 on Ser241

In response to environmental cues, TOR triggers cellular processes through phosphorylation of several downstream effector proteins. The phosphorylation sites within these effectors serve as markers of TOR activity in various species, typically by generating antibodies specific to the phosphorylated form and detecting them in Western blots (Xiong and Sheen 2012; Dobrenel et al. 2016; Saliba et al. 2018). This is an effective tool to investigate TOR signalling at the cellular level. We aimed to develop this approach for Physcomitrella.

Using an antibody against phosphorylated Thr389 in HsS6K1, which also recognizes phosphorylated Thr449 and Thr455 in Arabidopsis S6K1 and S6K2, respectively (Xiong and Sheen 2012), our attempts to detect phosphorylated ribosomal S6 kinases in Physcomitrella were not successful. Most likely, this is due to their low abundance rather than a lack of conservation of the TOR phosphorylation motif FLGFTYVAP in human S6K1 (**Supplementary Figure S5**). This hypothesis is consistent with findings in Arabidopsis, where successful detection with this antibody often requires transgenic plants overexpressing AtS6K1 (Xiong and Sheen 2012; Primo et al. 2022). We therefore shifted to assaying the phosphorylation of RPS6, which is phosphorylated by S6K in a TOR-dependent manner. In Physcomitrella, four *RPS6* genes exist and their expression levels are up to 5-fold higher than those of S6K (**Supplementary**

Figure S6). Despite the overall high sequence identity of the Physcomitrella RPS6 isoforms with RPS6A from Arabidopsis (**Figure 7A**), the sequence window around the known phosphorylation site of AtRPS6A (SRLSSAAAKPSVTA; Dobrenel et al. 2016) is far less conserved (**Figure 7B**). Consequently, the commercially available antibody against phosphorylated Ser240 in AtRPS6A could not be used (Agrisera, personal communication).

Therefore, we aimed to establish a mass spectrometry-based assay to determine which residues in PpRPS6 undergo phosphorylation in a TOR-dependent manner. Whereas in Arabidopsis two consecutive serines (Ser240 and Ser241) exist, Physcomitrella RPS6 proteins have only a single serine residue (Ser241). We collected protonema from suspensions treated with 10 µM AZD8055 for 60 min, alongside DMSO-treated controls, enriched phospho-peptides by Ti-NTA affinity chromatography and identified the enriched phospho-peptides by LC-MS/MS in data-independent acquisition (DIA) mode. We identified peptides spanning the potential phosphorylation site of interest (around Ser241) for all four PpRPS6 proteins. Among those peptides, Ser241 was identified to be phosphorylated in all four isoforms. Two additional phosphorylation sites were detected, namely Ser238 and Ser248, whereas Ser248 was only found in PpRPS6_1 and PpRPS6_4 (**Figure 7C**). Of those three sites, only phosphorylation of Ser241 showed a significant decrease after 60 min treatment with AZD8055. This effect was observed in the three isoforms PpRPS6_2, PpRPS6_3, and PpRPS6_4. Although a similar trend was noted for PpRPS6_1, the number of data points was insufficient for statistical analysis in this isoform (**Figure 7C**).

Taken together, Physcomitrella TOR, likely acting through ribosomal S6 kinases, mediates PpRPS6 phosphorylation at Ser241. This finding reveals that another key component of the TOR signalling pathway, well characterized in other eukaryotes, is conserved in Physcomitrella.

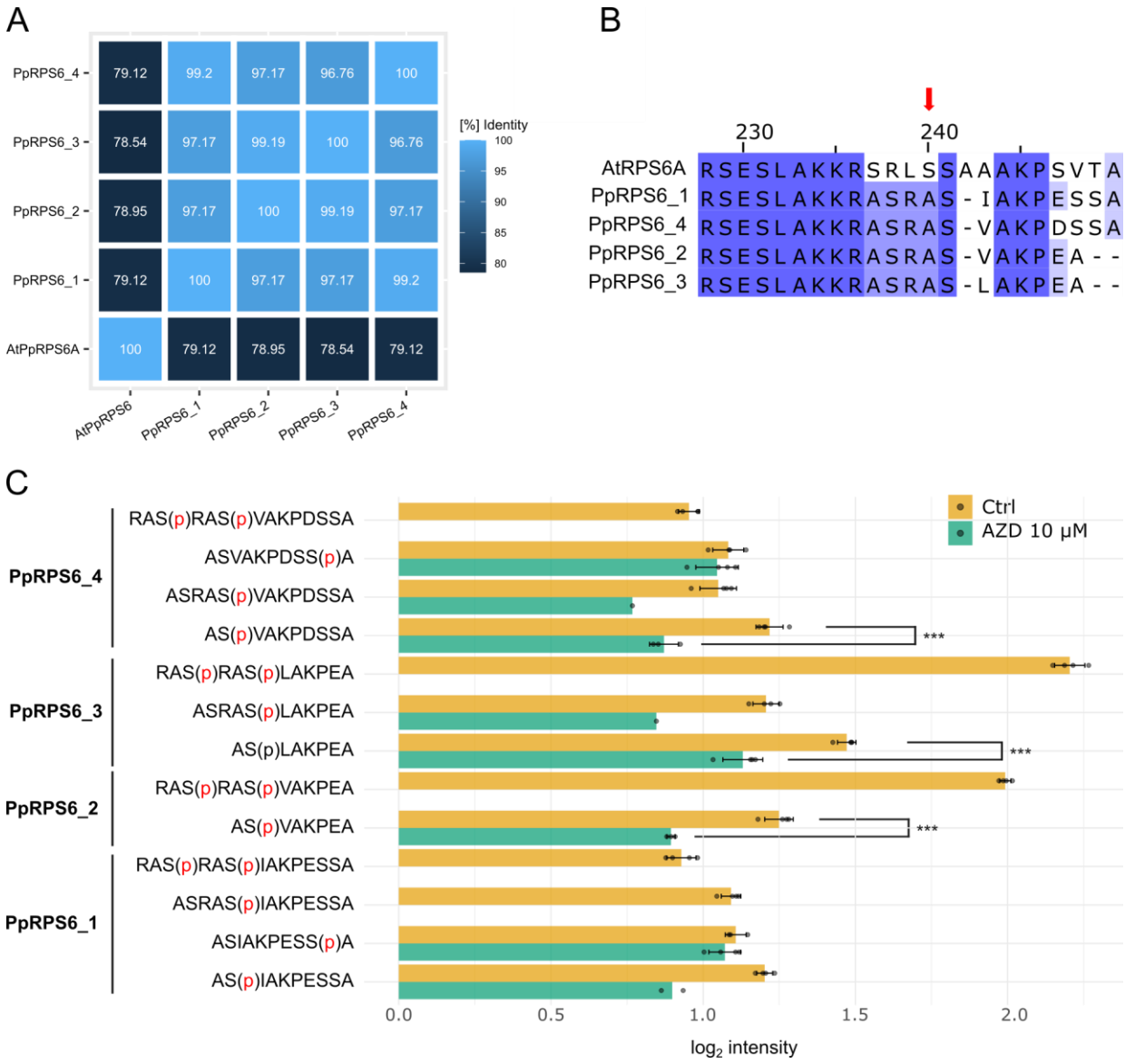

Fig. 7 Sequence identity between Physcomitrella and Arabidopsis RPS6 isoforms and analysis of TOR-dependent phosphorylation of Physcomitrella RPS6.
A Percentage identity matrix of Physcomitrella RPS6 isoforms (PpRPS6_1: Pp3c11_21120V3.1; PpRPS6_2: Pp3c15_25430V3.1; PpRPS6_3: Pp3c15_25780V3.1; PpRPS6_4: Pp3c7_5780V3.1) with Arabidopsis AtRPS6A (AT4G31700.1). Sequences were aligned using *Clustal Omega* (V2.1, Sievers and Higgins 2018) on UNIPROT (https://www.uniprot.org/align). **B** Section of a multiple sequence alignment of Physcomitrella RPS6 isoforms with Arabidopsis AtRPS6A. Sequences were aligned in *Jalview* (2.11.4.1, Waterhouse et al. 2009) using *Mafft* with defaults (Katoh and Standley 2013). Serine 240 in AtRPS6A that is phosphorylated in a TOR-dependent manner is indicated with a red arrow. **C** Phosphorylation level of the Physcomitrella RPS6 C-terminal peptides following the addition of AZD8055 for 60 min. Bars represent mean median normalized intensity values with standard deviation. Each datapoint represents the summed intensity for a peptide per replicate (including different charge states). Significance levels (***p<0.001) are based on a Welch test. The Welch test was only calculated for peptides with at least three data points (biological replicates).

Discussion

The signalling hub TOR is studied in algae and flowering plants, yet its role in non-vascular plants remained less clear. Here, we present evidence of TOR signalling in the non-vascular moss plant Physcomitrella. In yeast and animals, TOR signalling is inhibited by rapamycin, a macrolide antibiotic that played a pivotal role in the discovery of this pathway (Heitman et al. 1991a). Due to the essential nature of the *TOR* gene, rapamycin sensitivity has been key for dissecting TOR function in these organisms. However, assessing this in photosynthetic organisms has been challenging, as most of them are resistant to rapamycin. This has been attributed to an FKBP12 protein lacking critical amino acids needed to form an effective ternary complex with rapamycin and TOR, a low cellular abundance of FKBP12, or a combination of both. Similar to other plants, we found that Physcomitrella is not sensitive to rapamycin, primarily due to low expression of the *PpFKBP12* gene. By generating a transgenic line overexpressing PpFKBP12, we demonstrated that rapamycin treatment delays protonemal growth and differentiation, induces chlorosis, inhibits photosynthesis, reduces total protein content, and delays cell cycle progression. These phenotypic and physiological changes were similarly induced by treatment with the ATP-competitive TOR inhibitor AZD8055. While no TORC2-specific components such as RICTOR or SIN1 are encoded by the moss genome, we identified and functionally characterised key TORC1 components, including LST8, RAPTOR, and the downstream target RPS6, which undergoes TOR-dependent phosphorylation at Ser241. These findings reveal that the evolutionary conserved TORC1 pathway is present and functional in Physcomitrella. We infer TOR engagement from convergent pharmacological responses and the decrease in RPS6 Ser241 phosphorylation, recognizing that moss-specific inhibitor specificity remains to be formally validated.

Although overexpression of *PpFKBP12* rendered Physcomitrella sensitive to rapamycin, the yeast complementation assay of the *Scfkbp12Δ* mutant indicated that the sequence of PpFKBP12 is not optimal for full interaction with the drug. Whereas the W40D substitution resulted in a loss-of-function mutant, all other aa changes within the rapamycin-binding pocket aimed at getting a human- or yeast-like PpFKBP12 variant, resulted in proteins that complemented the *Scfkbp12Δ* strain better than WT PpFKBP12. One mutant, PpFKBP12^{C26Y}, exhibited an ScFKBP12-like function

capacity. The presence of a tyrosine instead of a cysteine at position 26 in PpFKBP12 appeared to be important for efficient rapamycin binding as it reversed the phenotype of the W40D substitution. What could be the reason behind these observations? Unique to land plant FKBP12 proteins are two cysteines at fixed positions (Cys26 and Cys80), reported to be spatially adjacent to potentially form disulphide linkage (Xu et al. 1998), whereas homologues from other organisms contain no or only one cysteine at variable positions. Even though the reduction of this disulphide bridge was shown to decrease the affinity of *Vicia faba* FKBP12 towards its ligands *in vitro* (Xu et al. 1998), it is possible that disruption of this bridge could lead to an increased affinity of FKBP12 *in vivo*. Our complementation assay of the *Scfkbp12Δ* mutant with PpFKBP12^{C80I} indicate that this is the case, at least in PpFKBP12. PpFKBP12^{C80I} was as efficient as PpFKBP12^{C26Y} in inhibiting yeast growth in the presence of rapamycin. However, the effects of these two mutations in Arabidopsis FKBP12 could not be replicated, as only AtFKBP12^{C26Y} showed a slightly increased affinity to rapamycin. This contingency could be due to differences in the aa sequences between PpFKBP12 and AtFFKBP12, which might mask the expected phenotype. Therefore, further experiments are needed to validate the above hypothesis. For instance, by combining the C26Y or C80I substitutions in AtFKBP12 with other aa changes within the rapamycin-binding domain to make AtFKBP12 more yeast-, human-, or Physcomitrella-like. Or, to check whether the introduction of these substitutions in other plant FKBP12 sequences could enhance their affinity to rapamycin. In contrast to Chlamydomonas FKBP12, which has no cysteines in its protein sequence, FKBP12 proteins from *Cyanidioschyzon merolae* and *Auxenochlorella pyrenoidosa* have one cysteine homologous to C80 in land plant FKBP12, and additional cysteines in their extra regions at their N-terminus. These extra regions are believed to prohibit rapamycin binding (Zhu et al. 2022). Therefore, one could test if the deletion of these extra regions could make these two algal species sensitive to the drug. It would also be interesting to test whether other bryophyte species are sensitive to rapamycin. These plants express an FKBP12 protein. Intriguingly, the FKBP12 protein sequences of the three mosses *Takakia lepidozioides*, *Calohypnum plumiforme*, and *Sphagnum magellanicum* contain a glutamine at position 58, equivalent to the one in ScFKBP12. Since we showed that introducing this glutamine in PpFKBP12 enhances its affinity to rapamycin, it is reasonable to consider that FKBP12 proteins from these species may have a higher affinity to the inhibitor, than the native Physcomitrella FKBP12 has.

The proteins TOR, LST8, and RAPTOR are the main subunits of TORC1 (Loewith et al. 2002). In Chlamydomonas and Arabidopsis, TOR interacts with LST8 *in vitro* and *in vivo* (Díaz-Troya et al. 2008; Moreau et al. 2012). Here, we show that Physcomitrella LST8 substitutes ScLST8 to allow yeast growth, indicating that PpLST8 can be integrated in the yeast TOR complex. It remains to be determined that the above proteins interact with each other in Physcomitrella. Our ESPB003 line that overexpresses PpFKBP12 is highly suited for such an analysis. In fact, in this line, the PpFKBP12 protein is fused at its C-terminus to cMyc, which did not impair its function and could be used to detect the protein in Western blots. Since rapamycin bridges FKBP12 and TOR together, one could use this condition to immunoprecipitate PpFKBP12-cMyc using anti-cMyc magnetic beads, and the subsequent detection of the interacting proteins via Western-blot or LC-MS. However, it should be considered to perform this immunoprecipitation *in vitro* and in the presence of a cross-linker to facilitate protein interactions, as described for Chlamydomonas (Díaz-Troya et al. 2008).

In Arabidopsis, TOR plays an essential role throughout all stages of development (Liu et al. 2025). Our results with rapamycin and AZD8055 reveal that Physcomitrella TOR not only controls protonema growth but is also required for developmental progression to gametophores. The Physcomitrella life cycle starts with spores that germinate into protonema, composed of chloronema and caulonema cells. From the protonema, buds develop into leaf-like gametophores bearing male and female sex organs and having root-like structures, called rhizoids. After fertilization, the zygote grows into a sporophyte consisting of a foot, stalk, and capsule, wherein meiosis produces new haploid spores to continue the life cycle (Lueth and Reski 2023). It would be interesting to investigate whether TOR also regulates other developmental stages of Physcomitrella, beyond protonema growth and gametophore formation, especially sexual reproduction (Lüth et al. 2023). The induction by estradiol of the RNAi systems to target PpTORC1 subunit transcripts also affected gametophore formation. However, we had anticipated a more pronounced phenotype, based on observations in Arabidopsis, where a similar system was used (Xiong and Sheen 2012). To our knowledge, the estradiol-inducible RNAi system to downregulate essential genes in Physcomitrella has been predominantly assessed in terms of cell division and viability (Kubo et al. 2013; Kubo et al. 2019). Therefore, comparative data are lacking to place

our results into context. In addition, the tendency of the expression cassettes to leak has complicated the selection process. Therefore, additional clones will need to be analysed in order to identify the most suitable lines.

In vascular plants, TOR activity is modulated by diverse environmental cues such as nutrients, energy, light, hormones, biotic and abiotic stresses. This is mediated through well characterized upstream regulators as sensors of these variations (Saliba et al. 2021; Primo et al. 2022; Liu et al. 2025). The downstream effectors through which TOR transduces these signals are also well defined (Liu et al. 2025). Such knowledge was missing for non-vascular plants. In the present study, we identified Physcomitrella S6K and RPS6, and showed via LC-MS/MS that AZD8055 impacts PpRPS6 phosphorylation on serine 241. Given that the Physcomitrella genome is sequenced and well annotated (Lang et al. 2018), identification of additional TOR pathway components should be feasible. Future large-scale phosphoproteomic or other omics studies employing TOR inhibitors, together with genetic and biochemical approaches, will broaden our understanding of the various components of the TOR signalling pathway in this species. The identification of PpRPS6 phosphorylation at Ser241 in a TOR-dependent manner provides a valuable molecular marker that could be used to develop a sensitive Western blot assay of TOR activity using antibodies raised against phosphorylated Ser241 (Dobrenel et al. 2016). Once established, this assay could be used to determine whether Physcomitrella TOR activity responds to the environmental cues described above. As this moss can be grown in large quantities in bioreactors under highly standardized conditions (Decker and Reski 2004), testing the effects of different environmental parameters is quite straightforward.

Conclusion

This study closes the knowledge gap about TOR signalling in non-vascular plants, such as mosses. We found a remarkable evolutionary conservation of key components, as well as specific differences, such as the expansion of the *RAPTOR* genes in Physcomitrella compared to Arabidopsis. Such a gene expansion suggests neofunctionalization of its proteins and indicates differences in signal integration for environmental cues between vascular and non-vascular plants, especially as RAPTOR proteins are regulatory proteins of the TOR complex. Based on sequences

analyses, we suggest that other moss species, such as the living fossil *Takakia* may have an enhanced sensitivity to rapamycin, underscoring the necessity for analysing a phylogenetically divers set of plant species. The tools established here will help to further dissect TOR signalling in Physcomitrella in order to elucidate signalling integration via TORC1 in plants.

Materials and methods

Plant material, culture conditions, and dry weight measurement

Physcomitrella WT (new species name: *Physcomitrium patens* (Hedw.) Mitt.; Medina et al. 2019), ecotype "Gransden 2004" (IMSC accession number 41269) and its derivative transgenic lines were cultivated in Knop medium (pH 5.8) supplemented with microelements (ME) as described previously (Frank et al. 2005; Horst et al. 2016). For cultivation on solid medium, 12 g/L agar was added to the Knop ME preparation. Unless noted otherwise, Physcomitrella was grown under standard light conditions (70 µmol photons m^{-2} s^{-1}) at 22 °C in a 16 h/8 h light/dark cycle. For stock suspension cultures, moss tissues were grown in 500 mL Erlenmeyer flasks containing 180 mL of Knop ME (pH 5.8). Tissues were disrupted weekly with an ULTRA-TURRAX (IKA, Staufen, Germany) at 18,000 rpm for 60 s to maintain them as protonema. All suspension cultures were subjected to shaking at a speed of 125 rpm. Axenity of the cultures were monitored according to Heck et al. (2021). For dry weight (DW) measurement, 10-25 mL of tissue suspension were vacuum-filtered, dried for 2 h at 105 °C, and then weighed. All measurements were conducted on at least two to three biological replicates. All photos showing Physcomitrella plants on plates or in flasks were taken with either a Canon EOS 400D or Canon EOS 2000D.

Yeast complementation

Coding sequences were amplified from either yeast genomic DNA or Physcomitrella cDNA and cloned into linearized plasmids (p415 GAL1 or pRL614) using Gibson assembly (Gibson et al. 2009). Point mutations were introduced into *PpFKBP12* (systematic number *Pp3c1_27870*) by site-directed mutagenesis using PCR with synthesized mutagenic primers. The primers were designed to contain the desired nucleotide substitution near the centre of the sequence (all primer sequences are listed in **Supplementary Table S1**). PCR amplification was performed using

Phusion™ Plus DNA Polymerase (Thermo Fisher Scientific, Waltham, USA) with plasmids containing *PpFKBP12* (pESPB003) or *PpFKBP12*$^{C26Y\text{-}W40D}$ (pESPB010) as DNA templates. All generated plasmids were verified by sequencing and are listed in **Table 1**. Yeast strains used in this study were obtained from the laboratory of M.N. Hall (Biozentrum, University of Basel, Switzerland) and are listed in **Table 2**. Plasmids were introduced into yeast cells by transformation using the lithium acetate method (Gietz et al. 1992). Detailed growth conditions for yeast strains are provided in the Figure legends. SD-Leu refers to yeast synthetic dextrose (SD) medium, and SGal-Leu to yeast synthetic galactose (SGal), both of them lacking leucine. Unless otherwise indicated, uracil, tryptophan, and histidine were added to the synthetic media to complement the yeast auxotrophies.

Table 1. Plasmids used in this study for experiments in yeast

Plasmid	IMSC accession #	Description	Reference
p415 GAL1		YCp-GAL1p (LEU2)	Gift from Barbara Di Ventura
pESPB001	2078	YCp-GAL1p-ScFKBP12 (LEU2)	This study
pESPB003	2080	YCp-GAL1p-Pp3c1_27870/PpFKBP12 (LEU2)	This study
pESPB006	2083	YCp-GAL1p-PpFKBP12-C26Y (LEU2)	This study
pESPB008	2084	YCp-GAL1p-PpFKBP12-W40D (LEU2)	This study
pESPB010	2085	YCp-GAL1p-PpFKBP12-C26Y-W40D (LEU2)	This study
pESPB012	2086	YCp-GAL1p-PpFKBP12-M56V-R58Q (LEU2)	This study
pESPB014	2087	YCp-GAL1p-PpFKBP12-M56K-G57Q-R58E (LEU2)	This study
pESPB016	2089	YCp-GAL1p-PpFKBP12-C26Y-W40D-M56V-R58Q (LEU2)	This study
pESPB018	2090	YCp-GAL1p-PpFKBP12-C26Y-W40D-M56K-G57Q-R58E (LEU2)	This study
pRL614		YEp-GPDp-GST-ALY2-CYC1t (LEU2)	Gift from Riko Hatakeyama
pESPB019	2105	YEp-GPDp-SpeI-XhoI-CYC1t (LEU2)	This study
pESPB020	2106	YEp-GPDp-Pp3c11_25160/PpLST8-CYC1t (LEU2)	This study
pESPB022	2118	YEp-GPDp-Pp3c6_4910/PpTOR-CYC1t (LEU2)	This study

pESPB024	2126	YEp-GPDp-Pp3c9_4770/PpRAPTOR1-CYC1t (LEU2)	This study
pESPB026	2127	YEp-GPDp-Pp3c25_7220/PpRAPTOR2-CYC1t (LEU2)	This study
pESPB029	2129	YEp-GPDp-Pp3c17_3950/PpRAPTOR3-CYC1t (LEU2)	This study
pESPB032	2132	YEp-GPDp-Pp3c15_3360/PpRAPTOR4-CYC1t (LEU2)	This study
pCHD001		YCp-ScKOG1/ScRAPTOR (LEU2)	Gift from Bruno André

Table 2. Yeast strains used in this study

Strain	Genotype
MH272-3c	MATa *leu2-3,112 ura3-52 rme1 trp1 his3*
MH274-1a	MATa *fpr1/fkbp12::URA3 leu2-3,112 ura3-52 rme1 trp1 his3*
TB50a	MATa *leu2-3,112 ura3-52 rme1 trp1 his3*
SW137-4b	MATa *[HIS3MX6]-GAL1-pTOR2 tor1::[kanMX4] LST8-13myc-[kanMX4] leu2-3,112 ura3-52 rme1 trp1 his3*
RL57-2d	MATa *[kanMX4]-GAL1p-LST8 leu2-3,112 ura3-52 rme1 trp1 his3*
RL93a	MATa *[kanMX4]-GAL1p-KOG1/RAPTOR leu2-3,112 ura3-52 rme1 trp1 his3*

FKBP12 overexpression lines

DNA constructs for the targeted integration into the Physcomitrella genome of the different *FKBP12* variants fused to *cMyc* were cloned via Gibson assembly. All parts were compiled into a vector backbone containing left (bL) and right (bR) borders of the Physcomitrella intergenic 1 (PIG1) locus, a neutral integration site in the genome (Okano et al. 2009). For each construct, the assembly resulted in a vector that can be linearized via enzymatic digestion to release the following DNA cassette: *PIG1bR-CaMV 35Sp-FKBP12-cMyc-CaMV 35St-PIG1bL*. Coding sequences (CDS) of *ScFKBP12*, *PpFKBP12* and *PpFKBP12-C26Y* were amplified from plasmids pESPB001, pESPB003, and pESPB006, respectively. The CDS of *HsFKBP12* was amplified from *pDONR223-HsFKBP1A/HsFKBP12 SpectR* (gift from Ekkehard Schulze). Transgenic lines were created via highly efficient homologous recombination (Wiedemann et al. 2018) in transformed WT protoplasts (Hohe and

Reski 2002; Hohe et al. 2004). At each time, the linear DNA cassette and a co-transfection vector conferring resistance on hygromycin B were used for transfection as described before. All DNA materials used for transfection were purified and sterilized via ethanol precipitation before usage (Sambrook and Russell 2006).

Screening of plants surviving hygromycin B selection was done by PCR to validate correct integration of the linear DNA cassette at the PIG1 locus. For this purpose, we used two different primer pairs: one pair (5_Up_173long_PIG1-5 and 3_103_35S-T(inv)) binds to a region in the genome upstream of PIG1bL and in the CaMV 35S terminator, while the other (5_52_35S-P(inv) and 3_Down_81_PIG1-3) binds in the CaMV 35S promoter and a region in the genome downstream of PIG1bR. Because untargeted integrations can still take place, transgene copy numbers were quantified via qPCR as described in Noy-Malka et al. (2014). Genomic DNA was isolated from 100 mg fresh weight (FW) of frozen protonema tissue using the GeneJET Plant Genomic DNA Purification Kit (Thermo Fisher Scientific), following the manufacturer's protocol. DNA samples were normalized to a concentration of 3 ng/µL prior to qPCR analysis. Reactions were set up using primers targeting PIG1bL (5-qPCR-PIG1-5HR-a and 3-qPCR-PIG1-5HR-a) and PIG1bR (5-qPCR-PIG1-3HR-b and 3-qPCR-PIG1-3HR-b), as well as primers specific for the CaMV 35S promoter (5-qPCR-35Sp(mAV)-c and 3-qPCR-35Sp(mAV)-c). To serve as an internal reference, primers amplifying the single-copy gene *CLF* (*Pp3c22_2940V3*) were included. All primer sequences are listed in **Supplementary Table S2**. WT plants and an in-house reference line (Δ*PpAARE3 #17*; Hoernstein et al. 2023) with a confirmed single integration of a DNA cassette were used as controls. All qPCR reactions were performed using 2x SensiFAST Mix (Bioline, London, UK) on a Lightcycler 480 II system (Roche, Basel, Switzerland).

Inducible RNA interference lines

To generate the estradiol-inducible *tor*, *lst8*, and *raptors* RNA interference (RNAi) lines of Physcomitrella, we followed the method of Miki et al. (2016) with minor modifications. For the construction of the different RNAi systems destined for a targeted integration at the PIG1 locus, we used the pGG624 plasmid (Miki et al. 2016). For each *TORC* gene subunit, two distinct regions within the transcript sequence were selected as RNAi targets. This approach reduces the likelihood of off-target effects, as consistent phenotypes across both targets strengthen evidence for a gene-specific

knockdown. For *PpTOR*, these regions were of 500 and 510 bp length, and covered regions 561-1060 and 2496-3005 in the CDS, respectively. For *PpLST8*, the first target sequence was 500 bp long and covered region 213-712 in the CDS. The second was 435 bp long and was located in the 5'UTR prior to the start codon. To downregulate the expression of the four *PpRAPTOR* paralogs with a single RNAi construct, regions in their CDS that are highly similar were selected. This strategy was described before and was proven successful (Miki et al. 2016). Thus, the first *Ppraptor* RNAi construct contained region 1656-2166 (511 bp) from the CDS of *PpRAPTOR1*. The second contained region 3662-4103 (442 bp) from *PpRAPTOR2*. These regions were 74-85% similar between the four paralogs. All primers used for cloning are listed in **Supplementary Table S3**. β-Estradiol (E8875, Sigma-Aldrich, St. Louis, USA) was used to induce gene silencing.

Crude extracts and Western blotting

Crude extracts for Western blot analysis were prepared from 100 mg of FW protonema, which were vacuum-filtered, collected in 2 mL Safe-Lock tube, and frozen in liquid nitrogen. Tissues were homogenized and disrupted using two beads (glass and metal) in a bead mill (MM 400; Retsch, Haan, Germany) for 3 min at 30 Hz. To the ground plant material, 500 µL of extraction buffer (25 mM HEPES-KOH pH 7.5, 100 mM NaCl, 0.2 mM DTT, 2 mM EDTA, 0.5% Triton, 1% plant protease inhibitor cocktail P9599 from Sigma Aldrich) were added to each sample, followed by sonication for 15 min using a cold ultrasound bath (Sonorex RK52, Bandelin, Berlin, Germany), and then centrifuged at 20,000 x g for 30 min at 2°C. Collected supernatants were subjected to another round of centrifugation for 5 min, and at the end collected into new tubes. Samples were quantified using the Pierce™ BCA Protein Assay Kit (Thermo Fisher Scientific) according to the manufacturer's protocol. Before loading on SDS gel, samples were reduced by heating 10 min at 95°C following the addition of 50 mM DTT and 4x Laemmli sample buffer (Bio-Rad Laboratories, Hercules, USA). 30 µg of total protein were loaded on a 12% acrylamide gel (Mini-PROTEAN® TGX™ Stain-Free™ gels, Bio-Rad Laboratories) and run for 90 min at 120 V. Proteins were transferred to a PVDF membrane (Hybond P0.45, Amersham, Cytiva, Marlborough, USA) in a Trans-Blot SD Semi-Dry Electrophoretic Cell (Bio-Rad Laboratories) for 80 min with 1.5 mA/cm^2. After blocking with 4% ECL™ Blocking Agent (Cytiva, Amersham), the membrane was probed with mouse monoclonal anti-

cMyc antibody (dilution 1:5000 in 1x TBST; clone 9E10, Roche). Anti-cMyc antibody was detected with a horseradish-peroxidase-conjugated anti-mouse IgG secondary antibody from sheep (Cytiva), followed by enhanced chemiluminescence (dilution 1:5000 in 1x TBST; Amersham ECL Prime Western Blotting Detection Reagent, Cytiva). Western blot signals were visualized using autoradiography films (CL-XPosure™ Film, Thermo Scientific, Cat. No. 34090). Transfer quality and total protein levels were monitored by PageBlue™ (Thermo Fisher Scientific) staining of the SDS gels.

Chlorophyll content

Chlorophyll was extracted from 20 mg protonema (vacuum-filtered material and frozen in liquid nitrogen). Tissues in a 2 mL Safe-Lock tube were homogenized and disrupted using two beads (glass and metal) in a mixer mill (MM 400, Retsch GmbH) for 3 min at 30 Hz, followed by addition of 480 µL cold 80% acetone and incubation on ice. After mixing for 5 min at Vmax using an Eppendorf ThermoMixer, samples were centrifuged at 20,000 x g for 10 min at 2°C and 400 µL of supernatants were collected. After an additional round of centrifugation for 5 min, three technical replicates of 100 µL of each supernatant were loaded on a 96-well microplate (Greiner, PS, F-Bottom, Crystal-Clear) and absorbance was read at 645 nm and at 663 nm using a POLARstar Omega or a SPECTROstar^{Nano} microplate reader (BMG LABTECH, Ortenberg, Germany). Total chlorophyll was calculated as chlorophyll *a* + chlorophyll *b* (mg g^{-1} FW) using the following formula as described in Ruibal et al. (2020): Chl *a* ($mg \cdot g^{-1}$ FW) = [(12.7 × A_{663}) - (2.6 × A_{645})] × (mL acetone/mg FW); Chl *b* ($mg \cdot g^{-1}$ FW) = [(22.9 × A_{645}) - (4.68 × A_{663})] × (mL acetone/mg FW).

Light microscopy

A Zeiss Axioplan 2 optical microscope equipped with an AxioCam MRc5 (Zeiss) was used to visualize protonema tissues. For this purpose, 15 µL of protonema suspension were placed on a glass slide, which was then covered with a coverslip before visualization at 10x magnification.

Chlorophyll fluorescence

Protonema suspension cultures at a density of 250 mg/L DW were dark-adapted for 10 min, and chlorophyll fluorescence was measured via pulse-amplitude modulation (PAM) in an imaging PAM instrument (IMAG-MAX/L, Walz, Effeltrich, Germany)

equipped with a Maxi-head (IMAG-K7, Walz). PSII maximum quantum yield (F_v/F_m) was recorded after F_0 and F_m determination. All experiments on photosynthetic parameters were repeated independently three times.

Total protein content

Total protein content was determined from 20 mg protonema (vacuum-filtered material and frozen in liquid nitrogen). Tissues in a 2 mL Safe-Lock tube were homogenized and disrupted using two beads (glass and metal) in a mixer mill (MM 400, Retsch GmbH) for 3 min at 30 Hz, followed by addition of 100 µL extraction buffer (50 mM PBS and 1 mM EDTA). Samples were vigorously hand-shaken, centrifuged for 5 sec at 1.5 x g, and vortexed for 10 sec. To enhance extraction, samples were further processed in the mixer mill for 5 min at 20 Hz. This was followed by sonication in a cold ultrasonic bath (Sonorex RK52, Bandelin) for 15 min. The lysates were centrifuged at 20,000 × g for 30 min at 2°C. The supernatants were carefully collected and subjected to a second centrifugation step (5 min), after which the supernatants were transferred to new tubes. Total protein content was determined from 1:4 diluted samples in extraction buffer using the Pierce™ BCA Protein Assay Kit (Thermo Fisher Scientific) according to the manufacturer's instructions.

Flow cytometry

Flow cytometry analysis was conducted as previously described (Heck et al. 2021) with slight modifications. Protonema tissues were chopped with a razor blade in a small petri dish (6 cm diameter) containing 0.5 mL of DAPI-buffer (0.01 mg/L 4′,6-Diamidin-2-phenylindol (DAPI), 1.07 g/L MgCl2 ×6 H2O, 5 g/L NaCl, 21.11 g/L Tris, 0.1% Triton, pH 7). Subsequently, 1.5 mL DAPI-buffer was added to the preparation, which was then filtered through a sieve of 30 µm pore size. The filtrate was analysed with a Partec CyFlow® Space flow cytometer (Sysmex Partec, Görlitz, Germany) equipped with a 365 nm UV-LED.

AZD treatment for phospho-proteomic analysis

Moss suspension culture normalised to 180 mg/L was divided into 50 mL Erlenmeyer flasks and cultivated for 24 h under standard growth conditions. Subsequently, they were incubated for 1 h with either 10 µM AZD8055 (AZD), or an equivalent amount of DMSO as a control. Treated tissue was harvested by vacuum-filtration, transferred to 2 mL SafeLock reaction tube (Eppendorf) containing one 3 mm tungsten carbide bead

(Qiagen) and one glass bead. Samples were snap-frozen in liquid nitrogen and ground to fine powder at 28 Hz for 2 min in a homogenizer (MM 400, Retsch). Lysis buffer according to Lang et al. (2011) containing 7.5 M urea, 2.5 M thiourea, 12.5% glycerol, 62.5 mM Tris-HCl, 2.5% (w/v) n-octyl glucoside (octyl β-D-glucopyranoside), 1.25 mM protease inhibitor P2714 (Sigma-Aldrich) was supplemented with PhosStop phosphatase inhibitor (Roche) and added to the ground tissue. Samples were vortexed until dissolved, incubated for 15 min in an ultrasound bath, and centrifuged at 20,000 x g and 16 °C for 30 min. Finally, the supernatant containing the extracted protein was transferred to a fresh reaction tube. The protein concentration was determined using the Quick Start Bradford Protein Assay (Bio-Rad) according to the manufacturer's instructions.

SP3 clean up, tryptic digest and phospho-peptide enrichment

The extracted proteins were further processed using an adapted single-pot, solid-phase-enhanced sample-preparation (SP3) method (Hughes et al. 2019). Briefly, samples (200 µg input) were reduced with 2 mM tris(2-carboxyethyl) phosphine (TCEP) for 30 min at 37 °C, then alkylated with 50 mM chloroacetamide (CAA) for 30 min in the dark, and finally, the reaction was quenched with 50 mM DTT for 20 min at RT. Sera-Mag SpeedBead magnetic carboxylate-modified particles (Cytiva) were washed twice with 10x volume of ELGA H_2O, then added in a 1:10 bead to proteome ratio to the samples and incubated for 20 min at RT in a high organic solution of 80% EtOH to allow the proteins to bind to the beads. The beads were bound using a magnetic rack and washed twice with 10x volume of 90% acetonitrile (ACN). To resuspend the beads in between washing steps, the tubes were placed in an ultrasonic water bath. After washing, remaining liquid was removed, and the beads were resuspended in 100 mM ammonium bicarbonate (AMBIC). Trypsin was added in a 1:100 protease to proteome ratio and incubated at 37 °C for 16 h and shaking at 1,200 rpm. Digested peptides were desalted using µSpin C18-disc cartridges (Affinisep) following the manufacturer's instructions. After elution in 50 % ACN and 0.5 % acetic acid (HAC) the peptides were dried using a Speedvac concentrator (Eppendorf).

Peptides were reconstituted in 1 µL binding buffer (80% ACN, 1% trifluoracetic acid (TFA), 3% (w/v) glycolic acid (GA)) per 1 µg dried peptide. The magnetic Ti-NTA beads (Cube Biotech, Monheim, Germany) were washed three times in 10 vol of binding

buffer, resuspended in binding buffer, then incubated for 30 min at 25 °C and 1200 rpm with the peptides in a 10:1 (w/w) bead to peptide ratio. After binding, the beads were washed twice in wash buffer 1 (80% ACN, 1% TFA), and once in wash buffer 2 (10 % ACN, 0.2% TFA), in between wash steps, the beads were placed in an ultrasonic water bath and incubated for 2 min at 25 °C and 1200 rpm. Finally, the peptides were incubated for 30 min at 25 °C and 1200 rpm in elution buffer (1% ammonium hydroxide (NH_4OH)), then the supernatant containing the eluted peptides was transferred to a fresh reaction tube and acidified to pH <3 using formic acid.

Acidified peptides were desalted using self-packed SDB-RPS Stop and Go Extraction tips (StageTips) (Rappsilber et al. 2007) composed of three layers of 1.0 × 1.0 mm (AttractSPE Disks Bio RPS, Affinisep, Le Houlme, France). The StageTips were equilibrated sequentially with 100% methanol, 80% acetonitrile containing 0.1% FA, and twice with 0.1% FA. Acidified peptide solutions were loaded onto the StageTips and washed with 0.1% FA, 80% acetonitrile with 0.1% FA, and 80% methanol with 0.5% FA. The eluates were dried using a Speedvac concentrator (Eppendorf) and reconstituted in 0.1% FA prior to LC-MS measurement.

Measurement on a QExactive Orbitrap

For LC-MS analysis of the phospho-peptide enriched samples, an UltiMate 3000 RSLCnano system was online coupled to a QExactive mass spectrometer (both Thermo Fisher Scientific). The peptide mixture was washed and preconcentrated on a PepMap C18 trapping column (Thermo Fisher Scientific) with a flow rate of 30 µL/min and peptides were separated on a µPAC C18 pillar array column (200 cm bed length, Thermo Fisher Scientific) using a binary buffer system consisting of A (0.1% formic acid) and B (86% acetonitrile, 0.1% formic acid). Peptides were eluted applying a linear gradient from 5% to 50% B in 45 min and 50 to 99% B in 2 min at a flow rate of 1 µL/min. For electrospray ionization of peptides, a Nanospray Flex ion source (Thermo Fisher Scientific) with a liquid Junction PST-HV-NFU (MS Wil, Aarle-Rixtel, The Netherlands) and a fused silica emitter (20 µm inner diameter, 360 µm outer diameter, MicroOmics Technologies LLC) applying a source voltage of +1.800 V and an ion transfer tube temperature at 250°C was used. Cycles of data-independent acquisition (DIA) consisted of: one overview spectrum (RF lens of 50%, normalized AGC target of 3e6, maximum injection time of 60 ms, m/z range of 385 to 1.050,

resolution of 70.000 at 200m/z, profile mode) followed by MS^2 fragment spectra (RF lens of 50%, normalized AGC target of 1e6, maximum injection time of 60 ms) generated sequentially by higher-energy collision-induced dissociation (HCD) at a normalized energy of 26% in a precursor m/z range from 400 to 1.000 in 50 windows of 12.5 m/z isolation width overlapping by 0.25 m/z and recorded at a resolution of 35.000 in profile mode.

Database search with *FragPipe*

Raw mass spectrometry files of phospho-peptide enriched samples were analysed using *FragPipe* v22.0 configured for data independent acquisition (DIA). Peptide identification was performed using *MSFragger* (Kong et al. 2017) against a *Physcomitrium patens* protein database (48,582 entries; Lang et al. 2018) containing both target and decoy sequences for FDR estimation. The search was carried out with a precursor mass tolerance of -20 to +20 ppm, enzyme specificity set to trypsin, a peptide mass range of 500 to 5,000 Da, and a minimum peptide length of 7 and a maximum of 40 amino acids. Variable modifications included phosphorylation of serine, threonine, and tyrosine (S/T/Y), oxidation of methionine (M), deamidation of asparagine and glutamine (N/Q), pyro-glutamate conversion from N-terminal glutamine, glutamic acid, and cysteine (Q/E/C), as well as hydroxylation of proline (P). Validation of peptide-spectrum matches, and phospho-site assignments were performed using *MSBooster* (Yang et al. 2023), Percolator (Käll et al. 2007; The et al. 2017), and PTMProphet (Shteynberg et al. 2019). Quantification was conducted using *DIA-NN* (Demichev et al. 2020), applying a protein-level false discovery rate (FDR) threshold of 0.01.

Phospho-peptide data analysis with R

Phospho-peptide data analysis was performed in *R* (v4.4.3; R Core Team 2025), using a minimum site localization probability of 0.75 for serine, threonine, and tyrosine (S/T/Y) residues. Statistical significance of differences between conditions was assessed using a Welch test.

Protein sequence alignment and functional domain analysis

FKBP12 protein sequences from *A. thaliana* (AT5G64350.1) and *P. patens* (Pp3c1_27870V3.1) were complemented by homologs from *C. reinhardtii*, *Homo sapiens*, *O. sativa*, *S. cerevisiae*, *Schizosaccharomyces pombe* (Crespo et al. 2005),

A. pyrenoidosa (Zhu et al. 2022), *C. merolae* (Imamura et al. 2013), *S. lycopersicum* (Xiong et al. 2016), and *V. faba* (Xu et al. 1998). Based on this set we conducted proteome-wide sequence searches with Diamond (v2.1.10.164; Buchfink et al. 2021) against *Anthoceros angustus* (Zhang et al. 2020), *Calohypnum plumiforme* (Mao et al. 2020), *Ceratopteris richardii* (Marchant et al. 2022), *Marchantia polymorpha* (Bowman et al. 2017), *Populus trichocarpa* (Tuskan et al. 2006), *Selaginella moellendorffii* (Banks et al. 2011), *Sphagnum magellanicum* (Healey et al. 2023), *Takakia lepidozioides* (Hu et al. 2023), and *Vitis vinifera* (Jaillon et al. 2007). InterProScan (v5.71-102.0; Jones et al. 2014) was used to infer functional domain annotation. Initial hits were filtered for assignment to the Panther (Thomas et al. 2022) family "PEPTIDYL-PROLYL CIS-TRANS ISOMERASE" (PTHR10516), manually curated and aligned with Mafft (v7.490; Katoh and Standley 2013) in "globalpair" mode.

We inferred functional domains for TOR, RAPTOR and LST8 homologs from *A. thaliana*, *O. sativa*, *P. patens*, and *S. cerevisiae* (Liu et al. 2025) using InterProScan (v5.71-102.0; Jones et al. 2014). Pfam (Paysan-Lafosse et al. 2024) domains "FKBP12-rapamycin binding domain" (PF08771), "FAT domain" (PF02259), "Phosphatidylinositol 3- and 4-kinase" (PF00454), "FATC domain" (PF02260), and "Raptor N-terminal CASPase like domain" (PF14538) were relabelled as "FRB", "FAT", "KD", "FATC", and "RNC", respectively. Superfamily (Pandurangan et al. 2018) annotations "ARM repeat" (SSF48371), and "WD40 repeat-like" (SSF50978) were relabelled as "HEAT", and "WD40", respectively, and consecutive "WD40" domains were concatenated for sequence comparison and visualization. Pairwise sequence identity was calculated using R (v4.4.3; R Core Team 2025) and the pwalign package (v1.2.0; Aboyoun et al. 2025), and protein domain plots were generated using the seqvisr (v0.2.7; vragh 2022) package.

Statistical analysis

Graphs and statistical analyses were performed with the GraphPad Prism software version 10.0 for Windows (GraphPad software, San Diego, California, USA). Statistical differences were analysed with one-way Anova with subsequent post-hoc test in R. Statistical significance was accepted at $*p < 0.05$, $**p < 0.01$, and $***p < 0.001$.

Author contributions

E.S. designed research, acquired funding, performed experiments, analysed data, and wrote the manuscript. S.N.W.H., N.v.G, A.S., and K.M.V.H. designed research, performed experiments, analysed data, and helped writing the manuscript. J.P., E.L.D., and P.F.H. analysed data and helped writing the manuscript. H.T.S. supervised research. R.R. designed and supervised research, analysed data, acquired funding, and wrote the manuscript. All authors read and approved the final version of the manuscript.

Funding

This project was funded by the European Union Horizon's 2021 research and innovation program under the Marie Skłodowska-Curie Actions grant agreement No 101065000 to E.S., and by the German Research Foundation DFG under Germany's Excellence Strategy (CIBSS – EXC-2189 – Project ID 390939984) to R.R.

Data availability

The WT strain as well as the transgenic lines generated in this study are accessible via the International Moss Stock Center (IMSC, www.moss-stock-center.org). Their IMSC accession numbers are listed in **Supplementary Table S4**. The mass spectrometry proteomics data have been deposited at the ProteomeXchange Consortium via the PRIDE partner repository (Deutsch et al. 2023; Perez-Riverol et al. 2025) with the dataset identifier PXD069889.

Conflict of interest

All authors declare no conflict of interest.

Short legends for Supporting Information

Supplementary Figure S1 Expression levels of TORC1 component genes in Physcomitrella at different culture conditions and developmental stages.

Supplementary Figure S2 Caulonema frequency increased with incubation time.

Supplementary Figure S3 Complementation of the yeast *tor* and *raptor* mutants with their Physcomitrella homologs.

Supplementary Figure S4 Gametophore counts over time in Physcomitrella WT.

Supplementary Figure S5 Expression levels of *PpS6K* genes in Physcomitrella at different culture conditions and developmental stages.

Supplementary Figure S6 Expression levels of *PpRPS6* genes in Physcomitrella at different culture conditions and developmental stages.

Supplementary Figure S7 Yeast complementation assay of the *fkbp12Δ* mutant with mutant FKBP12 variants from Physcomitrella and Arabidopsis.

Supplementary Table S1 Primers used to clone *ScFKBP12*, *PpFKBP12* WT and mutants in p415 GAL1 restricted with XbaI and XhoI.

Supplementary Table S2 Primers used to generate the vectors containing the different *PIG1bL-CaMV 35Sp-FKBP12-cMyc-CaMV 35St-PIG1bR* DNA constructs, to validate via PCR their correct integration at the PIG1 locus, and to determine via qPCR their copy number in the Physcomitrella genome.

Supplementary Table S3 Primers used to generate the estradiol-inducible *lst8*, *tor*, and *raptors* RNA interference (RNAi) systems destined for a targeted integration at the PIG1 locus in the Physcomitrella genome

Supplementary Table S4 International Moss Stock Center (IMSC, www.mossstock-center.org) accession numbers of the lines used in this study.

References

Aboyoun P, Gentleman R, Pages H (2025) pwalign: Perform pairwise sequence alignments. Bioconductor. doi: 10.18129/B9.bioc.pwalign

Adami A, García-Alvarez B, Arias-Palomo E, Barford D, Llorca O (2007) Structure of TOR and its complex with KOG1. Mol Cell 27:509-516. doi: 10.1016/j.molcel.2007.05.040

Bakshi A, Moin M, Kumar MU, Reddy ABM, Ren MZ, Datla R, Siddiq EA, Kirti PB (2017) Ectopic expression of *Arabidopsis Target of Rapamycin* (*AtTOR*) improves water-use efficiency and yield potential in rice. Sci Rep 7:42835. doi: 10.1038/srep42835

Banks JA, Nishiyama T, Hasebe M, Bowman JL, Gribskov M, dePamphilis C, Albert VA, Aono N, Aoyama T, Ambrose BA, Ashton NW, Axtell MJ, Barker E, Barker MS, Bennetzen JL, Bonawitz ND, Chapple C, Cheng C, Correa LGG, Dacre M, DeBarry J, Dreyer I, Elias M, Engstrom EM, Estelle M, Feng L, Finet C, Floyd SK, Frommer WB, Fujita T, Gramzow L, Gutensohn M, Harholt J, Hattori M, Heyl A, Hirai T, Hiwatashi Y, Ishikawa M, Iwata M, Karol KG, Koehler B, Kolukisaoglu U, Kubo M, Kurata T, Lalonde S, Li K, Li Y, Litt A, Lyons E, Manning G, Maruyama T, Michael TP, Mikami K, Miyazaki S, Morinaga S, Murata T, Mueller-Roeber B, Nelson DR, Obara M, Oguri Y, Olmstead RG, Onodera N, Petersen BL, Pils B, Prigge M, Rensing SA, Riaño-Pachón DM, Roberts AW, Sato Y, Scheller HV, Schulz B, Schulz C, Shakirov EV, Shibagaki N, Shinohara N, Shippen DE, Sørensen I, Sotooka R, Sugimoto N, Sugita M, Sumikawa N, Tanurdzic M, Theissen G, Ulvskov P, Wakazuki S, Weng JK, Willats WWGT, Wipf D, Wolf PG, Yang L, Zimmer AD, Zhu Q, Mitros T, Hellsten U, Loqué D, Otillar R, Salamov A, Schmutz J, Shapiro H, Lindquist E, Lucas S, Rokhsar D, Grigoriev IV (2011) The *Selaginella* genome identifies genetic changes associated with the evolution of vascular plants. Science 332:960-963. doi: 10.1126/science.1203810

Barbet NC, Schneider U, Helliwell SB, Stansfield I, Tuite MF, Hall MN (1996) TOR controls translation initiation and early G1 progression in yeast. Mol Bio Cell 7:25-42. doi: 10.1091/mbc.7.1.25

Battaglioni S, Benjamin D, Wälchli M, Maier T, Hall MN (2022) mTOR substrate phosphorylation in growth control. Cell 185:1814-1836. doi: 10.1016/j.cell.2022.04.013

Beike AK, Lang D, Zimmer AD, Wüst F, Trautmann D, Wiedemann G, Beyer P, Decker EL, Reski R (2015) Insights from the cold transcriptome of *Physcomitrella patens*: global specialization pattern of conserved transcriptional regulators and identification of orphan genes involved in cold acclimation. New Phytol 205:869–881. doi: 10.1111/nph.13004

Bowman JL, Kohchi T, Yamato KT, Jenkins J, Shu S, Ishizaki K, Yamaoka S, Nishihama R, Nakamura Y, Berger F, Adam C, Aki SS, Althoff F, Araki T, Arteaga-Vazquez MA, Balasubrmanian S, Barry K, Bauer D, Boehm CR, Briginshaw L, Caballero-Perez J, Catarino B, Chen F, Chiyoda S, Chovatia M, Davies KM, Delmans M, Demura T, Dierschke T, Dolan L, Dorantes-Acosta AE, Eklund DM, Florent SN, Flores-Sandoval E, Fujiyama A, Fukuzawa H, Galik B, Grimanelli D, Grimwood J, Grossniklaus U, Hamada T, Haseloff J, Hetherington AJ, Higo A, Hirakawa Y, Hundley HN, Ikeda Y, Inoue K, Inoue S, Ishida S, Jia Q, Kakita M, Kanazawa T, Kawai Y, Kawashima T, Kennedy M, Kinose K, Kinoshita T, Kohara Y, Koide E, Komatsu K, Kopischke S, Kubo M, Kyozuka J, Lagercrantz U, Lin SS, Lindquist E, Lipzen AM, Lu CW, De Luna E, Martienssen RA, Minamino N, Mizutani M, Mizutani M, Mochizuki N, Monte I, Mosher R, Nagasaki H, Nakagami H, Naramoto S, Nishitani K, Ohtani M, Okamoto T, Okumura M, Phillips J, Pollak B, Reinders A, Rövekamp M, Sano R, Sawa S, Schmid MW, Shirakawa M, Solano R, Spunde A, Suetsugu N, Sugano S, Sugiyama A, Sun R, Suzuki Y, Takenaka M, Takezawa D, Tomogane H, Tsuzuki M, Ueda T, Umeda M, Ward JM, Watanabe Y, Yazaki K, Yokoyama R, Yoshitake Y, Yotsui I, Zachgo S, Schmutz J (2017) Insights into land plant evolution garnered from the *Marchantia polymorpha* genome. Cell 171:287-304. doi: 10.1016/j.cell.2017.09.030

Buchfink B, Reuter K, Drost HG (2021) Sensitive protein alignments at tree-of-life scale using DIAMOND. Nat Methods 18:366-368. doi: 10.1038/s41592-021-01101-x

Caldana C, Li Y, Leisse A, Zhang Y, Bartholomaeus L, Fernie AR, Willmitzer L, Giavalisco P (2013) Systemic analysis of inducible target of rapamycin mutants reveal a general metabolic switch controlling growth in *Arabidopsis thaliana*. Plant J 73:897-909. doi: 10.1111/tpj.12080

Choi JW, Chen J, Schreiber SL, Clardy J (1996) Structure of the FKBP12-rapamycin complex interacting with the binding domain of human FRAP. Science 273:239-242. doi: 10.1126/science.273.5272.239

Chresta CM, Davies BR, Hickson I, Harding T, Cosulich S, Critchlow SE, Vincent JP, Ellston R, Jones D, Sini P, James D, Howard Z, Dudley P, Hughes G, Smith L, Maguire S, Hummersone M, Malagu K, Menear K, Jenkins R, Jacobsen M, Smith GCM, Guichard S, Pass M (2010) AZD8055 is a potent, selective, and orally bioavailable ATP-competitive mammalian Target of Rapamycin kinase inhibitor with *in vitro* and *in vivo* antitumor activity. Cancer Res 70:288-298. doi: 10.1158/0008-5472.CAN-09-1751

Couso I, Smythers AL, Ford MM, Umen JG, Crespo JL, Hicks LM (2021) Inositol phosphates and target of rapamycin signalling govern photosystem II protein phosphorylation and photosynthetic function under light stress in *Chlamydomonas*. New Phytol 232:2011-2025. doi: 10.1111/nph.17741

Crespo JL, Diaz-Troya S, Florencio FJ (2005) Inhibition of target of rapamycin signaling by rapamycin in the unicellular green alga *Chlamydomonas reinhardtii*. Plant Phys 139:1736-1749. doi: 10.1104/pp.105.070847

D'Alessandro S, Velay F, Lebrun R, Zafirov D, Mehrez M, Romand S, Saadouni R, Forzani C, Citerne S, Montane MH (2024) Posttranslational regulation of photosynthetic activity via the TOR kinase in plants. Sci Adv 10:eadj3268 doi: 10.1126/sciadv.adj3268

Decker EL, Reski R (2004) The moss bioreactor. Curr Op Plant Bio 7:166-170. doi: 10.1016/j.pbi.2004.01.002

Decker E, Reski R (2007) Moss bioreactor producing improved biopharmaceuticals. Curr Op Biotech 18:393-398. doi: 10.1016/j.copbio.2007.07.012

Deprost D, Truong HN, Robaglia C, Meyer C (2005) An *Arabidopsis* homolog of RAPTOR/KOG1 is essential for early embryo development. Biochem Biophys Res Comm 326:844-850. doi: 10.1016/j.bbrc.2004.11.117

Deprost D, Yao L, Sormani R, Moreau M, Leterreux G, Nicolai M, Bedu M, Robaglia C, Meyer C (2007) The Arabidopsis TOR kinase links plant growth, yield, stress

resistance and mRNA translation. EMBO Rep 8:864-870. doi: 10.1038/sj.embor.7401043

Deutsch EW, Bandeira N, Perez-Riverol Y, Sharma V, Carver JJ, Mendoza L, Kundu DJ, Wang S, Bandla C, Kamatchinathan S, Hewapathirana S, Pullman BS, Wertz J, Sun Z, Kawano S, Okuda S, Watanabe Y, MacLean B, MacCoss MJ, Zhu Y, Ishihama Y, Vizcaíno JA (2023) The ProteomeXchange consortium at 10 years: 2023 update. Nucl Acids Res 51:D1539-D1548. doi: 10.1093/nar/gkac1040

Díaz-Troya S, Florencio FJ, Crespo JL (2008) Target of rapamycin and LST8 proteins associate with membranes from the endoplasmic reticulum in the unicellular green alga *Chlamydomonas reinhardtii*. Eukar Cell 7:212-222. doi: 10.1128/EC.00361-07

Demichev V, Messner CB, Vernardis SI, Lilley KS, Ralser M (2020) DIA-NN: neuronal networks and interference correction enable deep proteome coverage in high throughput. Nat Methods 17:41-44. doi: 10.1038/s41592-019-0638-x

Dobrenel T, Mancera-Martinez E, Forzani C, Azzopardi M, Davanture M, Moreau M, Schepetilnikov M, Chicher J, Langella O, Zivy M, Robaglia C, Ryabova LA, Hanson J, Meyer C (2016) The Arabidopsis TOR kinase specifically regulates the expression of nuclear genes coding for plastidic ribosomal proteins and the phosphorylation of the cytosolic ribosomal protein S6. Front Plant Sci 7:1611. doi: 10.3389/fpls.2016.01611

Egener T, Granado J, Guitton MC, Hohe A, Holtorf H, Lucht JM, Rensing SA, Schlink K, Schulte J, Schween G, Zimmermann S, Duwenig E, Rak B, Reski R (2002) High frequency of phenotypic deviations in *Physcomitrella patens* plants transformed with a gene-disruption library. BMC Plant Bio 2:6. doi: 10.1186/1471-2229-2-6

Ermert AL, Nogue F, Stahl F, Gans T, Hughes J (2019) CRISPR/Cas9-mediated knockout of *Physcomitrella patens* phytochromes. Meth Mol Bio 2026:237-263. doi: 10.1007/978-1-4939-9612-4_20

Feng L, Li XB, Zheng XA, Zheng Z, Liu QR, Liu CL, Zhu QL, Shen WJ, Yang C, Li HB (2025) SnRK1 and TOR: central regulators of autophagy in plant energy stress responses. ABIOTECH. doi: 10.1007/s42994-025-00218-3

Fernandez-Pozo N (2023) PEATMOSS: A gene expression atlas for bryophytes. Meth Mol Bio 2703:91-107. doi: 10.1007/978-1-0716-3389-2_8

Frank W, Decker EL, Reski R (2005) Molecular tools to study *Physcomitrella patens*. Plant Bio 7:220-227. doi: 10.1055/s-2005-865645

Gibson DG, Young L, Chuang RY, Venter JC, Hutchison CA, Smith HO (2009) Enzymatic assembly of DNA molecules up to several hundred kilobases. Nat Methods 6:343-345. doi: 10.1038/NMETH.1318

Gietz D, St. Jean A, Woods RA, Schiestl RH (1992) Improved method for high-efficiency transformation of intact yeast-cells. Nucl Ac Res 20:1425. doi: 10.1093/nar/20.6.1425

Hadeler B, Scholz S, Reski R (1995) Gelrite and agar differently influence cytokinin-sensitivity of a moss. J Plant Phys 146:369-371. doi: 10.1016/S0176-1617(11)82071-7

Healey AL, Piatkowski B, Lovell JT, Sreedasyam A, Carey SB, Mamidi S, Shu S, Plott C, Jenkins J, Lawrence T, Aguero B, Carrell AA, Nieto-Lugilde M, Talag J, Duffy A, Jawdy S, Carter KR, Boston L-B, Jones T, Jaramillo-Chico J, Harkess A, Barry K, Keymanesh K, Bauer D, Grimwood J, Gunter L, Schmutz J, Weston DJ, Shaw AJ (2023) Newly identified sex chromosomes in the *Sphagnum* (peat moss) genome alter carbon sequestration and ecosystem dynamics. Nat Plants 9:238-254. doi: 10.1038/s41477-022-01333-5

Heck MA, Lüth VM, van Gessel N, Krebs M, Kohl M, Prager A, Joosten H, Decker EL, Reski R (2021) Axenic *in vitro* cultivation of 19 peat moss (*Sphagnum* L.) species as a resource for basic biology, biotechnology, and paludiculture. New Phytol 229:861-876. doi: 10.1111/nph.16922

Heitman J, Movva NR, Hall MN (1991a) Targets for cell-cycle arrest by the immunosuppressant rapamycin in yeast. Science 253:905-909. doi: 11.1126/science.1715094

Heitman J, Movva NR, Hiestand PC, Hall MN (1991b) FK 506-binding protein proline rotamase is a target for the immunosuppressive agent FK 506 in *Saccharomyces cerevisiae*. Proc Natl Acad Sci USA 88:1948-1952. doi: 10.1073/pnas.88.5.1948

Hoernstein SNW Oezdemir B, van Gessel N, Miniera AA, Rogalla von Bieberstein B, Nilges L, Schweikert Farinha J, Komoll R, Glauz S, Weckerle T, Scherzinger F,

Rodriguez-Franco M, Mueller-Schuessele SJ, Reski R (2023) A deeply conserved protease, acylamino acid-releasing enzyme (AARE), acts in ageing in Physcomitrella and Arabidopsis. Comm Bio 6:61. doi: 10.1038/s42003-023-04428-7

Hohe A, Reski R (2002) Optimisation of a bioreactor culture of the moss *Physcomitrella patens* for mass production of protoplasts. Plant Sci 163:69-74. doi: 10.1016/S0168-9452(02)00059-6

Hohe A, Reski R (2005) Control of growth and differentiation of bioreactor cultures of *Physcomitrella* by environmental parameters. Plant Cell Tiss Org Cult 81:307-311. doi: 10.1007/s11240-004-6656-z

Hohe A, Decker E, Gorr G, Schween G, Reski R (2002) Tight control of growth and cell differentiation in photoautotrophically growing moss (*Physcomitrella patens*) bioreactor cultures. Plant Cell Rep 20:1135-1140. doi: 10.1007/s00299-002-0463-y

Hohe A, Egener T, Lucht JM, Holtorf H, Reinhard C, Schween G, Reski R (2004) An improved and highly standardised transformation procedure allows efficient production of single and multiple targeted gene-knockouts in a moss, *Physcomitrella patens*. Curr Genet 44:339-347. doi: 10.1007/s00294-003-0458-4

Horst NA, Katz A, Pereman I, Decker EL, Ohad N, Reski R (2016) A single homeobox gene triggers phase transition, embryogenesis and asexual reproduction. Nat Plants 2:15209. doi: 10.1038/NPLANTS.2015.209

Horstmann V, Huether CM, Jost W, Reski R, Decker EL (2004) Quantitative promoter analysis in *Physcomitrella patens*: a set of plant vectors activating gene expression within three orders of magnitude. BMC Biotech 4:13. doi: 10.1186/1472-6750-4-13

Hu R, Li X, Hu Y, Zhang R, Lv Q, Zhang M, Sheng X, Zhao F, Chen Z, Ding Y, Yuan H, Wu X, Xing S, Yan X, Bao F, Wan P, Xiao L, Wang X, Xiao W, Decker EL, van Gessel N, Renault H, Wiedemann G, Horst NA, Haas FB, Wilhelmsson PKI, Ullrich KK, Neumann E, Lv B, Liang C, Du H, Lu H, Gao Q, Cheng Z, You H, Xin P, Chu J, Huang CH, Liu Y, Dong S, Zhang L, Chen F, Deng L, Duan F, Zhao W, Li K, Li Z, Li X, Cui H, Zhang YE, Ma C, Zhu R, Jia Y, Wang M, Hasebe M, Fu J, Goffinet B, Ma H, Rensing SA, Reski R, He Y (2023) Adaptive evolution of the enigmatic *Takakia* now facing climate change in Tibet. Cell 186:3558-3576. doi: 10.1016/j.cell.2023.07.003

Hughes CS, Moggridge S, Müller T, Sorensen PH, Morin GB, Krijgsveld J (2019) Single-pot, solid-phase-enhanced sample preparation for proteomics experiments. Nat Protocols 14:68-85. doi: 10.1038/s41596-018-0082-x

Imamura S, Ishiwata A, Watanabe S, Yoshikawa H, Tanaka K (2013) Expression of budding yeast FKBP12 confers rapamycin susceptibility to the unicellular red alga *Cyanidioschyzon merolae*. Biochem Biophys Res Comm 439:264-269. doi: 10.1016/j.bbrc.2013.08.045

Jacinto E, Lorberg A (2008) TOR regulation of AGC kinases in yeast and mammals. Biochem J 410:19-37. doi: 10.1042/BJ20071518

Jaillon O, Aury J-M, Noel B, Policriti A, Clepet C, Casagrande A, Choisne N, Aubourg S, Vitulo N, Jubin C, Vezzi A, Legeai F, Hugueney P, Dasilva C, Horner D, Mica E, Jublot D, Poulain J, Bruyère C, Billault A, Segurens B, Gouyvenoux M, Ugarte E, Cattonaro F, Anthouard V, Vico V, Del Fabbro C, Alaux M, Di Gaspero G, Dumas V, Felice N, Paillard S, Juman I, Moroldo M, Scalabrin S, Canaguier A, Le Clainche I, Malacrida G, Durand É, Pesole G, Laucou V, Chatelet P, Merdinoglu D, Delledonne M, Pezzotti M, Lecharny A, Scarpelli C, Artiguenave F, Pè ME, Valle G, Morgante M, Caboche M, Adam-Blondon AF, Weissenbach J, Quétier F, Wincker P (2007) The grapevine genome sequence suggests ancestral hexaploidization in major angiosperm phyla. Nature 449:463-467. doi: 10.1038/nature06148

Jones P, Binns D, Chang H-Y, Fraser M, Li W, McAnulla C, McWilliam H, Maslen J, Mitchell A, Nuka G, Pesseat S, Quinn AF, Sangrador-Vegas A, Scheremetjew M, Yong SY, Lopez R, Hunter S (2014) InterProScan 5: genome-scale protein function classification. Bioinform 30:1236-1240. doi: 10.1093/bioinformatics/btu031

Jordan NJ, Dutkowski CM, Barrow D, Mottram HJ, Hutcheson IR, Nicholson RI, Guichard SM, Gee JMW (2014) Impact of dual mTORC1/2 mTOR kinase inhibitor AZD8055 on acquired endocrine resistance in breast cancer *in vitro*. Breast Canc Res 16:R12. doi: 10.1186/bcr3604

Kamisugi Y, Schlink K, Rensing SA, Schween G, von Stackelberg M, Cuming AC, Reski R, Cove DJ (2006) The mechanism of gene targeting in *Physcomitrella patens*: homologous recombination, concatenation and multiple integration. Nucl Acids Res 34:6205-6214. doi: 10.1093/nar/gkl832

Katoh K, Standley DM (2013) MAFFT multiple sequence alignment software version 7: improvements in performance and usability. Mol Biol Evol 30:772-780. doi: 10.1093/molbev/mst010.

Katoh K, Rozewicki J, Yamada KD (2019) MAFFT online service: multiple sequence alignment, interactive sequence choice and visualization. Brief Bioinform 20:1160-1166. doi: 10.1093/bib/bbx108

Käll L, Canterbury JD, Weston J, Noble WS, MacCoss MJ (2007) Semi-supervised learning for peptide identification from shotgun proteomics datasets. Nat Methods 4:923-925. doi: 10.1038/nmeth1113

Keith CT, Schreiber SL (1995) PIK-related kinases - DNA-repair, recombination, and cell-cycle checkpoints. Science 270:50-51. doi: 10.1126/science.270.5233.50

Kim DH, Sarbassov DD, Ali SM, King JE, Latek RR, Erdjument-Bromage H, Tempst P, Sabatini DM (2002) mTOR interacts with Raptor to form a nutrient-sensitive complex that signals to the cell-growth machinery. Cell 110:163-175. doi: 10.1016/S0092-8674(02)00808-5

Khraiwesh B, Arif MA, Seumel GI, Ossowski S, Weigel D, Reski R, Frank W (2010) Transcriptional control of gene expression by microRNAs. Cell 140:111-122. doi: 10.1016/j.cell.2009.12.023

Kong AT, Leprevost FV, Avtonomov DM, Mellacheruvu D, Nesvizhskii AI (2017) MSFragger: ultrafast and comprehensive peptide identification in mass spectrometry-based proteomics. Nat Methods 14:513-520. doi: 10.1038/NMETH.4256

Kozgunova E, Yoshida MW, Reski R, Goshima G (2022) Spindle motility skews division site determination during asymmetric cell division in Physcomitrella. Nat Comm 13:2488. doi: 10.1038/s41467-022-30239-1

Kubo M, Imai A, Nishiyama T, Ishikawa M, Sato Y, Kurata T, Hiwatashi Y, Reski R, Hasebe M (2013) System for stable β-estradiol-inducible gene expression in the moss *Physcomitrella patens*. PLOS ONE 8:e77356. doi: 10.1371/journal.pone.0077356

Kubo M, Nishiyama T, Tamada Y, Sano R, Ishikawa M, Murata T, Imai A, Lang D, Demura T, Reski R, Hasebe M (2019) Single-cell transcriptome analysis of

Physcomitrella leaf cells during reprogramming using microcapillary manipulation. Nucl Acids Res 47:4539-4553. doi: 10.1093/nar/gkz181

Lang EG, Mueller SJ, Hoernstein SNW, Porankiewicz-Asplund J, Vervliet-Scheebaum M, Reski R (2011). Simultaneous isolation of pure and intact chloroplasts and mitochondria from moss as the basis for sub-cellular proteomics. Plant Cell Rep 30:205-215. doi: 10.1007/s00299-010-0935-4

Lang D, Ullrich KK, Murat F, Fuchs J, Jenkins J, Haas FB, Piednoel M, Gundlach H, Van Bel M, Meyberg R, Vives C, Morata J, Symeonidi A, Hiss M, Muchero W, Kamisugi Y, Saleh O, Blanc G, Decker EL, van Gessel N, Grimwood J, Hayes RD, Graham SW, Gunter LE, McDaniel SF, Hoernstein SNW, Larsson A, Li FW, Perroud PF, Phillips J, Ranjan P, Rokshar DS, Rothfels CJ, Schneider L, Shu S, Stevenson DW, Thümmler F, Tillich M, Villarreal Aguilar JC, Widiez T, Wong GKS, Wymore A, Zhang Y, Zimmer AD, Quatrano RS, Mayer KFX, Goodstein D, Casacuberta JM, Vandepoele K, Reski R, Cuming AC, Tuskan GA, Maumus F, Salse J, Schmutz J, Rensing SA (2018) The *Physcomitrella patens* chromosome-scale assembly reveals moss genome structure and evolution. Plant J 93:515-533. doi: 10.1111/tpj.13801

Li XJ, Cai WG, Liu YL, Li H, Fu LW, Liu ZY, Xu L, Liu HT, Xu TD, Xiong Y (2017) Differential TOR activation and cell proliferation in *Arabidopsis* root and shoot apexes. Proc Natl Acad Sci USA 114:2765-2770. doi: 10.1073/pnas.1618782114

Liu YL, Xiong Y (2022) Plant target of rapamycin network: complexes, conservations and specificities. J Integr Plant Bio 64:342-370. doi: 10.1111/jipb.13212

Liu Q, Hao T, Lin Z, Fang YP, Li L, Huang DQ, Wu JB, Zhao YC, Zhang X (2024) AZD8055 is more effective than rapamycin in inhibiting proliferation and promoting mitochondrial clearance in erythroid differentiation. Anal Cell Patho 2024:2639464. doi: 10.1155/2024/2639464

Liu YL, Hu J, Duan XL, Ding WL, Xu ML, Xiong Y (2025) Target of Rapamycin (TOR): A master regulator in plant growth, development, and stress responses. Ann Rev Plant Bio 76:341-371. doi: 10.1146/annurev-arplant-083123-050311

Loewith R, Jacinto E, Wullschleger S, Lorberg A, Crespo JL, Bonenfant D, Oppliger W, Jenoe P, Hall MN (2002) Two TOR complexes, only one of which is rapamycin

sensitive, have distinct roles in cell growth control. Mol Cell 10:457-468. doi: 10.1016/S1097-2765(02)00636-6

Loewith R, Hall MN (2011) Target of rapamycin (TOR) in nutrient signalling and growth control. Genet 189:1177-1201. doi: 10.1534/genetics.111.1333363

Lorenz S, Tintelnot S, Reski R, Decker EL (2003) Cyclin D-knockout uncouples developmental progression from sugar availability. Plant Mol Bio 53:227-236.doi: 10.1023/B:PLAN.0000009295.07016.87

Lueth VM, Reski R (2023) Mosses. Curr Bio 33:R1175-R1181. doi: 10.1016/j.cub.2023.09.042

Lüth VM, Rempfer C, van Gessel N, Herzog O, Hanser M, Braun M, Decker EL, Reski R (2023) A Physcomitrella PIN protein acts in spermatogenesis and sporophyte retention. New Phytol 237:2118-2135. doi: 10.1111/nph.18691

Maegawa K, Takii R, Ushimaru T, Kozaki A (2015) Evolutionary conservation of TORC1 components, TOR, Raptor, and LST8, between rice and yeast. Mol Gen Genom 290:2019-2030. doi: 10.1007/s00438-015-1056-0

Mao L, Kawaide H, Higuchi T, Chen M, Miyamoto K, Hirata Y, Kimura H, Miyazaki S, Teruya M, Fujiwara K, Tomita K, Yamane H, Hayashi K-I, Nojiri H, Jia L, Qiu J, Ye C, Timko MP, Fan L, Okada K (2020) Genomic evidence for convergent evolution of gene clusters for momilactone biosynthesis in land plants. Proc Natl Acad Sci USA 117:12472–12480. doi: 10.1073/pnas.1914373117

Marchant DB, Chen G, Cai S, Chen F, Schafran P, Jenkins J, Shu S, Plott C, Webber J, Lovell JT, He G, Sandor, L, Williams, M, Rajasekar S, Healey A, Barry K, Zhang Y, Sessa E, Dhakal RR, Wolf PG, Harkess A, Li FW, Rössner C, Becker A, Gramzow L, Xue D, Wu Y, Tong T, Wang Y, Dai F, Hua S, Wang H, Xu S, Xu F, Duan H, Theißen G, McKain MR, Li Z, McKibben MTW, Barker MS, Schmitz RJ, Stevenson DW, Zumajo-Cardona C, Ambrose BA, Leebens-Mack JH, Grimwood J, Schmutz J, Soltis PS, Soltis DE, Chen ZH (2022) Dynamic genome evolution in a model fern. Nat Plants 8:1038–1051. doi: 10.1038/s41477-022-01226-7

Medina R, Johnson MG, Liu Y, Wickett NJ, Shaw AJ, Goffinet B (2019) Phylogenomic delineation of *Physcomitrium* (Bryophyta: Funariaceae) based on targeted sequencing

of nuclear exons and their flanking regions rejects the retention of *Physcomitrella*, *Physcomitridium* and *Aphanorrhegma*. J Syst Evol 57:404-417. doi: 10.1111/jse.12516

Menand B, Desnos T, Nussaume L, Berger F, Bouchez D, Meyer C, Robaglia C (2002) Expression and disruption of the *Arabidopsis TOR* (target of rapamycin) gene. Proc Natl Acad Sci USA 99:6422-6427. doi: 10.1073/pnas.09214899

Miki T, Nakaoka Y, Goshima G (2016) Live cell microscopy-based RNAi screening in the moss *Physcomitrella patens*. Meth Mol Bio 1470:225-246. doi: 10.1007/978-1-4939-6337-9_18

Montané MH, Menand B (2013) ATP-competitive mTOR kinase inhibitors delay plant growth by triggering early differentiation of meristematic cells but no developmental patterning. J Exp Bot 64:4361-4374. doi: 10.1093/jxb/ert242

Moreau M, Azzopardi M, Clément G, Dobrenel T, Marchive C, Renne C, Martin-Magniette ML, Taconnat L, Renou JP, Robaglia C, Meyer C (2012) Mutations in the *Arabidopsis* homolog of LST8/GβL, a partner of the Target of Rapamycin kinase, impair plant growth, flowering, and metabolic adaptation to long days. Plant Cell 24:463-481. doi: 10.1105/tpc.111.091306

Nakaoka Y, Miki T, Fujioka R, Uehara R, Tomioka A, Obuse C, Kubo M, Hiwatashi Y, Goshima G (2012) An inducible RNA interference system in *Physcomitrella patens* reveals a dominant role of augmin in phragmoplast microtubule generation. Plant Cell 24:1478-1493. doi: 10.1105/tpc.112.098509

Neufeld TP (2010) TOR-dependent control of autophagy: biting the hand that feeds. Curr Op Cell Bio 22:157-168. doi: 10.1016/j.ceb.2009.11.005

Niederau PA, Eglé P, Willig S, Parsons J, Hoernstein SNW, Decker EL, Reski R (2024) Multifactorial analysis of terminator performance on heterologous gene expression in Physcomitrella. Plant Cell Rep 43:43. doi: 10.1007/s00299-023-03088-5

Noy-Malka C, Yaari R, Itzhaki R, Mosquna A, Gershovitz NA, Katz A, Ohad N (2014) A single CMT methyltransferase homolog is involved in CHG DNA methylation and development of *Physcomitrella patens*. Plant Mol Bio 84:719-735. doi: 10.1007/s11103-013-0165-6

Okano Y, Aono N, Hiwatashi Y, Murata T, Nishiyama T, Ishikawa T, Kubo M, Hasebe M (2009) A polycomb repressive complex 2 gene regulates apogamy and gives evolutionary insights into early land plant evolution. Proc Natl Acad Sci USA 106:16321-16326. doi: 10.1073/pnas.0906997106

Ostendorf AK, van Gessel N, Malkowsky Y, Sabovljevic MS, Rensing SA, Roth-Nebelsick A, Reski R (2021) Polyploidization within the Funariaceae – a key principle behind speciation, sporophyte reduction and the high variance of spore diameters? Bryoph Divers Evol 43:164-179. doi: 10.11646/BDE.43.1.13

Pandurangan AP, Stahlhacke J, Oates ME, Smithers B, Gough J (2018) The SUPERFAMILY 2.0 database: a significant proteome update and a new webserver. Nucl Acids Res 47:D490-D494. doi: 10.1093/nar/gky1130

Paysan-Lafosse T, Andreeva A, Blum M, Chuguransky S, Grego T, Lazaro Pinto B, Salazar GA, Bileschi ML, Llinares-López F, Meng-Papaxanthos L, Colwell LJ, Grishin NV, Schaeffer RD, Clementel D, Tosatto SCE, Sonnhammer E, Wood V, Bateman A (2024) The Pfam protein families database: embracing AI/ML. Nucl Acids Res 53:D523-D534. doi: 10.1093/nar/gkae997

Perdoux R, Barrada A, Boulaiz M, Garau C, Belbachir C, Lecampion C, Montané MH, Menand B (2024) A drug-resistant mutation in plant target of rapamycin validates the specificity of ATP-competitive TOR inhibitors *in vivo*. Plant J 117:1344-1355. doi: 10.1111/tpj.16564

Perez-Riverol Y, Bandla C, Kundu DJ, Kamatchinathan S, Bai J, Hewapathirana S, John NS, Prakash A, Walzer M, Wang S, Vizcaíno, JA (2025) The PRIDE database at 20 years: 2025 update. Nucl Acids Res 53:D543-D553. doi: 10.1093/nar/gkae1011

Primo C, Navarre C, Chaumont F, André B (2022) Plasma membrane H^+-ATPases promote TORC1 activation in plant suspension cells. iScience 25:104238. doi: 10.1016/j.isci.2022.104238

R Core Team (2025). R: A language and environment for statistical computing. R Foundation for Statistical Computing, Vienna, Austria. https://www.R-project.org

Rappsilber J, Mann M, Ishihama Y (2007) Protocol for micro-purification, enrichment, pre-fractionation and storage of peptides for proteomics using StageTips. Nat Protocols 2:1896-1906. doi: 10.1038/nprot.2007.261

Reinke A, Anderson S, McCaffery JM, Yates J III, Aronova S, Chu S, Fairclough S, Iverson C, Wedaman KP, Powers T (2004) TOR complex 1 includes a novel component, Tco89p (YPL180w), and cooperates with Ssd1p to maintain cellular integrity in *Saccharomyces cerevisiae*. J Biol Chem 279:14752-14762. doi: 10.1074/jbc.M313062200

Ren MZ, Venglat P, Qiu SQ, Feng L, Cao YG, Wang E, Xiang DQ, Wang JH, Alexander D, Chalivendra S, Logan D, Mattoo A, Selvaraj G, Datla R (2012) Target of Rapamycin signaling regulates metabolism, growth, and life span in *Arabidopsis*. Plant Cell 24:4850-4874. doi: 10.1105/tpc.112.107144

Rensing SA, Goffinet B, Meyberg R, Wu SZ, Bezanilla M (2020) The moss *Physcomitrium* (*Physcomitrella*) *patens*: A model organism for non-seed plants. Plant Cell 32:1361-1376. doi: 10.1105/tpc.19.00828

Resemann HC, Herrfurth C, Feussner K, Hornung E, Ostendorf AK, Gömann J, Mittag J, van Gessel N, de Vries J, Ludwig-Müller J, Markham J, Reski R, Feussner I (2021) Convergence of sphingolipid desaturation across over 500 million years of plant evolution. Nat Plants 7:219-232. doi: 10.1038/s41477-020-00844-3

Reski R (1998) Development, genetics and molecular biology of mosses. Bot Acta 111:1-15. doi: 10.1111/j.1438-8677.1998.tb00670.x

Reski R (2018) Quantitative moss cell biology. Curr Op Plant Bio 46:39-47. doi: 10.1016/j.pbi.2018.07.005

Reski R, Abel WO (1985) Induction of budding on chloronemata and caulonemata of the moss, *Physcomitrella patens*, using isopentenyladenine. Planta 165:354-358. doi: 10.1007/BF00392232

Reski R, Cove DJ (2004) *Physcomitrella patens*. Curr Bio 14:R261-R262. doi: 10.1016/j.cub.2004.03.016

Ruiz-Molina N, Parsons J, Schroeder S, Posten C, Reski R, Decker EL (2022) Process engineering of biopharmaceutical production in moss bioreactors via model-based

description and evaluation of phytohormone impact. Front Bioeng Biotech 10:837965. doi: 10.3389/fbioe.2022.837965

Saliba E, Evangelinos M, Gournas C, Corrillon F, Georis I, André B (2018) The yeast H^+-ATPase Pma1 promotes Rag/Gtr-dependent TORC1 activation in response to H^+-coupled nutrient uptake. eLife 7:e31981. doi: 10.7554/eLIFE.31981

Saliba E, Primo C, Guarini N, André B (2021) A plant plasma-membrane H^+-ATPase promotes yeast TORC1 activation via its carboxy-terminal tail. Sci Rep 11:4788. doi: 10.1038/s41598-021-83525-1

Sambrook J, Russell DW (2006) Standard ethanol precipitation of DNA in microcentrifuge tubes. CSH Protocols 2006:1116-1120. doi: 10.1101/pdb.prot4456

Shteynberg DD, Deutsch EW, Campbell DS, Hoopmann MR, Kusebauch U, Lee D, Mendoza L, Midha MK, Sun Z, Whetton AD, Moritz RL (2019) PTMProphet: Fast and accurate mass modification localization for the trans-proteomic pipeline. J Proteome Res 18:4262–4272. doi: 10.1021/acs.jproteome.9b00205

The M, MacCoss MJ, Noble WS, Käll L (2016) Fast and accurate protein false discovery rates on large-scale proteomics data sets with Percolator 3.0. J Am Soc Mass Spec 27:1719-1727. doi: 10.1007/s13361-016-1460-7

Roux PP, Shahbazian D, Vu H, Holz MK, Cohen MS, Taunton J, Sonnenberg N, Blenis J (2007) RAS/ERK signalling promotes site-specific ribosomal protein S6 phosphorylation via RSK and stimulates cap-dependent translation. J Biol Chem 282:14056-14064. doi: 10.1074/jbc.M700906200

Ruibal C, Castro A, Fleitas AL, Quezada J, Quero G, Vidal S (2020) A chloroplast COR413 protein from *Physcomitrella patens* is required for growth regulation under high light and ABA responses. Front Plant Sci 11:845. doi: 10.3389/fpls.2020.00845

Schepetilnikov M, Kobayashi K, Geldreich A, Caranta C, Robaglia C, Keller M, Ryabova LA (2011) Viral factor TAV recruits TOR/S6K1 signalling to activate reinitiation after long ORF translation. EMBO J 30:1343-1356. doi: 10.1038/emboj.2011.39

Schween G, Gorr G, Hohe A, Reski R (2003) Unique tissue-specific cell cycle in *Physcomitrella*. Plant Bio 5:50-58. doi: 10.1055/s-2003-37984

Schween G, Egener T, Fritzowsky D, Granado J, Guitton MC, Hartmann N, Hohe A, Holtorf H, Lang D, Lucht JM, Reinhard C, Rensing SA, Schlink K, Schulte J, Reski R (2005) Large-scale analysis of 73,329 *Physcomitrella* plants transformed with different gene disruption libraries: Production parameters and mutant phenotypes. Plant Bio 7:228-237. doi: 10.1055/s-2005-837692

Sehgal SN, Baker H, Vezina C (1975) Rapamycin (AY-22,989), a new antifungal antibiotic. 2. Fermentation, isolation and characterization. J Antibiot 28:727-732. doi: 10.7164/antibiotics.28.727

Sievers F, Higgins DG (2018) Clustal Omega for making accurate alignments of many protein sequences. Protein Sci 27:135-145. doi: 10.1002/pro.3290

Sormani R, Yao L, Menand B, Ennar N, Lecampion C, Meyer C, Robaglia C (2007) *Saccharomyces cerevisiae* FKBP12 binds *Arabidopsis thaliana* TOR and its expression in plants leads to rapamycin susceptibility. BMC Plant Bio 7:26. doi: 10.1186/1471-2229-7-26

Steger M, Demichev V, Backmann M, Ohmayer U, Ihmor P, Müller S, Ralser M, Daub H (2021) Time-resolved *in vivo* ubiquitinome profiling by DIA-MS reveals USP7 targets on a proteome-wide scale. Nat Comm 12:5399. doi: 10.1038/s41467-021-25454-1

Strepp R, Scholz S, Kruse S, Speth V, Reski R (1998) Plant nuclear gene knockout reveals a role in plastid division for the homolog of the bacterial cell division protein FtsZ, an ancestral tubulin. Proc Natl Acad Sci USA 95:4368-4373. doi: 10.1073/pnas.95.8.4368

Tatebe H, Shiozaki K (2017) Evolutionary conservation of the components in the TOR signaling pathways. Biomolec 7:77. doi: 10.3390/biom7040077

Thomas PD, Ebert D, Muruganujan A, Mushayahama T, Albou LP, Mi H (2022) PANTHER: Making genome-scale phylogenetics accessible to all. Protein Sci 31:8-22. doi: 10.1002/pro.4218

Tuskan GA, Difazio S, Jansson S, Bohlmann J, Grigoriev I, Hellsten U, Putnam N, Ralph S, Rombauts S, Salamov A, Schein J, Sterck L, Aerts A, Bhalerao RR, Bhalerao RP, Blaudez D, Boerjan W, Brun A, Brunner A, Busov V, Campbell M, Carlson J, Chalot M, Chapman J, Chen GL, Cooper D, Coutinho PM, Couturier J, Covert S, Cronk

Q, Cunningham R, Davis J, Degroeve S, Déjardin A, Depamphilis C, Detter J, Dirks B, Dubchak I, Duplessis S, Ehlting J, Ellis B, Gendler K, Goodstein D, Gribskov M, Grimwood J, Groover A, Gunter L, Hamberger B, Heinze B, Helariutta Y, Henrissat B, Holligan D, Holt R, Huang W, Islam-Faridi N, Jones S, Jones-Rhoades M, Jorgensen R, Joshi C, Kangasjärvi J, Karlsson J, Kelleher C, Kirkpatrick R, Kirst M, Kohler A, Kalluri U, Larimer F, Leebens-Mack J, Leplé JC, Locascio P, Lou Y, Lucas S, Martin F, Montanini B, Napoli C, Nelson DR, Nelson C, Nieminen K, Nilsson O, Pereda V, Peter G, Philippe R, Pilate G, Poliakov A, Razumovskaya J, Richardson P, Rinaldi C, Ritland K, Rouzé P, Ryaboy D, Schmutz J, Schrader J, Segerman B, Shin H, Siddiqui A, Sterky F, Terry A, Tsai CJ, Uberbacher E, Unneberg P, Vahala J, Wall K, Wessler S, Yang G, Yin T, Douglas C, Marra M, Sandberg G, Van de Peer Y, Rokhsar D (2006) The genome of black cottonwood, *Populus trichocarpa* (Torr. & Gray). Science 313:1596-1604. doi: 10.1126/science.1128691

Upadhyaya S, Rao BJ (2019) Reciprocal regulation of photosynthesis and mitochondrial respiration by TOR kinase in *Chlamydomonas reinhardtii*. Plant Direct 3:e00184. doi: 10.1002/pld3.184

Van Leene J, Han C, Gadeyne A, Eeckhout D, Matthijs C, Cannoot B, De Winne N, Persiau G, Van de Slijke E, Van de Cotte B, Stes E, Van Bel M, Storme V, Impens F, Gevaert K, Vandepoele K, De Smet I, De Jaeger G (2019) Capturing the phosphorylation and protein interaction landscape of the plant TOR kinase. Nat Plants 5:316-327. doi: 10.1038/s41477-019-0378-z

Vezina C, Kudelski A, Sehgal SN (1975) Rapamycin (AY-22,989), a new antifungal antibiotic. 1. Taxonomy of producing streptomycete and isolation of active principle. J Antibiot 28:721-726. doi: 10.7164/antibiotics.28.721

vragh (2022) vragh/seqvisr: v0.2.7. Zenodo. doi: 10.5281/zenodo.7342841

Wang X, Liu ZZ, Yuan DY, Lu YJ, Chen S, He XJ (2025) Nutrient-driven TOR signaling controls a chromatin-associated complex for orchestrating plant growth and stress tolerance. Nat Plants 11:2115-2129. doi: 10.1038/s41477-025-02107-5

Waterhouse AM, Procter JB, Martin DMA, Clamp M, Barton GJ (2009) Jalview Version 2 – a multiple sequence alignment editor and analysis workbench. Bioinform 25:1189-1191. doi: 10.1093/bioinformatics/btp033

Weeks Z, Chaturvedi G, Day E, Kelly S, Moody LA (2025) A FLOE-related protein regulates the two-dimensional to three-dimensional growth transition in the moss *Physcomitrium patens*. Development 152:dev204508. doi: 10.1242/dev.204508

Weisman R, Choder M, Koltin Y (1997) Rapamycin specifically interferes with the developmental response of fission yeast to starvation. J Bac 179:6325-6334. doi: 10.1128/jb.179.20.6325-6334.1997

Wiedemann G, van Gessel N, Köchl F, Hunn L, Schulze K, Maloukh L, Nogue F, Decker EL, Hartung F, Reski R (2018) RecQ helicase function in development, DNA repair, and gene targeting in *Physcomitrella patens*. Plant Cell 30:717-736. doi: 10.1105/tpc.17.00632

Wullschleger S, Loewith R, Oppliger W, Hall MN (2005) Molecular organization of target of rapamycin complex 2. J Bio Chem 280:30697-30704. doi: 10.1074/jbc.M505553200

Xiong Y, Sheen J (2012) Rapamycin and glucose-target of rapamycin (TOR) protein signaling in plants. J Bio Chem 287:2836-2842. doi: 10.1074/jbc.M111.300749

Xiong FJ, Dong P, Liu M, Xie GX, Wang K, Zhuo FP, Feng L, Yang L, Li ZG, Ren MZ (2016) Tomato FK506 Binding Protein 12KD (FKBP12) mediates the interaction between rapamycin and Target of Rapamycin (TOR). Front Plant Sci 7:1746. doi: 10.3389/fpls.2016.01746

Xu Q, Liang S, Kudla J, Luan S (1998) Molecular characterization of a plant FKBP12 that does not mediate action of FK506 and rapamycin. Plant J 15:511-519. doi: 10.1046/j.1365-313X.1998.00232.x

Yang KL, Yu F, Teo GC, Li K, Demichev V, Ralser M, Nesvizhskii AI (2023) MSBooster: improving peptide identification rates using deep learning-based features. Nat Comm 14:4539. doi: 10.1038/s41467-023-40129-9

Yang HJ, Rudge DG, Koos JD, Vaidialingam B, Yang HJ, Pavletich NP (2013) mTOR kinase structure, mechanism and regulation. Nature 497:217-223. doi: 10.1038/nature.12122

Yu FC, Teo GC, Kong AT, Fröhlich K, Li GX, Demichev V, Nesvizhskii AI (2023) Analysis of DIA proteomics data using MSFragger and FragPipe computational platform. Nat Comm 14:4154. doi: 10.1038/s41467-023-39869-5

Zhang J, Fu XX, Li RQ, Zhao X, Liu Y, Li MH, Zwaenepoel A, Ma H, Goffinet B, Guan YL, Xue JY, Liao YY, Wang QF, Wang QH, Wang QH, Wang JY, Zhang GQ, Wang ZW, Jia Y, Wang MZ, Dong SS, Yang JF, Jiao YN, Guo YL, Kong HZ, Lu AM, Yang HM, Zhang SZ, Van de Peer Y, Liu ZJ, Chen ZD (2020) The hornwort genome and early land plant evolution. Nat Plants 6:107-118. doi: 10.1038/s41477-019-0588-4

Zhu TT, Li LX, Chang HM, Zhan JS, Ren MZ (2022) Target of Rapamycin regulates photosynthesis and cell growth in *Auxenochlorella pyrenoidosa*. Int J Mol Sci 23:11309. doi: 10.3390/ijms231911309

Supplementary information

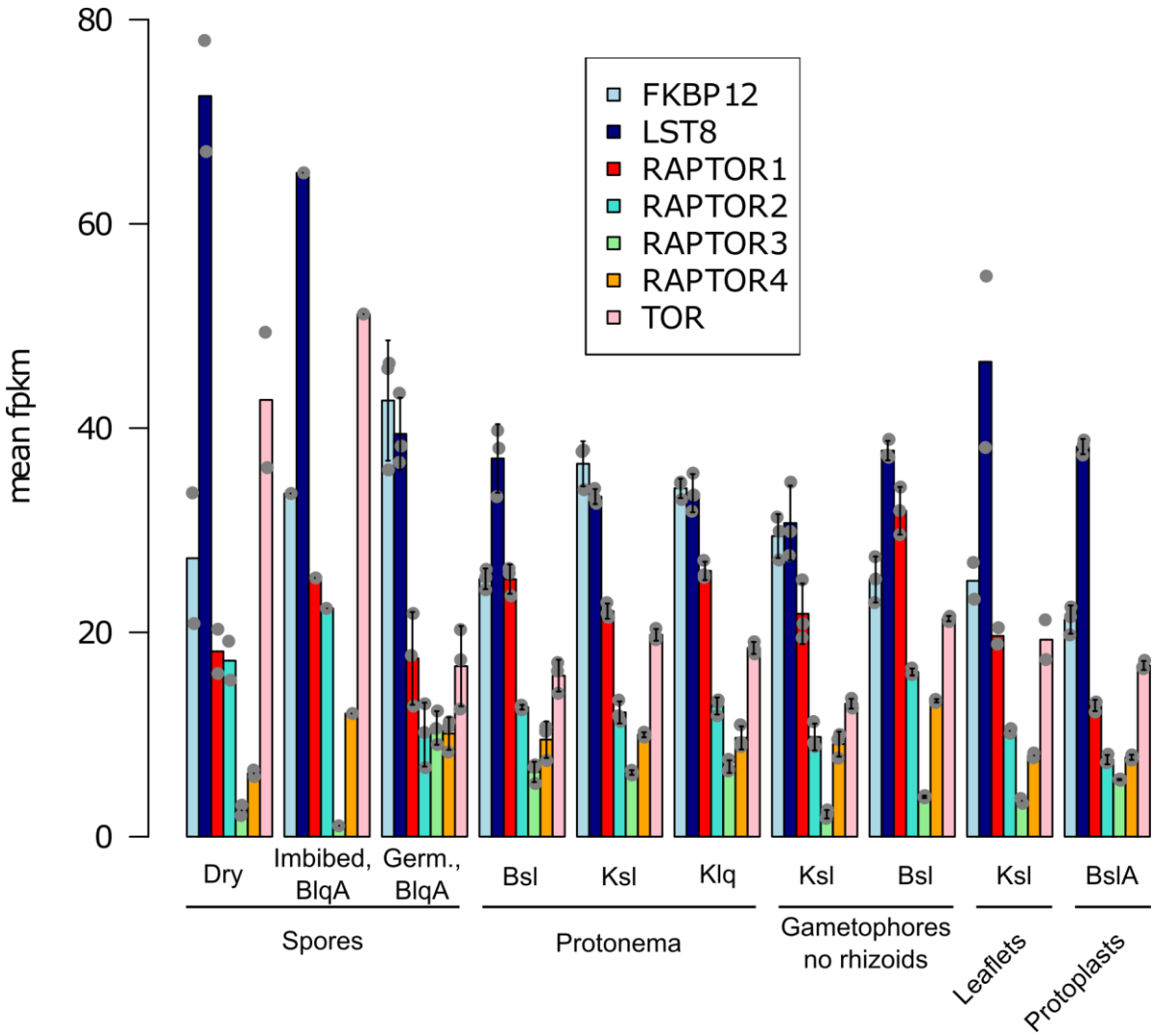

Supplementary Figure S1 Expression levels of TORC1 component genes in Physcomitrella at different culture conditions and developmental stages. Expression data were retrieved from *PEATmoss* (https://peatmoss.plantcode.cup.uni-freiburg.de/expression_viewer/input). Values represent mean FPKM values (Fragments Per Kilobase Million) and standard deviation. Data points represent biological replicates. Abbreviations: B = BCD medium; lq = liquid; A = ammonium tartrate; sl = solid; K = Knop medium; Germ. = germinating.

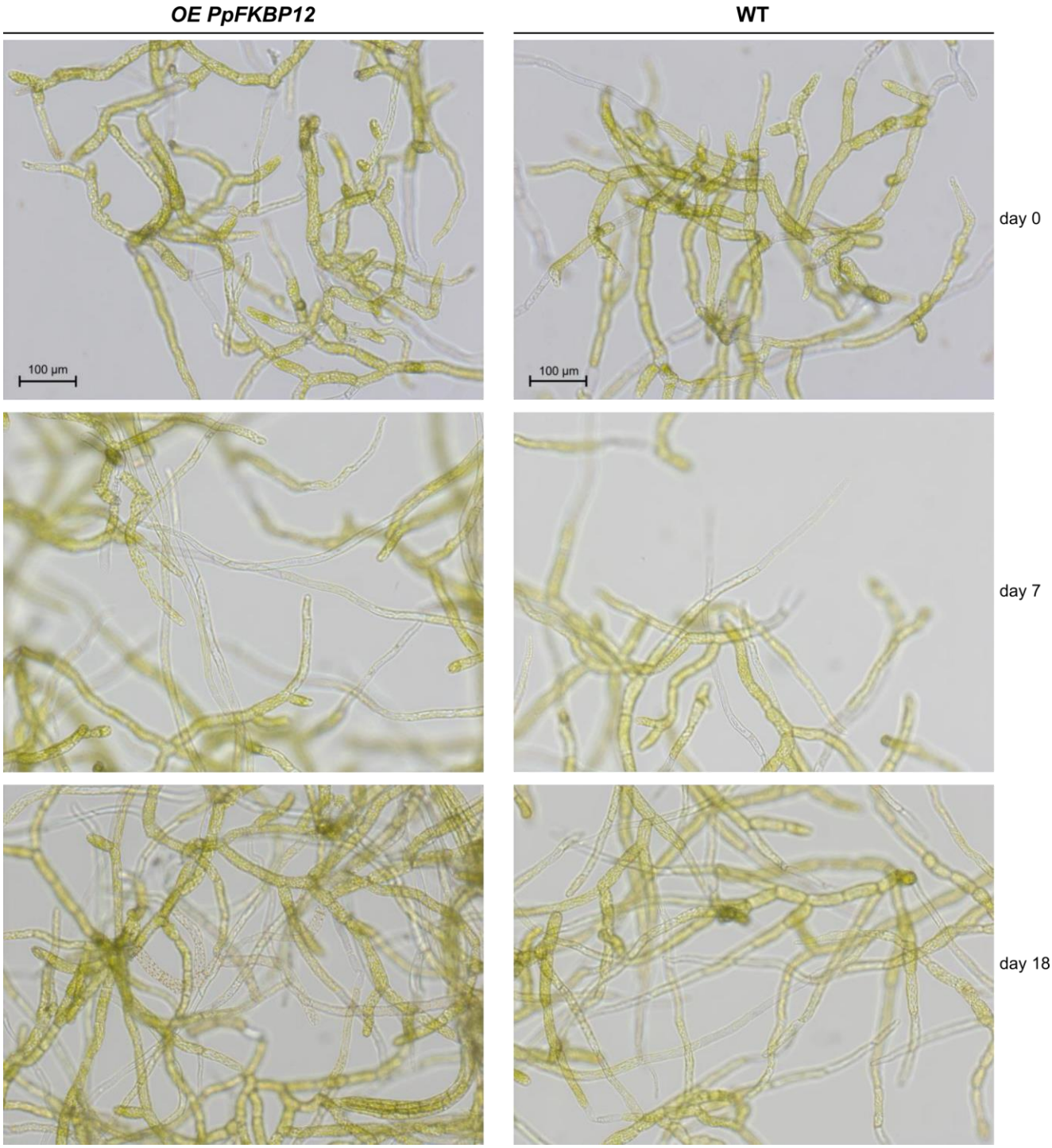

Supplementary Figure S2 Caulonema frequency increased with incubation time. Light microscopy images of protonemata in suspension cultures treated with DMSO 0.01 % and incubated for 7 and 18 days. Culture conditions are similar to those in Figure 1.

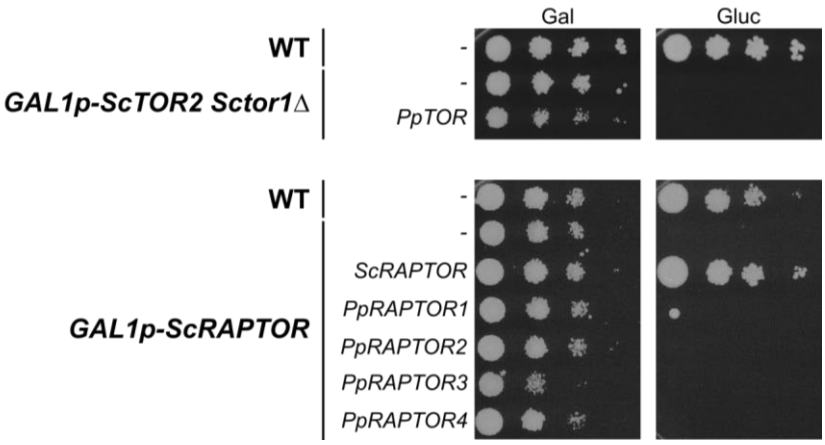

Supplementary Figure S3 Complementation of the yeast *tor* and *raptor* mutants with their Physcomitrella homologs.

A Wild-type TB50a yeast strain and mutant SW137-4b expressing *ScTOR2* from the galactose-inducible GAL1 promoter were initially grown as suspensions in rich medium containing galactose as a carbon source (YPGal). Strains were transformed with pESPB019 (empty vector) or pESPB022 (pESPB019-derived vector expressing *PpTOR*) and selected on SGal-Leu plates. Selected transformants were grown for 6 h at 30°C in SD-Leu suspension cultures. Cultures were normalized to an OD (660 nm) of 0.2, subjected to 10-fold serial dilutions, and 15 µl of each dilution were spotted onto SGal-Leu or SD-Leu plates, which were incubated at 30°C for 5 days. Plates were scanned upside down with the lid open on a Canon CanoScan 9000F scanner. **B** Same growth conditions as in panel A. Strain RL93a expressing yeast *RAPTOR* from the GAL1 promoter was transformed with pESPB019 (empty vector), pESPB019-derived vectors each containing one of the Physcomitrella RAPTOR paralogs (pESPB024, pESPB026, pESPB029, and pESPB032), or pCHD001 expressing *ScRAPTOR*.

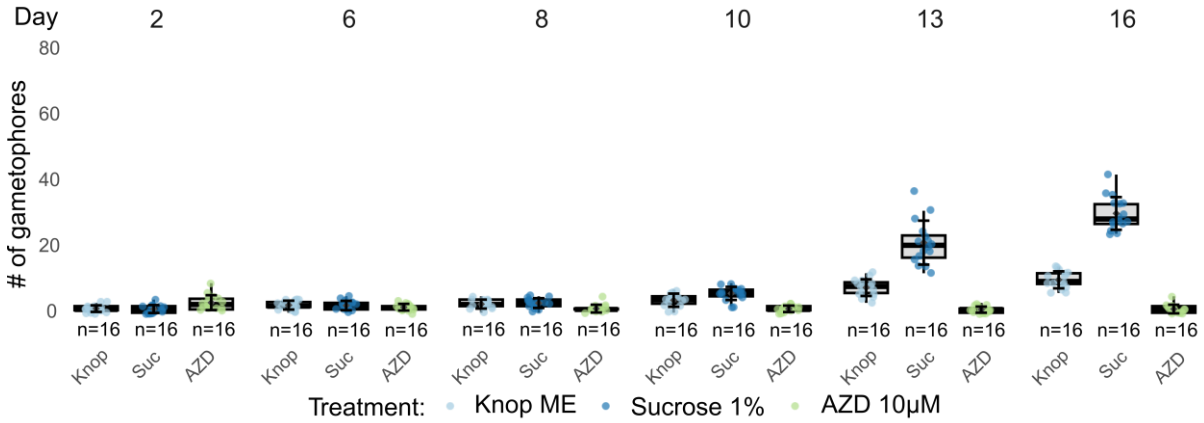

Supplementary Figure S4 Gametophore counts over time in Physcomitrella WT. Protonema at a density of 440 mg DW/L was spotted on solid medium plates (15 µL) containing either only Knop ME or additionally 1% Sucrose or 10 µM AZD8055. Arising gametophores were counted over 16 days. Each data point represents a single spot at which gametophores were counted. n = 16 colonies per treatment.

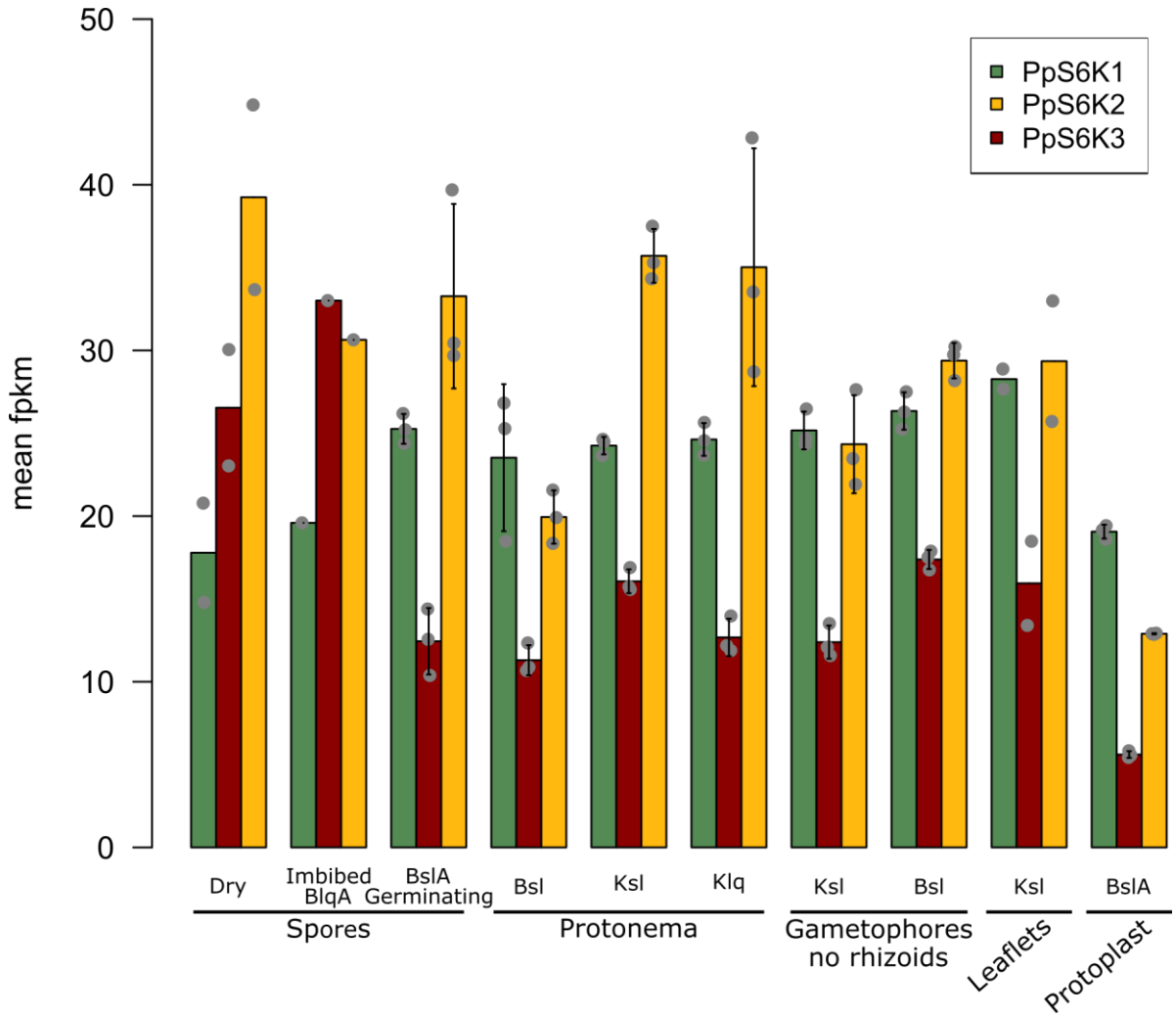

Supplementary Figure S5 Expression levels of *PpS6K* genes in Physcomitrella at different culture conditions and developmental stages.

Expression data were retrieved from *PEATmoss* (https://peatmoss.plantcode.cup.uni-freiburg.de/expression_viewer/input). Values represent mean FPKM values (Fragments Per Kilobase Million) and standard deviation. Data points represent biological replicates. Abbreviations: B = BCD medium; lq = liquid; A = ammonium tartrate; sl = solid; K = Knop medium; Germ. = germinating. PpS6K1: Pp3c12_22360V3.1; PpS6K2: Pp3c25_14820V3.1; PpS6K3: Pp3c16_24840V3.1

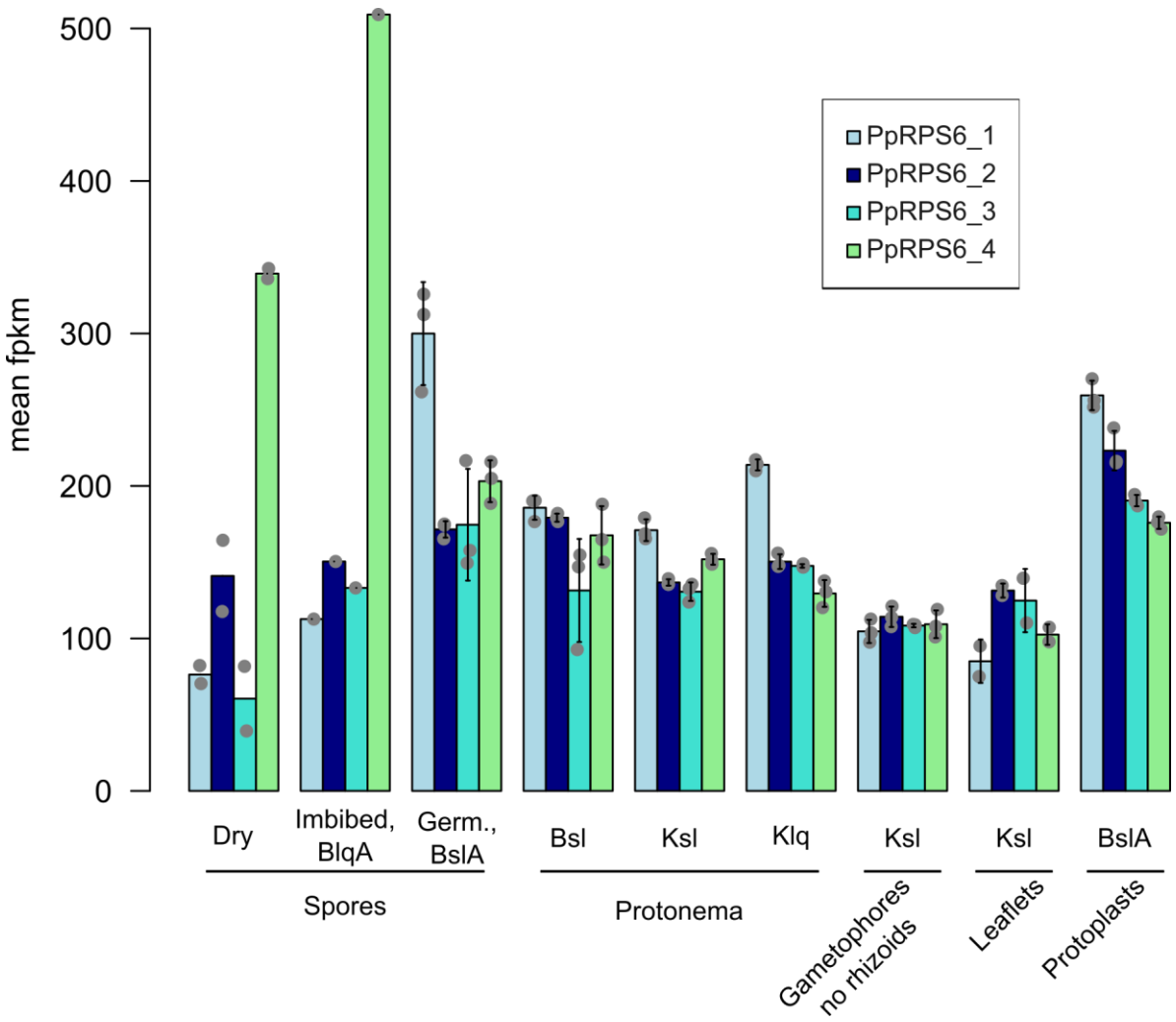

Supplementary Figure S6 Expression levels of *PpRPS6* genes in Physcomitrella at different culture conditions and developmental stages.

Expression data were retrieved from *PEATmoss* (https://peatmoss.plantcode.cup.uni-freiburg.de/expression_viewer/input). Values represent mean FPKM values (Fragments Per Kilobase Million) and standard deviation. Data points represent biological replicates. Abbreviations: B = BCD medium; lq = liquid; A = ammonium tartrate; sl = solid; K = Knop medium; Germ. = germinating. PpRPS6_1: Pp3c11_21120V3.1; PpRPS6_2: Pp3c15_25430V3.1; PpRPS6_3: Pp3c15_25780V3.1; PpRPS6_4: Pp3c7_5780V3.1

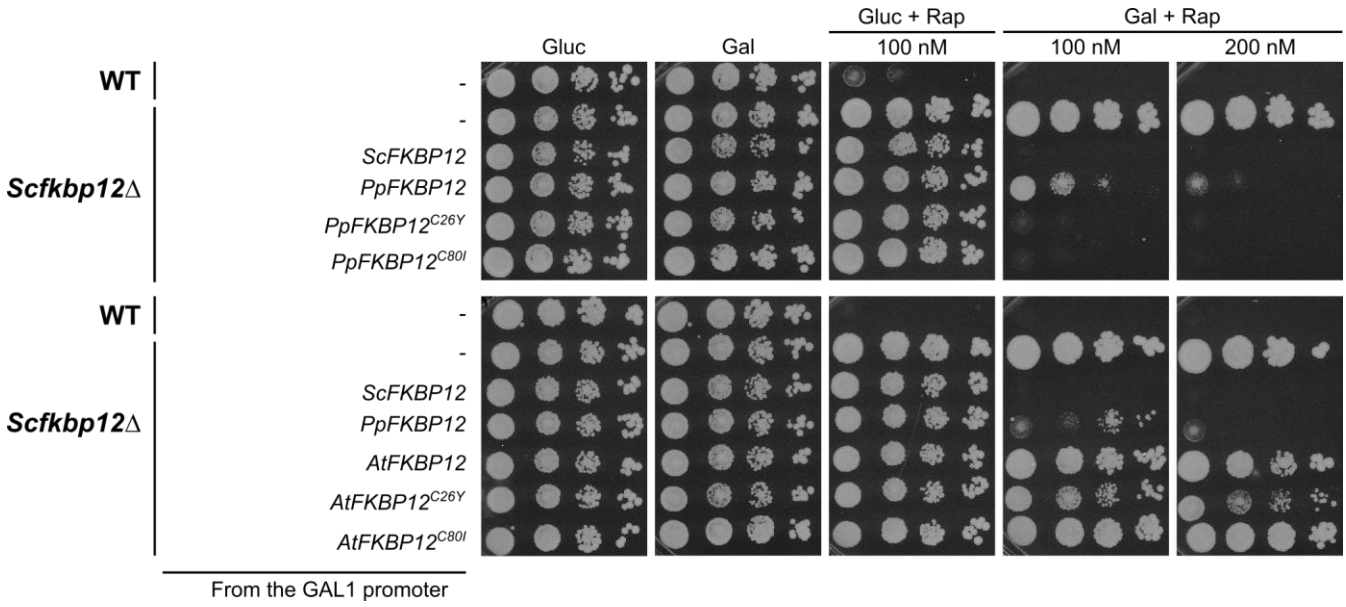

Supplementary Figure S7 Yeast complementation assay of the *fkbp12Δ* mutant with mutant FKBP12 variants from Physcomitrella and Arabidopsis.

Wild-type MH272-3c yeast strain transformed with an empty vector (p415 GAL1), and mutant MH274-1a (*fkbp12Δ*) strain transformed with either p415 GAL1 or p415 GAL1-derived vectors expressing different *FKBP12* variants, were grown in SD-Leu or SGal-Leu suspension cultures. Cultures were normalized to an optical density (OD) at 660 nm of 0.1, subjected to 10-fold serial dilutions, and 15 µL of each dilution were spotted onto SD-Leu or SGal-Leu plates supplemented with DMSO (0.02%) or with rapamycin at 100 or 200 nM. Plates were incubated at 30°C for 5 days.

Supplementary Table S1

Primers used to clone *ScFKBP12*, *PpFKBP12* WT and mutants in p415 GAL1 restricted with XbaI and XhoI. Grey font colours indicate that the primers have been re-used.

Plasmid	DNA template	Primer name	Primer sequence
pESPB001	Yeast gDNA	5_Cl_ScFKBP12	ACGTCAAGGAGAAAAAACCCCGGATTCTAGAatgtctgaagtaattgaaggtaac
		3_Cl_ScFKBP12	AAGCGTGACATAACTAATTACATGACTCGAGttagttgaccttcaacaattcgac
pESPB003	Physcomitrella cDNA	5_Cl_PpFKBP12wt	ACGTCAAGGAGAAAAAACCCCGGATTCTAGAatggggtacgagaaagaaatc
		3_Cl_PpFKBP12wt	AAGCGTGACATAACTAATTACATGACTCGAGtcactgggcgctgagc
pESPB006	pESPB003	5_Cl_PpFKBP12wt	ACGTCAAGGAGAAAAAACCCCGGATTCTAGAatggggtacgagaaagaaatc
		3_Cl_57_PpFKBP12C26Y	GAACTTCTCATTCAGGTCCCTATTCTTGCCATAGCCGGTGTagtggacagtgacggtttg
		5_Cl_57_PpFKBP12C26Y	CAAACCGTCACTGTCCACTAcaccggctatggcaagaatagggacctgaatgagaagttc
		3_Cl_PpFKBP12wt	AAGCGTGACATAACTAATTACATGACTCGAGtcactgggcgctgagc
pESPB008	pESPB003	5_Cl_PpFKBP12wt	ACGTCAAGGAGAAAAAACCCCGGATTCTAGAatggggtacgagaaagaaatc
		3_Cl_77_PpFKBP12W40D	GCCAGGGTCCTTTGTACTATCgaacttctcattcaggtccctattcttgccatagccggtg
		5_Cl_77_PpFKBP12W40D	CACCGGCTATGGCAAGAATAGGGACCTGAATGAGAAGTTCGATagtacaaaggaccctggc
		3_Cl_PpFKBP12wt	AAGCGTGACATAACTAATTACATGACTCGAGtcactgggcgctgagc
pESPB010	pESPB003	5_Cl_PpFKBP12wt	ACGTCAAGGAGAAAAAACCCCGGATTCTAGAatggggtacgagaaagaaatc
		3_Cl_57_PpFKBP12C26Y	GAACTTCTCATTCAGGTCCCTATTCTTGCCATAGCCGGTGTagtggacagtgacggtttg
		5_Cl_77_PpFKBP12W40D	CACCGGCTATGGCAAGAATAGGGACCTGAATGAGAAGTTCGATagtacaaaggaccctggc
		3_Cl_PpFKBP12wt	AAGCGTGACATAACTAATTACATGACTCGAGtcactgggcgctgagc
pESPB012	pESPB003	5_Cl_PpFKBP12wt	ACGTCAAGGAGAAAAAACCCCGGATTCTAGAatggggtacgagaaagaaatc

		3Cl_146_PpFKBP12M56V-R58Q	CATCCCAACCTTTGATCACTTGACCCA Cccctaactcaaactggaag
		5Cl_146_PpFKBP12M56V-R58Q	CTTCCAGTTTGAGTTAGGGGTGGGTCAa gtgatcaaaggttgggatg
		3_Cl_PpFKBP12wt	AAGCGTGACATAACTAATTACATGACT CGAGtcactgggcgctgagc
pESPB014	pESPB003	5_Cl_PpFKBP12wt	ACGTCAAGGAGAAAAAACCCCGGATT CTAGAatggggtacgagaaagaaatc
		3Cl_146_PpFKBP12- M56K-G57Q-R58E	CATCCCAACCTTTGATCACTTCCTGCTT ccctaactcaaactggaag
		5Cl_146_PpFKBP12- M56K-G57Q-R58E	CTTCCAGTTTGAGTTAGGGAAGCAGGA Agtgatcaaaggttgggatg
		3_Cl_PpFKBP12wt	AAGCGTGACATAACTAATTACATGACT CGAGtcactgggcgctgagc
pESPB016	pESPB010	5_Cl_PpFKBP12wt	ACGTCAAGGAGAAAAAACCCCGGATT CTAGAatggggtacgagaaagaaatc
		3Cl_146_PpFKBP12M56V-R58Q	CATCCCAACCTTTGATCACTTGACCCA Cccctaactcaaactggaag
		5Cl_146_PpFKBP12M56V-R58Q	CTTCCAGTTTGAGTTAGGGGTGGGTCAa gtgatcaaaggttgggatg
		3_Cl_PpFKBP12wt	AAGCGTGACATAACTAATTACATGACT CGAGtcactgggcgctgagc
pESPB018	pESPB010	5_Cl_PpFKBP12wt	ACGTCAAGGAGAAAAAACCCCGGATT CTAGAatggggtacgagaaagaaatc
		3Cl_146_PpFKBP12- M56K-G57Q-R58E	CATCCCAACCTTTGATCACTTCCTGCTT ccctaactcaaactggaag
		5Cl_146_PpFKBP12- M56K-G57Q-R58E	CTTCCAGTTTGAGTTAGGGAAGCAGGA Agtgatcaaaggttgggatg
		3_Cl_PpFKBP12wt	AAGCGTGACATAACTAATTACATGACT CGAGtcactgggcgctgagc

Supplementary Table S2

Primers used to generate the vectors containing the different *PIG1bL-CaMV 35Sp-FKBP12-cMyc-CaMV 35St-PIG1bR* DNA constructs, to validate via PCR their correct integration at the PIG1 locus, and to determine via qPCR their copy number in the Physcomitrella genome. Grey font colours indicate that the primers have been re-used.

Purpose	Obtained vector name	DNA template used for PCR	Primer name	Primer sequence
DNA construct for the targeted integration of *PpFKBP12* fused to *cMyc*	pESPB033	Bel5-PIG1b-Act5	3Cl_5HR-PIG1	TGTATTCTATTTGATTGATAAGAAAAATGATAATAGTTTAAAGAGC
			5Cl_5HR-PIG1	AAAACATGAATAACCAAATTAAAATATTAATAATTCATAGGG
		mAV4-hpt	5Cl_5HR-PIG1_35S-P	GCTCTTTAAACTATTATCATTTTTCTTATCAATCAAATAGAATACAGCGGCCGCctgcaggtccccagattagc
			3Cl_35S-P	TCTAGAtgttctctccaaatgaaatgaacttcc
		2027_pluc-nosp_35st	5Cl_Myc_35S-T	GAACAAAAACTCATCTCAGAAGAGGATCTGTGACTCGAGgtccgcaaaaatcaccagtc
			3Cl_5HR-PIG1_35S-T	CCCTATGAATTATTAATATTTTAATTTGGTTATTCATGTTTTGCGGCCGCgtcactggattttggttttagg
		pESPB003	5Cl_35S-P_PpFKBP12	GGAAGTTCATTTCATTTGGAGAGAACATCTAGAatggggtacgagaaagaaatcatccggcc
			3Cl_Myc_PpFKBP12	CAGATCCTCTTCTGAGATGAGTTTTTGTTCctgggcgctgagcacctcgatttc
DNA construct for the targeted integration of *PpFKBP12-C26Y* fused to *cMyc*	pESPB035	Bel5-PIG1b-Act5	3Cl_5HR-PIG1	TGTATTCTATTTGATTGATAAGAAAAATGATAATAGTTTAAAGAGC
			5Cl_5HR-PIG1	AAAACATGAATAACCAAATTAAAATATTAATAATTCATAGGG
		mAV4-hpt	5Cl_5HR-PIG1_35S-P	GCTCTTTAAACTATTATCATTTTTCTTATCAATCAAATAGAATACAGCGGCCGCctgcaggtccccagattagc
			3Cl_35S-P	TCTAGAtgttctctccaaatgaaatgaacttcc
		2027_pluc-nosp_35st	5Cl_Myc_35S-T	GAACAAAAACTCATCTCAGAAGAGGATCTGTGACTCGAGgtccgcaaaaatcaccagtc
			3Cl_5HR-PIG1_35S-T	CCCTATGAATTATTAATATTTTAATTTGGTTATTCATGTTTTGCGGCCGCgtcactggattttggttttagg

		pESPB006	5Cl_35S-P_PpFKBP12	GGAAGTTCATTTCATTTGGAGAGAACATCTAGAatggggtacgagaaagaaatcatccggcc
			3Cl_Myc_PpFKBP12	CAGATCCTCTTCTGAGATGAGTTTTTGTTCctgggcgctgagcacctcgatttc
DNA construct for the targeted integration of *PpFKBP12-C26Y* fused to *cMyc*	pESPB037	Bel5-PIG1b-Act5	3Cl_5HR-PIG1	TGTATTCTATTTGATTGATAAGAAAAATGATAATAGTTTAAAGAGC
			5Cl_5HR-PIG1	AAAACATGAATAACCAAATTAAAATATTAATAATTCATAGGG
		mAV4-hpt	5Cl_5HR-PIG1_35S-P	GCTCTTTAAACTATTATCATTTTTCTTATCAATCAAATAGAATACAGCGGCCGCctgcaggtccccagattagc
			3Cl_35S-P	TCTAGAtgttctctccaaatgaaatgaacttcc
		2027_pluc-nosp_35st	5Cl_Myc_35S-T	GAACAAAAACTCATCTCAGAAGAGGATCTGTGACTCGAGgtccgcaaaaatcaccagtc
			3Cl_5HR-PIG1_35S-T	CCCTATGAATTATTAATATTTTAATTTGGTTATTCATGTTTTGCGGCCGCgtcactggattttggttttagg
		pESPB001	5Cl_ 35S-P_ScFPR1	GGAAGTTCATTTCATTTGGAGAGAACATCTAGAatgtctgaagtaattgaaggtaacgtc
			3Cl_Myc_ScFPR1	CAGATCCTCTTCTGAGATGAGTTTTTGTTCgttgaccttcaacaattcgacgtc
DNA construct for the targeted integration of *PpFKBP12-C26Y* fused to *cMyc*	pESPB039	Bel5-PIG1b-Act5	3Cl_5HR-PIG1	TGTATTCTATTTGATTGATAAGAAAAATGATAATAGTTTAAAGAGC
			5Cl_5HR-PIG1	AAAACATGAATAACCAAATTAAAATATTAATAATTCATAGGG
		mAV4-hpt	5Cl_5HR-PIG1_35S-P	GCTCTTTAAACTATTATCATTTTTCTTATCAATCAAATAGAATACAGCGGCCGCctgcaggtccccagattagc
			3Cl_35S-P	TCTAGAtgttctctccaaatgaaatgaacttcc
		2027_pluc-nosp_35st	5Cl_Myc_35S-T	GAACAAAAACTCATCTCAGAAGAGGATCTGTGACTCGAGgtccgcaaaaatcaccagtc
			3Cl_5HR-PIG1_35S-T	CCCTATGAATTATTAATATTTTAATTTGGTTATTCATGTTTTGCGGCCGCgtcactggattttggttttagg
		pDONR223-HsFKBP1A/HsFKBP12 SpectR	5Cl_ 35S-P_HsFKBP1A	GGAAGTTCATTTCATTTGGAGAGAACATCTAGAatgggagtgcaggtggaaac
			3Cl_Myc_HsFKBP1A	CAGATCCTCTTCTGAGATGAGTTTTTGTTCttccagttttagaagctccacatc
PCR to validate correct integration at the PIG1		Physcomitrella gDNA	5_Up_173long_PIG1-5	TTGTTGCAACATTTGGAGTTGGC
			3_103_35S-T(inv)	GGTTTCGCTCATGTGTTGAGC
			5_52_35S-P(inv)	CTGCGTAAGCCTCTCTAACCATC

locus of the linear DNA cassette			3_Down_81_PIG1-3	CCAATCTGGGAATAGCTTGTTATTGTC
Transgene copy number determination via qPCR		Physcomitrella gDNA	5-qPCR-PIG1-5HR-a	TTTCTATGCACGGATAGCAAC
			3-qPCR-PIG1-5HR-a	ACACCACACCCATCTATAGC
			5-qPCR-PIG1-3HR-b	AGACGGTTGATAGCTTGGC
			3-qPCR-PIG1-3HR-b	GCATGCTATGGACCCAAATTG
			5-qPCR-35Sp(mAV)-c	AAGGGTCTTGCGAAGGATAG
			3-qPCR-35Sp(mAV)-c	CGTTCCAACCACGTCTTC

Supplementary Table S3

Primers used to generate the estradiol-inducible *lst8*, *tor*, and *raptors* RNA interference (RNAi) systems destined for a targeted integration at the PIG1 locus in the Physcomitrella genome

Purpose	Obtained vector name	DNA template used for PCR	Primer name	Primer sequence
Estradiol-inducible *lst8* RNAi system #1	pESPB061	pESPB020	5Cl_pENTR-PpLST8_RNAi_1st	CACCGTTGACTTATGAATCGCATATGAAC
			3Cl_pENTR-PpLST8_RNAi_1st	TGTGATCAGAGGACGTTGTAG
Estradiol-inducible *lst8* RNAi system #2	pESPB063	Physcomitrella cDNA	5Cl_pENTR-PpLST8_RNAi_2nd	GCGGCCGCTGCCCCTGTACAGCAAAG
			3Cl_pENTR-PpLST8_RNAi_2nd	GGCGCGCCCGTTTCTGACACTCACTTGC
Estradiol-inducible *tor* RNAi system #1	pESPB065	pESPB022	5Cl_pENTR-PpTOR_RNAi_1st	TGTACAAAAAAGCAGGCTCCGCGGCCGCAAAAATGCAAGTCCGAG
			3Cl_pENTR-PpTOR_RNAi_1st	TTGTACAAGAAAGCTGGGTCGGCGCGCCGATTTATCGCATCCTTC
Estradiol-inducible *tor* RNAi system #2	pESPB067	pESPB022	5Cl_pENTR-PpTOR_RNAi_2nd	TGTACAAAAAAGCAGGCTCCGCGGCCGCTGTCGAGCTTCTTCAATCTG
			3Cl_pENTR-PpTOR_RNAi_2nd	TTGTACAAGAAAGCTGGGTCGGCGCGCCAGAACAGTAACACAAAGGCG
Estradiol-inducible *raptors* RNAi system #1	pESPB069	pESPB024	5Cl_pENTR-PpRAPTORs_RNAi_1st	TGTACAAAAAAGCAGGCTCCGCGGCCGCGTGTCTGAACCTGGAGTTG
			3Cl_pENTR-PpRAPTORs_RNAi_1st	TTGTACAAGAAAGCTGGGTCGGCGCGCCACCGCTCGCAGAATGCATTC
Estradiol-inducible *raptors* RNAi system #2	pESPB071	pESPB026	5Cl_pENTR-PpRAPTORs_RNAi_2nd	TGTACAAAAAAGCAGGCTCCGCGGCCGCTGCCAGAATCTACATTTTTCAAGTGG
			3Cl_pENTR-PpRAPTORs_RNAi_2nd	TTGTACAAGAAAGCTGGGTCGGCGCGCCCTCCTTCTGTGTATAGTCTC

Supplementary Table S4

International Moss Stock Center (IMSC, www.mossstock-center.org) accession numbers of the lines used in this study.

Code	IMSC accession #	Genotype
Wild type	41269	
ESPB001	40976	*PIG1bR-CaMV 35Sp-PpFKBP12-cMyc-CaMV 35St-PIG1bL*
ESPB002	40977	*PIG1bR-CaMV 35Sp-PpFKBP12-cMyc-CaMV 35St-PIG1bL*
ESPB003	40978	*PIG1bR-CaMV 35Sp-PpFKBP12-cMyc-CaMV 35St-PIG1bL*
ESPB004	40979	*PIG1bR-CaMV 35Sp-PpFKBP12-cMyc-CaMV 35St-PIG1bL*
ESPB006	40980	*PIG1bR-CaMV 35Sp-PpFKBP12^{C26Y}-cMyc-CaMV 35St-PIG1bL*
ESPB007	40981	*PIG1bR-CaMV 35Sp-PpFKBP12^{C26Y}-cMyc-CaMV 35St-PIG1bL*
ESPB010	40982	*PIG1bR-CaMV 35Sp-ScFKBP12-cMyc-CaMV 35St-PIG1bL*
ESPB011	40983	*PIG1bR-CaMV 35Sp-ScFKBP12-cMyc-CaMV 35St-PIG1bL*
ESPB012	40984	*PIG1bR-CaMV 35Sp-ScFKBP12-cMyc-CaMV 35St-PIG1bL*
ESPB014	40985	*PIG1bR-CaMV 35Sp-HsFKBP12-cMyc-CaMV 35St-PIG1bL*
ESPB015	40986	*PIG1bR-CaMV 35Sp-HsFKBP12-cMyc-CaMV 35St-PIG1bL*
ESPB016	40987	*PIG1bR-CaMV 35Sp-HsFKBP12-cMyc-CaMV 35St-PIG1bL*
ESPB017	40988	*PIG1bR-CaMV 35Sp-PpFKBP12-cMyc-CaMV 35St-PIG1bL*
ESPB018	40989	*PIG1bR-CaMV 35Sp-PpFKBP12-cMyc-CaMV 35St-PIG1bL*
ESPB020	40990	*Pplst8-RNAi-61'-40*
ESPB024	40991	*Pplst8-RNAi-63'-38*
ESPB027	40992	*Pptor-RNAi-65'-27*
ESPB032	40993	*Pptor-RNAi-67'-17*
ESPB035	40994	*Ppraptors-RNAi-69'-14*
ESPB040	40995	*Ppraptors-RNAi-71'-25*